Critical Reviews™ in Biomedical Engineering, 29(4):1–70 (2001)

Computational Modeling of Ligament Mechanics

Jeffrey A. Weiss and John C. Gardiner*

University of Utah, Department of Bioengineering, Salt Lake City, Utah 84112

*Address all correspondence to: Jeffrey A. Weiss, University of Utah, 50 South Central Campus Drive, Room 2480, Salt Lake City, UT 84112

ABSTRACT: This article provides a critical review of past and current techniques for the computational modeling of ligaments and tendons. A brief overview of relevant concepts from the fields of continuum mechanics and finite element analysis is provided. The structure and function of ligaments and tendons are reviewed in detail, with emphasis on the relationship of microstructural tissue features to the continuum mechanical behavior. Experimental techniques for the material characterization of biological soft tissues are discussed. Past and current efforts related to the constitutive modeling of ligaments and tendons are classified by the particular technique and dimensionality. Applications of one-dimensional and three-dimensional constitutive models in the representation of the mechanical behavior of joints are presented. Future research directions are identified.

KEY WORDS: ligament, soft tissue mechanics, constitutive modeling, finite element

CONVENTIONS

Vectors and vector fields and tensors are indicated in boldface. Material quantities are indicated in upper case. Spatial quantities are indicated in lower case. All numbers, vectors, matrices, functions, and so forth are real.

NOMENCLATURE

$\cdot$	inner product of a 2nd order tensor with a vector (i.e., $\boldsymbol{A} \cdot \boldsymbol{b}$) or a vector with a vector (i.e., $\boldsymbol{b} \cdot \boldsymbol{b}$)
:	inner product of two tensors of 2nd order or higher (i.e., $\boldsymbol{D} : \boldsymbol{C}$)
$\otimes$	outer product (i.e., $(\boldsymbol{A} \otimes \boldsymbol{B})_{ijkl} = A_{ij} B_{kl}$)
$\boldsymbol{A}^2$	The square of a matrix $\boldsymbol{A}$. In index notation, $(\boldsymbol{A}^2)_{ij} = A_{ik}A_{kj}$
tr	trace of a matrix (i.e., tr $\boldsymbol{C} = C_{11} + C_{22} + C_{33}$)
div	divergence of a vector; $\boldsymbol{A}^T$, transpose of a matrix $\boldsymbol{A}$
∇	gradient referred to the deformed configuration

0278-940X/01/$5.00

SYMBOLS (IN ORDER OF APPEARANCE)

II. Mechanics Background

A. Continuum Mechanics

$\boldsymbol{X}$ Position of a particle in the reference configuration

$\boldsymbol{x}$ Position of a particle in the deformed (current) configuration

$\boldsymbol{f}$ A deformation $\boldsymbol{f} = \boldsymbol{x}(\boldsymbol{X})$ is a mapping of a closed bounded region into another closed bounded region

R_0 Reference closed bounded region

R Deformed closed bounded region

$\boldsymbol{F}$ The deformation gradient tensor, $\boldsymbol{F} = \partial \boldsymbol{x}/\partial \boldsymbol{X}$

J The Jabobian of the deformation, $J = \det \boldsymbol{F}$

ρ_0 Density in reference configuration

ρ Density in deformed configuration

$\boldsymbol{C}$ The right Cauchy-Green deformation tensor, $\boldsymbol{C} = \boldsymbol{F}^T\boldsymbol{F}$

$\boldsymbol{B}$ The left Cauchy-Green deformation tensor, $\boldsymbol{B} = \boldsymbol{F}\boldsymbol{F}^T$

Stress and strain tensors

$\boldsymbol{E}$ Green-Lagrange strain tensor, $\boldsymbol{E} = \frac{1}{2}(\boldsymbol{F}^T\boldsymbol{F} - \boldsymbol{1}) = \frac{1}{2}(\boldsymbol{C} - \boldsymbol{1})$

$\boldsymbol{1}$ Identity tensor

ε Infinitesimal strain tensor, $\varepsilon = \frac{1}{2}(\boldsymbol{F} + \boldsymbol{F}^T - 2\boldsymbol{1})$

$\boldsymbol{T}$ Cauchy stress tensor

$\boldsymbol{P}$ First Piola-Kirchhoff stress tensor, $\boldsymbol{P} = J\boldsymbol{F}^{-1}\boldsymbol{T}$

$\boldsymbol{S}$ Second Piola-Kirchhoff stress tensor, $\boldsymbol{S} = J\boldsymbol{F}^{-1}\boldsymbol{T}\boldsymbol{F}^{-T} = \boldsymbol{P}\boldsymbol{F}^{-T}$

B. Constitutive Modeling

Hyperelasticity

$W, \widetilde{W}, \overline{W}$ Strain energy

I_1 The first invariant of $\boldsymbol{C}$, $I_1 = \text{tr}\,\boldsymbol{C}$

I_2 The second invariant of $\boldsymbol{C}$, $I_2 = \frac{1}{2}((\text{tr}\,\boldsymbol{C})^2 - \text{tr}\,\boldsymbol{C}^2)$

I_3 The third invariant of $\boldsymbol{C}$, $I_3 = \det \boldsymbol{C} = (\rho_0/\rho)^2 = J^2$

Elasticity tensors

C 4th order material elasticity tensor

C. Finite Element Modeling

Π Potential energy function

Π_{ext} Potential energy of the external loading

$\boldsymbol{R}_0$ Reference configuration

$\boldsymbol{v}$ Material variations

$\boldsymbol{T} : \nabla \boldsymbol{v}$ Internal stresses

$\boldsymbol{b} \cdot \boldsymbol{v}$ Body force

$\bar{t} \cdot \boldsymbol{v}$ Surface traction
$\boldsymbol{K}_{NL}$ Nonlinear stiffness matrix
$\boldsymbol{K}_{L}$ Linear stiffness matrix
$\Delta \boldsymbol{u}$ Incremental displacement vector
$\boldsymbol{F}_{ext}$ External forces
$\boldsymbol{F}_{int}$ Internal forces
$\boldsymbol{B}_{NL}$ Nonlinear strain displacement matrix
$\boldsymbol{B}_{L}$ Linear strain displacement matrix
$\boldsymbol{M}$ Mass matrix
$\boldsymbol{K}$ Stiffness matrix
$\boldsymbol{D}$ Global damping matrix; for Raleigh damping, $\boldsymbol{D} = \alpha_{mass}\,\boldsymbol{M} + \alpha_{stiff}\,\boldsymbol{K}$
α_{mass} Mass damping coefficient
α_{stiff} Stiffness damping coefficient

C. Finite Element Modeling
Π Potential energy function
Π_{ext} Potential energy of the external loading
$\boldsymbol{R}_0$ Reference configuration
$\boldsymbol{v}$ Material variations
$\boldsymbol{T}:\nabla \boldsymbol{v}$ Internal stresses
$\boldsymbol{b} \cdot \boldsymbol{v}$ Body force
$\bar{t} \cdot \boldsymbol{v}$ Surface traction
$\boldsymbol{K}_{NL}$ Nonlinear stiffness matrix
$\boldsymbol{K}_{L}$ Linear stiffness matrix
$\Delta \boldsymbol{u}$ Incremental displacement vector
$\boldsymbol{F}_{ext}$ External forces
$\boldsymbol{F}_{int}$ Internal forces
$\boldsymbol{B}_{NL}$ Nonlinear strain displacement matrix
$\boldsymbol{B}_{L}$ Linear strain displacement matrix
$\boldsymbol{M}$ Mass matrix
$\boldsymbol{K}$ Stiffness matrix
$\boldsymbol{D}$ Global damping matrix; for Raleigh damping, $\boldsymbol{D} = \alpha_{mass}\,\boldsymbol{M} + \alpha_{stiff}\,\boldsymbol{K}$
α_{mass} Mass damping coefficient
α_{stiff} Stiffness damping coefficient

IV. Material Models for Ligaments
B. Elastic Models
λ Stretch along fiber direction
W_{λ} Strain energy contribution from the collagen fibers
$\boldsymbol{a}$ Unit vector describing the local fiber direction
p Hydrostatic pressure
$\boldsymbol{a}^0$ Unit vector describing the local fiber direction in the reference configuration
F_1 Strain energy functional of isotropic ground substance
F_2 Strain energy functional for collagen fibers
F_3 Strain energy functional for fiber/matrix interaction
W_{α} Shorthand notation for $\partial W/\partial I_{\alpha}$

λ^* Stretch at which the collagen fibers were straightened
C_3 Coefficient scaling the collagen exponential stresses
C_4 Coefficient controlling rate of collagen fiber uncrimping
C_5 Coefficient for modulus of straightened collagen fibers
C_6 Coefficient describing the *y*-intercept of the linear region

C. Viscoelastic Models
$\boldsymbol{S}(t)$ Time-dependent 2nd Piola-Kirchhoff stress tensor
$\boldsymbol{S}_e(\boldsymbol{C}(t))$ Equilibrium stress representing elastic behavior
$\boldsymbol{Z}$ Functional representing the history of the right deformation tensor C
$\boldsymbol{G}(t-s)$ General tensor-valued relaxation function
Υ General tensor-valued history function
$\boldsymbol{S}_v$ Viscous stress
$\boldsymbol{R}$ Strain-dependent tensorial relaxation function, $\boldsymbol{R} = \phi_0\boldsymbol{I} + \phi_1\boldsymbol{C} + \phi_2\boldsymbol{C}^2$
ϕ_0, ϕ_1, ϕ_2 Principal invariants of $\boldsymbol{C}$
$G(t-s)$ General scalar-valued relaxation function
C_0 Initial modulus
C_∞ Long-time modulus
γ C_∞/C_0
μ Shear modulus
$I(s)$ tr $\boldsymbol{C}(s)$

$E_1(t)$ Exponential integral function $E_1(t) = \int_z^\infty \frac{e^{-t}}{t} t$

c Dimensionless constant scaling the degree to which viscous effects are present
τ_1 Time constant bounding the lower limit of the constant damping range
τ_2 Time constant bounding the upper limit of the constant damping range
G_e Equilibrium modulus
G_0 Initial modulus
N_d Span of the transition region in decades
10^{I_0} Lowest discernible relaxation time

D. Poroelastic Models
G Shear modulus
ν Poisson's ratio
e_0 Initial void ratio (fluid volume fraction/solid volume fraction)
p Internal pressure
Pt Elastic ultimate strength
ε_{vol}^{el} Elastic portio of volume change, $\varepsilon_{vol}^{el} = \ln(J^{el})$
κ Log bulk modulus
v Fluid velocity
k Permeability

E. Homogenization Models
$\{\varepsilon_{tissue}\}$ Total tissue strain
$\{\varepsilon_{app}\}$ Apparent strain
$\{\varepsilon^*\}$ Fluctuating strain component
$\boldsymbol{F}_{total}$ Total deformation gradient

$\boldsymbol{F}_{cont}$ Continuum level deformation gradient
$\boldsymbol{F}_{micro}$ Microstructural level deformation gradient

I. INTRODUCTION

The skeletal ligaments are short bands of tough fibrous connective tissue that bind bones together across joints. Their mechanical function is to guide normal joint motion and restrict abnormal joint movement. These functions are assisted by the congruent geometry of the articulating joint surfaces and musculotendinous forces. Ligaments can be subjected to extreme stress while performing their role in restricting abnormal joint motions and can be damaged or completely disrupted when overloaded. Excessive stretching or disruption can result in gross joint instability with some activities. Joint instability can cause altered joint kinematics, altered load distribution, and increased vulnerability to injury of other ligaments and musculoskeletal tissues. Eventually, degenerative joint disease may result from the alterations in loadbearing and joint kinematics.

Because the instability resulting from certain ligamentous injuries can greatly restrict the activity level of an individual and may result in degenerative disease, basic and applied research efforts have examined ligament injury mechanisms, techniques for ligament repair and reconstruction, and rehabilitation methods for use during the healing period. These studies have helped to elucidate details of the natural history of ligament injury and healing from biomechanical, histological, and biochemical viewpoints. However, fundamental mechanical questions regarding the role of individual ligaments, the mechanisms of ligament injury, and the efficacy of reparative/reconstructive procedures persist. This is in part due to the limitations associated with experimental measurements of basic kinematic and mechanical quantities in both *in vivo* and *in vitro* biomechanical studies.

Experimental studies of ligament mechanics are often technically difficult, costly, and prone to error. The stress and strain fields within ligaments are inhomogeneous, yet we are forced to measure these quantities between a small number of discrete points and assume that they are homogeneous. Other quantities such as pressure and contact area are extremely difficult to measure in an experimental setting. Also, parameterized studies require large numbers of animals or significant amounts of human tissue. This often results in prohibitively high costs and time requirements.

The emerging field of computational biomechanics offers a new set of tools for studies of solid and fluid biomechanics that can provide information that would otherwise be difficult or impossible to obtain from experiments. Advances in the fields of constitutive modeling, computational mechanics, numerical methods, and computer science have led to the widespread application of numerical procedures for the analysis of mechanical systems. Traditional engineering fields such as mechanical and civil engineering have utilized computational methods for the study of the mechanics in complex systems for over 20 years. In particular, the finite element (FE) method has provided a generalized procedure to analyze the stress/strain response of a structure. In the FE method, a body is discretized into small finite elements of material volume, for which the material and physical properties are known. The appropriate boundary conditions and initial conditions, including applied loading and displacements, must also be specified for the forward problem to be well posed. The solution procedure involves the consideration of overall energy minimization and/or other fundamental physical balance laws to determine unknown field variables

over the domain. From these variables, the stresses and strains (or other quantities of interest) can be determined throughout the body. The FE method provides a systematic method for assembling the response of a complex system from individual contributions of elements, and thus is ideal for the complex geometries often encountered in biomechanical systems. It also provides a consistent way to address material inhomogeneities and differences in constitutive models between disjoint or continuous parts of a model.

For the successful application of the FE method to studies of ligament and joint mechanics, a detailed mathematical description of the material behavior of the ligaments and a means by which to represent their interaction with other soft and hard tissues are necessary. A material model, referred to in continuum mechanics terminology as a constitutive model, may vary in complexity depending on the application. To develop such a constitutive model, detailed experimental measurements of the material structure and mechanical behavior are needed. The mechanical behavior of ligaments and tendons is somewhat complex. Ligaments consist largely of parallel-bundled collagen fibers embedded in a ground substance matrix holding large amounts of trapped water. The material properties imparted by this structure and composition enable ligaments to perform their role of guiding and restricting joint motions. These tissues possess both time- and rate-dependent properties due to the intrinsic viscoelastic nature of the solid phase and the interaction between the solid and fluid phases. This combination of properties makes accurate modeling of their material behavior a challenge. There are additional difficulties associated with modeling the mechanical behavior of ligaments in a joint such as the complex geometry, the large deformations, contact with other tissues, and the *in situ* stress that provides initial tension and joint stability. Many of these difficulties dictate the use of nonlinear solution procedures. However, these complications can be addressed in a uniform manner when properly formulated for use in FE analysis. During the last 20 years, numerous papers have reported the normal material behavior of soft and hard musculoskeletal tissues, as well as changes associated with injury, repair, immobilization, exercise, and other factors that can move the tissue away from an initially homeostatic state. It is possible to eventually include these effects directly into the constitutive models for the ligaments to model changes in material properties that occur with alterations in the mechanical or biological environment.

Substantial progress has been made in the areas of constitutive modeling and finite element methods that will facilitate the modeling of ligaments and joints. The objectives of this work are to provide a historical review of the efforts made to model ligament mechanics, identify current research relevant to constitutive modeling and the study of joint mechanics, and identify future directions for research and development. Efforts at modeling both isolated ligament tissue and ligaments interacting within larger models of joints are reviewed. The next section provides the reader with background material on basic concepts in continuum mechanics, constitutive modeling, and the finite element method. Section III describes the basic composition, structure, and function of ligaments. A detailed review of the experimental methods used to determine the material properties of ligaments is also provided. The variety of material models that have been proposed to represent ligament behavior is reviewed in Section IV. A critical review of published models of diarthroidal joints is presented in Section V. Finally, the closing section summarizes the work and identifies directions for future research.

II. MECHANICS BACKGROUND

A fundamental knowledge of mechanics is needed to understand the current state of research in computational modeling of ligaments. Because ligaments are subjected to large deformations and strains, concepts from finite deformation theory must be used to describe their stress and strain state. This section provides the reader with a brief review of basic concepts in finite deformation continuum mechanics, constitutive modeling, and finite element modeling that are used in later sections of this article. The reader is referred to the cited textbooks for detailed information on the topics of this section.

A. Continuum Mechanics

To apply continuum mechanics concepts to the analysis of a deformable material, the concept of a continuous medium must apply. In particular, the molecular structure of the material is disregarded in continuum mechanics analyses. In addition, there may not be any gaps or empty space in the continuum. All mathematical functions are assumed to be continuous over the domain of the material for the theory, except at interior surfaces separating regions. With these assumptions, the concept of the stress at a point in the material is well-defined, since the point does not occupy any volume. The continuum assumption is valid for many engineering applications but not all. A common example of a situation for which it is not valid would be the analysis of fatigue crack formation.

Following standard notational conventions,[1] $\boldsymbol{X}$ represents the position of a particle in the reference configuration, while $\boldsymbol{x}$ represents the particle in the deformed (current) configuration. A deformation $\boldsymbol{f} = \boldsymbol{x}(\boldsymbol{X})$ maps a closed bounded region R_0 into another closed bounded region $R = \boldsymbol{f}(R_0)$. The *deformation gradient*, $\boldsymbol{F}$, is defined as

$$\boldsymbol{F}(\boldsymbol{X}) = \nabla \boldsymbol{f} = \frac{\partial \boldsymbol{x}}{\partial \boldsymbol{X}} \tag{1}$$

The *Jacobian* of the deformation is

$$J = \det \boldsymbol{F} = \left(\frac{\rho_0}{\rho} \right) \tag{2}$$

where ρ_0 and ρ are the reference and current material densities, respectively. Physically, J can be interpreted as the ratio of the undeformed volume over the deformed volume for a homogeneous deformation at a material point. For an incompressible material, $J = 1$ for all admissable deformations. The *right* and *left Cauchy-Green deformation* tensors are, respectively,

$$\boldsymbol{C} = \boldsymbol{F}^T \boldsymbol{F} \quad \text{and} \quad \boldsymbol{B} = \boldsymbol{F}\boldsymbol{F}^F \tag{3}$$

These tensors provide measures of material stretching that are independent of rigid body rotation and form the basis of constitutive model development for soft tissues.

1. Stress and Strain Tensors

In finite deformation theory, different measures of stress and strain are employed, depending on whether the quantity is to be referred to the reference configuration or the deformed configuration. The Green-Lagrange strain tensor is used when strain is referred to the reference configuration:

$$\boldsymbol{E} = \frac{1}{2}(\boldsymbol{F}^T\boldsymbol{F} - \mathbf{1}) = \frac{1}{2}(\boldsymbol{C} - \mathbf{1}) \tag{4}$$

where $\mathbf{1}$ represents the identity tensor. As with all strain tensors that correctly describe large deformation, $\boldsymbol{E} = 0$ for rigid body motions.

When the deformation can be considered "small", (Equation 4) can be reduced to the infinitesimal strain tensor:

$$\varepsilon = \frac{1}{2}(\boldsymbol{F} + \boldsymbol{F}^T - 2\mathbf{1}) \tag{5}$$

ε is an approximate measure of strain that is only accurate for infinitesimal strains (less than 1%), whereas $\boldsymbol{E}$ provides an exact measure for both finite and infinitesimal strains. It should also be noted that for rigid body motions, $\varepsilon \neq 0$. A rigid rotation will cause straining as measured by this strain tensor. This is readily proven from the polar decomposition of the deformation gradient $\boldsymbol{F} = \boldsymbol{RU}$, where $\boldsymbol{R}$ represents a rigid rotation of the material point.

The Cauchy stress, $\boldsymbol{T}$, is defined as the force acting on the current or deformed configuration. Unfortunately, for large deformations the deformed configuration is typically not known *a priori*. For this reason, it is often advantageous to use a stress tensor that is defined in terms of the reference configuration. Two commonly used measures are the first and second Piola-Kirchoff stress tensors. They are defined respectively as

$$\boldsymbol{P} = J\boldsymbol{F}^{-1}\boldsymbol{T} \tag{6}$$

$$\boldsymbol{S} = J\boldsymbol{F}^{-1}\boldsymbol{T}\boldsymbol{F}^{-T} = \boldsymbol{P}\boldsymbol{F}^{-T} \tag{7}$$

The first Piola-Kirchoff stress, sometimes referred to as engineering stress, is the component of force in the current configuration on a surface that is normal to the axes in the reference configuration, measured per unit surface area in the reference configuration.[1] The components of $\boldsymbol{P}$ can be directly measured experimentally. Unfortunately, $\boldsymbol{P}$ is not symmetric. The stress tensor $\boldsymbol{S}$ is symmetric, but it does not have a direct physical interpretation. $\boldsymbol{S}$ is

used more commonly than $\boldsymbol{P}$ because it is energetically conjugate to the Green-Lagrange strain tensor $\boldsymbol{E}$. The tensors $\boldsymbol{S}$ and $\boldsymbol{E}$ often appear together in constitutive models for large deformation elasticity.

B. Constitutive Modeling

Constitutive equations are used to describe the mechanical behavior of ideal materials through specification of the dependence of stress on kinematic variables such as the deformation gradient, rate of deformation, temperature, and pressure. They can be used to distinguish one material from another but must be defined such that they obey dimensional homogeneity and independence of choice of coordinate system. Constitutive relations must also obey the *Principle of Material Frame Indifference*, which states that constitutive equations must be invariant under changes of observer frame of reference. This principle ensures that rigid body motions will not change the stress in a material. The accurate description and prediction of the mechanical behavior of soft tissues by constitutive equations remains one of the challenges for computational modeling of ligaments and other soft tissues.

Specific steps are generally followed in the development of constitutive relations for a material. The first step is to observe the material and classify it according to its behavior and composition. Examples of these classifications for a solid would include whether the material is elastic or viscoelastic, isotropic or anisotropic, linear or nonlinear, and homogeneous or heterogeneous. The second step is to choose an appropriate theoretical framework to develop a relationship between kinematic quantities and stress. Hyperelasticity is often utilized in the biomechanics field. The third step is to identify a specific constitutive equation. This step must take advantage of mathematical conditions such as observer independence to derive a relationship based on microstructural observations or experimental data. The fourth step is to perform experiments to determine values for the material parameters. The final step is independent validation of the model's predictive ability.

1. Hyperelasticity

For an *elastic material*, the stress at any point can be defined solely as a function of the deformation gradient $\boldsymbol{F}$ at that point. A change in stress arises only in response to a change in configuration, and the material is indifferent to the manner in which the change in configuration arises in space and time. For a *hyperelastic material*, the above definition applies, and in addition there is a scalar function from which the stress can be derived at each point $\boldsymbol{X}$. The scalar function is the stored energy or *strain energy function*, W, which can also be defined solely in terms of the deformation gradient:

$$W = \widetilde{W}(\boldsymbol{F}) \tag{8}$$

The strain energy, W, must obey the *Principle of Material Frame Indifference.* This principle ensures that rigid body motions will not change the value of the strain energy function. Consequently, W may be expressed in the form

$$W = \tilde{W}(\boldsymbol{C}) \tag{9}$$

The second Piola-Kirchhoff stress is derived directly from the strain energy as

$$\boldsymbol{S} = 2\frac{\partial W}{\partial \boldsymbol{C}} \tag{10}$$

Hyperelasticity provides a convenient framework for the formulation of constitutive equations for biological soft tissues because it allows for large deformations and anisotropy. It can also be easily extended to other material behaviors such as plasticity,[2] viscoelasticity,[3,4] poroelasticity,[5,6] and damage mechanics.[7]

Material symmetries will restrict the way in which the strain energy depends on $\boldsymbol{C}$. Specifically, any orthogonal transformation that is a member of the material symmetry group will leave its strain energy unaltered when applied to the material prior to deformation. For instance, if the material under consideration is *isotropic*, its symmetry group consists of the entire group of proper orthogonal transformations. For an isotropic material, W can depend on $\boldsymbol{C}$ through only the three principle invariants of $\boldsymbol{C}$:

$$W = W(I_1, I_2, I_3) \tag{11}$$

where

$$I_1 = \text{tr}\ \boldsymbol{C}\ I_2 = \frac{1}{2}[(\text{tr}\ \boldsymbol{C})^2 - \text{tr}\ \boldsymbol{C}^2] \qquad I_3 = \det\ \boldsymbol{C} \tag{12}$$

and "tr" denotes the trace of the tensor. The isotropic hyperelastic material reduces to linearized elasticity when appropriate assumptions regarding the magnitude of strains and rotations are made.

2. Elasticity Tensors

Small displacements from a known configuration of a material are governed by the "tangent" behavior of the material model. Mathematically, the elasticity tensor describes how infinitesimal variations in material configuration, or strain, will affect the stress tensor. Although typically termed the elasticity tensor, this tensor can be defined for any material, inelastic or elastic. For nonlinear FE analysis, the solution process often proceeds by searching for a configuration that is close to a known equilibrium state that provides a balance between incrementally applied loads and the current stress field in the material. In this case, the elasticity tensor plays an important role in the iterative solution process.

For a hyperelastic material, the material version of the second elasticity tensor is derived from the second derivative of the strain energy with respect to the right Cauchy-Green deformation tensor:

$$\mathbf{C} = 4\frac{\partial^2 W}{\partial \boldsymbol{C}\partial \boldsymbol{C}} = 2\frac{\partial \boldsymbol{S}}{\partial \boldsymbol{C}} \tag{13}$$

Note that the components of the 4th-order tensor $\mathbf{C}$ are not constant, but rather vary as a function of $\boldsymbol{C}$ in general. If this tensor is defined for an isotropic hyperelastic material at the reference configuration, it can be shown that the elasticity tensor defined above reduces to the elasticity tensor used in linearized elasticity theory to define the relationship between the infinitesimal strain tensor ε and engineering stress **s**. Similar analytic expressions for the elasticity tensor can be derived for other constitutive models.

C. Finite Element Modeling

In some cases, the equations of motion can be combined with an appropriate constitutive law to obtain closed-form mathematical solutions to problems with relatively simple geometry and boundary conditions. Unfortunately, most problems of interest in biomechanics are too complex to obtain closed-form solutions. This is due to inhomogeneous material properties, complex three-dimensional geometry, and unique boundary/initial conditions such as *in situ* stress or residual stress. In these cases, numerical solution techniques must be utilized. The FE method provides a powerful and commonly used methodology for the solution of complex problems in nonlinear solid and fluid biomechanics. Because of the importance of the finite element method in the computational modeling of joint mechanics, this section provides a brief overview of the key concepts and equations that characterize the FE method.

The FE method may be described as an analysis method for discrete systems.[8] The domain of interest is divided into a finite number of discrete elements. A form is assumed for the variation of the unknown functions over each element. Usually a polynomial form is assumed, and these polynomials are defined in terms of other independent variables. In solid mechanics, the unknown variation of displacements over the element is described by these polynomials, referred to as *shape functions*, in terms of the other nodal displacements. These shape functions are called *isoparametric* if they are used to define both the variation of element geometry between nodal points as well as the variation of displacement over the element. The equilibrium equations are cast in integral (weak) form, and the shape functions and nodal displacement values replacing the continuous functions. The requirement of stationarity yields a system of equations that can be assembled element by element. Numerical integration is used to evaluate the integrals for each element, and the result is a large (often nonlinear) system of simultaneous equations that can be solved for the nodal displacements that satisfy equilibrium.

In summary, steps in the analysis of a discrete system include the idealization of the system, establishment of equilibrium conditions, assemblage of the discrete element system into a set of simultaneous (possibly nonlinear) equations, and solution of these equations to determine the response of the state variables.[9] These steps are the same whether

the problem is steady-state or dynamic, linear or nonlinear, and regardless of the initial and boundary conditions. In contrast to other discretization methods, FE method has the ability to treat material inhomogeneities, complex boundary conditions, and complicated geometry in a systematic way.

For nonlinear elasticity, the weak form of the equilibrium equations can be obtained from the potential energy. The potential energy function, Π, is defined as the sum of the strain energy in the material (internal energy) and the energy due to externally applied body forces and surface tractions Π_{ext}. Both sources may be a function of the deformation map $\boldsymbol{f}$ over the reference configuration $\boldsymbol{R}_0$:

$$\Pi(\boldsymbol{f}) = \int_{\boldsymbol{R}_0} \{ W(\boldsymbol{X}, \boldsymbol{C}(\boldsymbol{f}(\boldsymbol{X}))) \} dV + \Pi_{ext}(\boldsymbol{f}) \tag{14}$$

The first variation of Π with respect to the deformation $\boldsymbol{F}$ in the direction $\boldsymbol{V}$ yields the "Euler equations". In the present case the Euler equations are simply a statement of the equilibrium equations in weak form. If these are transformed to the current configuration, with variations in configuration $\boldsymbol{v}$ taken with respect to the current configuration:

$$D\Pi \cdot \boldsymbol{v} = \int_{\boldsymbol{R}} \boldsymbol{T} : \nabla \boldsymbol{v} dv = \int_{\boldsymbol{R}} \boldsymbol{b} \cdot \boldsymbol{v} dv + \int_{S} \bar{\boldsymbol{t}} \cdot \boldsymbol{v} da \tag{15}$$

Note that this is equivalent to the virtual work approach. $\boldsymbol{T} : \nabla \boldsymbol{v}$ represents the internal stresses, $\boldsymbol{b} \cdot \boldsymbol{v}$ is the body force, and $\bar{\boldsymbol{t}} \cdot \boldsymbol{v}$ is the surface traction. This equation is in general highly nonlinear.

Two solution procedures are commonly employed at this point. An "explicit time integration" provides the solution to the equations of motion by including all inertial effects and using the central difference method to integrate the equations forward in time. This approach is limited by the Courant stability criterion and requires extremely small time step size. It is appropriate for high-rate and impact problems. The second approach is to linearize the equations (15) about a known configuration. After introduction of the FE shape functions, this results in a system of linearized matrix equations:

$$(\boldsymbol{K}_{NL} + \boldsymbol{K}_L) \cdot \Delta \boldsymbol{u} = \boldsymbol{F}_{ext} - \boldsymbol{F}_{int} \tag{16}$$

$\boldsymbol{K}_{NL}$ is the nonlinear stiffness, $\boldsymbol{K}_L$ is the linear stiffness, $\Delta \boldsymbol{u}$ is the incremental displacement vector, and $\boldsymbol{F}_{ext}$ and $\boldsymbol{F}_{int}$ represent the external and internal forces respectively. For a detailed derivation and description of the discrete form of the nonlinear FE equations, see Bathe.[9] This equation provides the starting point for an incremental-iterative solution strategy characterized by the Newton-Raphson method.

1. Contact

During deformation, two or more bodies may contact. The analysis of contact using the FE method can be an extremely difficult, nonlinear problem. In a FE context, contact may be enforced as an additional nonlinear constraint. The implementation of contact must be able to handle both static and dynamic situations, with our without frictional sliding. Three of the most common approaches for implementing contact in FE analyses are the penalty method,[9] the Lagrange multiplier method,[9,10] and the augmented Lagrangian method.[11] The penalty method is relatively easy to implement and it does not introduce any additional degrees of freedom to the global system of equations. However, it is difficult to choose the penalty parameter so that the contact constraint is sufficiently satisfied without causing ill-conditioning of the global stiffness matrix. Some penetration always occurs between the contacting bodies, and the challenge is to pick a penalty value that reduces the penetration to reasonable values for the analysis at hand without inducing numerical ill-conditioning. The Lagrange multiplier method exactly satisfies the contact constraint at the expense of introducing additional degrees of freedom to the global system. This causes an increase in the size of the stiffness matrix that must be inverted and thus increases the floating point and memory requirements of the analysis. The augmented Lagrangian method provides a compromise between the penalty and Lagrange multiplier methods. It does not introduce additional degrees of freedom or ill-conditioning as with the other methods. However, it requires additional Newton or quasi-Newton iterations that may increase the solution time when compared to the penalty method.

In recent years, there has been an increase in the availability and usage of commercial FE codes for nonlinear analysis. These software packages are rapidly becoming more powerful and user-friendly. Despite the apparent ease by which these programs can be learned in a superficial sense, it often takes many years before an analyst has the skill to confidently perform nonlinear analysis. Users must have a fundamental understanding of the approximations and limitations that are inherent with nonlinear FE analysis before reliable and consistent results can be expected. This is especially true in the analysis of ligament and joint mechanics because of the complex material behavior and boundary conditions.

III. STRUCTURE and FUNCTION of LIGAMENTS

Healthy articulating joints allow for nearly effortless motion along preferred anatomical directions, yet they must also restrict abnormal motions. The freedom of mobility is achieved by the lubricating action of cartilage that covers the articulating surfaces of the bones. Joint stability is maintained by a combination of bony geometry and ligament and other soft tissue interactions. Ligamentous restraints guide and restrict the motion, defining the normal envelope of passive joint motion. This section reviews the structure, function, mechanical testing, and material properties of ligaments. An undertanding of each of these topics is necessary for the critical evaluation of constitutive models for ligaments and tendons.

A. Ligament Structure

Ligaments are well suited to the physiological functions they perform. Ligaments are a biological composite consisting of a ground substance matrix reinforced by collagen and elastin. The ground substance matrix is composed of proteoglycans, glycolipids, and fibroblasts and holds large amounts of water.[12] Ligaments are relatively hypocellular with interconnected, elongated fibroblastic cells in their midsubstance and more rounded cells found near their insertions to bone.[13] The primary function of the cells is to maintain the collagen scaffold. This is consistent with other musculoskeletal soft tissues that have mechanical function as their main purpose. Water makes up about two-thirds of the weight of normal ligaments; 70 to 80% of the remaining weight is made up by the fibrillar protein collagen.[14] Collagen is the primary component resisting tensile stress in ligaments.

1. Collagen

Collagen is formed from a structural hierarchy. Figure 1 illustrates the hierarchy proposed by one investigator for the type I collagen in rat tail tendon. There appears to be some disagreement in the literature as to the exact levels of organization, and evidence suggests that it is tissue-specific. Type I collagen is one of the "fiber-forming" collagens, which also includes type II and type III collagens. Collagen molecules are synthesized and secreted by cells such as fibroblasts in connective tissue.[15] This process starts with the modification of

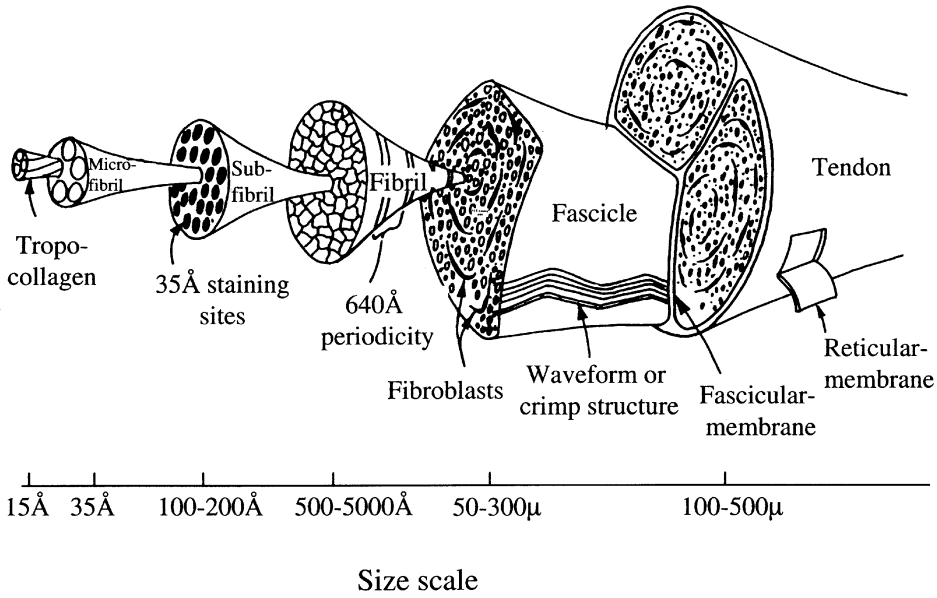

FIGURE1. The structural hierarchy of ligament and tendon. (Adapted from Kastelic etal.,1978.)

linear polypeptide chains to form alpha-helix chains. Three alpha-helix chains coil together to form the triple helix known as a tropocollagen molecule. The tropocollagen molecules are secreted and self-assemble in the extracellular matrix. Five tropocollagen molecules are wound together in a left-handed configuration with a quarter-staggered pattern, yielding a cross-striated collagen microfibril. This cross-striation can be seen in electron micrographs, and is reported to have a period of 640 to 680 Å. According to Viidik,[16] the diameter of the microfibril is about 40 Å. The microfibril is held together with hydrophobic interactions, but develops intermolecular cross-links during maturation. Kastelic illustrates that, for the case of rat tail tendon, microfibrils further associate to form subfibrils (100 to 200 Å diameter) and fibrils (500 to 5000 Å diameter) that are further grouped to form fascicles (50 to 300 μm diameter) (Figure 1). Viidik reports more generally that a fibril is an assembly of microfibrils for which the cross-striation is still evident, with diameters from 300 to 1500 Å. The fibrils are further packed together in parallel arrangements of fibers or fiber bundles, with diameters in the range of 1 to 12 μm. At this level they can be viewed using the light microscope. The unloaded fibers display a clear banding when viewed using polarized light microscopy.[17] The collagen has a visible longitudinal waveform referred to as the crimp pattern (Figure 2). The waveform represented in the collagen fiber crimp pattern has been debated. Some investigators believed the geometry was helical,[18] whereas others believed the fibers were planar sinusoidal or planar zig-zag.[19,20] From Figure 2, it is evident that there is variability in crimp period and amplitude with position within the tissue. The specimen in Figure 2 (rabbit Achilles tendon) appears to exhibit a planar waveform. The waveform disappears when the ligament or tendon is loaded in tension beyond the "toe region" of the stress-strain curve. The cause of the crimping is believed to be due to the shrinking of the surrounding matrix, transferring load to the fibers via collagen-interfibrillar interactions.[16,21] Because the distance between adjacent fibrils is too large to admit the possibility of cross-linking between fibrils, it is likely that the ground substance matrix and the associated proteoglycans bind the fibrils together.[16]

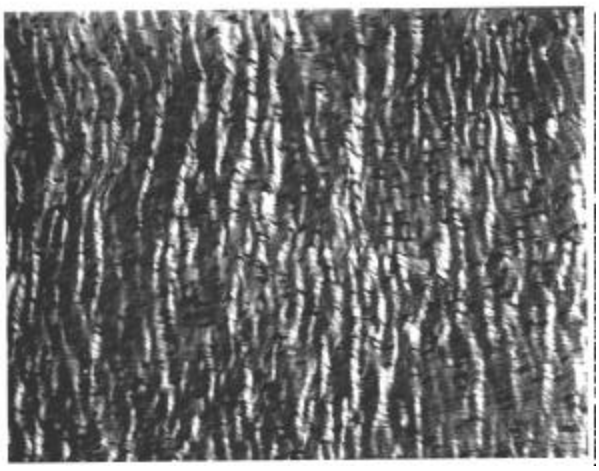

FIGURE2. Histological cross-section of a New Zealand White Rabbit achilles tendon showing the collagen crimp pattern.

The collagen of skeletal ligaments is a very stable biomolecule with unique material properties. The stability of collagen is due to its molecular coil configuration and its ability to form intramolecular and intermolecular crosslinks. Intramolecular cross-links occur between alpha-helix chains of the same tropocollagen molecule, whereas intermolecular cross-links join adjacent tropocollagen molecules with each other and with the ground substance matrix.[12] The cross-links are partially responsible for the high stiffness and tensile strength of collagen and its resistance to chemical and enzymatic attack.[22] Tissue maturation is accompanied by a reduction in the concentration of reducible cross-links.[23] Although collagen is quite stable, there is an ongoing balance between collagen synthesis and degradation in mature ligamentous tissue. Degradation of collagen occurs after the activation of specific collagenases. When activated, collagenases cleave the collagen triple helix leaving it susceptible to other proteases. The half-life of collagen has been estimated to be between 300 and 500 days.[24] The rate of collagen turnover can change drastically following injury or other stimuli.

2. Ground substance matrix

The connective tissue surrounding the collagen is referred to as the ground substance matrix. This tissue is partly responsible for holding the collagen together. The main constituent of the ground substance matrix is proteoglycan. Although these molecules constitute less than 1% of the ligament's total dry weight, they have a very important role in ligament function.[25] Ligament proteoglycans have a protein core and glycosaminoglycan side chains. Some proteoglycans are aggregated with hyaluronic acid to form hydrophilic molecules. These molecules associate with water to form the gel-like extracellular matrix. This interaction is responsible in part for the large amount of bound and unbound water in ligament: water typically comprises 60 to 70% of the total weight of normal ligaments (see for example Reference 26).

The interaction of water with the ground substance matrix and collagen is responsible for some of the time- and history-dependent viscoelastic behavior observed in ligaments. Movement of water within ligamentous tissue is inhibited by its entrapment between charged, proteoglycan molecules.[12] Exudation of water from ligamentous tissue has been shown to occur under cyclic loading.[26] In other collagenous soft tissues such as skin, the tissue retains most of its water even under high-pressure gradients.[27] Because of the large fraction of water in ligaments and tendons, many studies have made use of the incompressibility assumption in the development of constitutive equations. Recent work suggests that some volume change occurs during ligament deformation.[28,29] The actual change in volume that occurs during *in vivo* loading of ligaments is still a subject of debate. Further more, the mechanical and physiological significance of any such change in hydration and thus volume remains an open research area.

3. Elastin

The dry weight of most skeletal ligaments consists of less than 1% elastin.[30] The insoluble protein elastin takes on a complex coiled arrangement when unstressed. When elastin is stressed, the coiled arrangement stretches into a more ordered configuration.[31] The

behavior of elastin is responsible for a small part of a ligament's tensile resistance and its elastic recoverability.[32] Ligaments with a high elastin content have been shown to be less stiff and to undergo larger strains before failure when compared to ligaments with a lower elastin content.[33]

4. Insertion Sites

Ligament insertion sites transfer loads between components of the skeleton. They are designed to reduce the stress concentrations that naturally occur as forces are transferred across the ligament-bone interface. The junction between the soft tissue of ligaments and the hard tissue of bones is complex and can vary greatly from ligament to ligament as well as between the two ends of the same ligament. Ligament insertion sites have been broadly categorized into two categories, direct and indirect.

Direct insertion sites are generally well-defined areas with a sharp boundary between the bone and the attaching ligament occurring over a distance of less than 1 mm[13] (Figure 3). The collagen fibrils quickly pass out of normal ground substance matrix and continue through zones of fibrocartilage, mineralized fibrocartilage, and finally into bone.[34] Most of the fibrils at direct insertion sites are deep fibrils that meet the bone at approximately right angles. Examples of direct insertion sites include the femoral attachment of the medial collateral ligament (MCL) and anterior cruciate ligament (ACL) of the knee.

Indirect insertion sites attach to the bone over a broader area than direct insertion sites and have a more gradual transition between hard and soft tissue (Figure 4). The superficial fibers dominate at indirect sites and their attachment to bone occurs mainly through fibers blending with the periosteum. The deep fibers of indirect insertions have

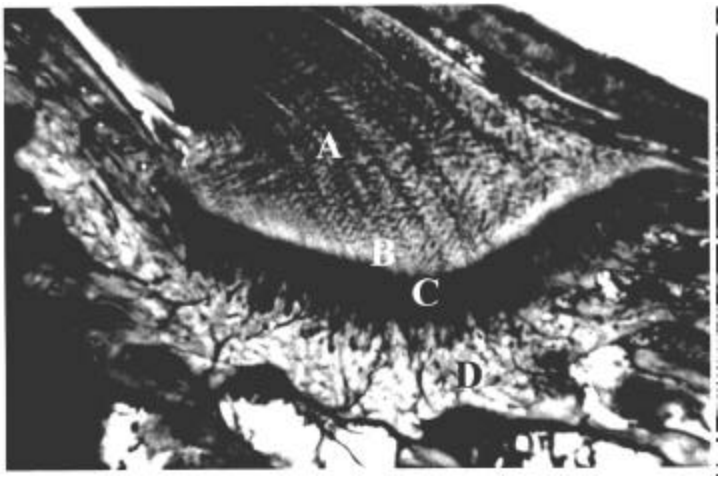

FIGURE3. Direct insertion site at the femoral insertion of a rabbit MCL. There are four distinct zones: ligament (A), uncalcified fibrocartilage (B), calcified fibrocartilage (C), and bone (D).

FIGURE4. Indirect insertion site at the tibial insertion of a rabbit MCL. The ligament fibers (A) insert obliquely into the bone (B).

been shown to attach directly to bone at acute angles without the fibrocartilagenous transitional zone observed in direct insertions.[35] Indirect insertions may be found at the tibial attachment of the MCL.

Despite the gradual change from soft to hard tissue, insertion sites are often the location of injuries. This is especially true when rapid remodeling of the insertion sites takes place during skeletal maturation or after joint immobilization.[36–39] Insertion sites have been shown to heal more slowly than ligament midsubstance tissue in response to injury or immobilization.[36,40] This may be due to the lack of a significant blood supply in the ligament substance near the insertion site. The different tissue microstructure found at insertion sites introduces inhomogeneous deformations throughout ligaments. Tissue strains near the insertion sites have been shown to differ from strains measured in the midsubstance of ligaments.[41,42]

B. Ligament Contribution to Joint Function

Joint kinematics are determined primarily by a combination of articulating bony geometry, ligament forces, and muscle and tendon forces. Ligaments contribute to maintaining proper joint kinematics by guiding normal motions and by providing a passive mechanical restraint to prevent abnormal motions. The anatomical geometry of ligaments and the location of their insertion sites have roles in dictating joint motion and stability. The majority of the load carried by ligaments is along the collagen fiber direction. As these loads are transferred to bones, the location of the insertion sites determines the orientation of the ligament-bone forces and thus greatly influences joint kinematics.

Although ligaments are generally considered to resist mainly uniaxial loads, they also experience shear and transverse loading *in vivo*. Complex loading patterns are especially common at the ligament insertions to bone.[43] In addition, ligaments wrap around bone surfaces in certain configurations and are subject to compressive contact stresses.[43–45] Weiss et al.[45] examined the contact between the MCL and the femur and between the MCL and tibia

during valgus rotation of the human knee joint by utilizing a three-dimensional finite element model. Loads as high as 700 N were transferred from the MCL to the tibia through contact under extreme valgus loading conditions. A two-dimensional FE model was created by Giori et al.[44] to study the stresses that develop as tendons wrap around bones. The study attempted to correlate the fibrocartilagenous tissue found in these regions to the mechanical state of stress. It was shown that the fibrocartilagenous areas correspond to areas with high levels of hydrostatic compressive stress. Matyas et al.[43] also predicted soft tissue compressive stresses near the insertion sites in a two-dimensional FE model of the rabbit MCL. These areas were correlated with regions of the ligament containing rounded, fibrocartilagenous cells rather than the elongated cells of ligament midsubstance.

When joints such as the knee are in neutral positions, the ligaments are still under some tension. This is usually referred to as *in situ* stress which is responsible for much of the joint stability in the absence of muscle and tendon forces. *In situ* strain has been measured experimentally in ligaments of the knee joint and has been shown to be nonuniform throughout individual ligaments and to vary depending on joint position.[46,47] Woo et al.[46] measured the *in situ* strain in anterior, middle, and posterior regions of the MCL in rabbits at three different flexion angles. For skeletally mature rabbits, it was shown that at 90 degrees of flexion the *in situ* strain was nearly uniform across the MCL width at 3.5%. A reduction in flexion angle caused an increase in loading of the posterior fibers and a decrease in anterior fiber loading. At increased flexion angles, the anterior portion of the MCL experienced an increase in *in situ* strain while the posterior region strain was reduced. Inclusion of *in situ* stress in computational models of joints is necessary to prevent an underestimation of the actual stress state in ligaments.

Ligament failures can occur through the tissue substance, by bony avulsion, or at insertion sites. Failure mechanism has been shown to be a function of age and activity level.[48,49] Substance failures are the most common failure mechanism in adults and are characterized by catastrophic rupture of collagen fibers. The ruptured fibers are often described as having a "mop-end" appearance. Avulsion and insertion site failures are less common. Bony avulsion failure occur in the cancellous bone located deep to the insertion sites. Bone fragments can be found on ligament ends that fail by bony avulsion. Insertion site failures can be distinguished from bony avulsions by the lack of bone present on the failed ligament end.

The knee has been the subject of a great number of both experimental and computational studies due to its high incidence of debilitating injuries. The knee is a six-degree-of-freedom joint, with three translational and three rotational degrees of freedom commonly described using the convention established by Grood and Suntay.[49] The four major ligaments of the knee are the ACL, posterior cruciate ligament (PCL), lateral collateral ligament (LCL), and MCL (Figure 5). These ligaments are made up of several discrete bands that are taut in different positions of the knee's range of motion in normal, stable joints.[50]

The specific functions of individual knee ligaments have been determined experimentally through the successive sectioning of ligaments in cadaveric knees. Primary and secondary roles of ligaments were determined by altering the order of ligament sectioning. The ACL has been shown to act as a primary restraint against anterior tibial displacements[51–53] and as a secondary restraint to tibial axial rotation.[52,54–56] The ACL also provides a minor secondary restraint to varus-valgus rotation at full extension.[52] The PCL provides the primary resistance to posterior tibial displacement[52,57–60] and also acts as a major secondary restraint to external tibial axial rotation[52,58,59] and a minor secondary

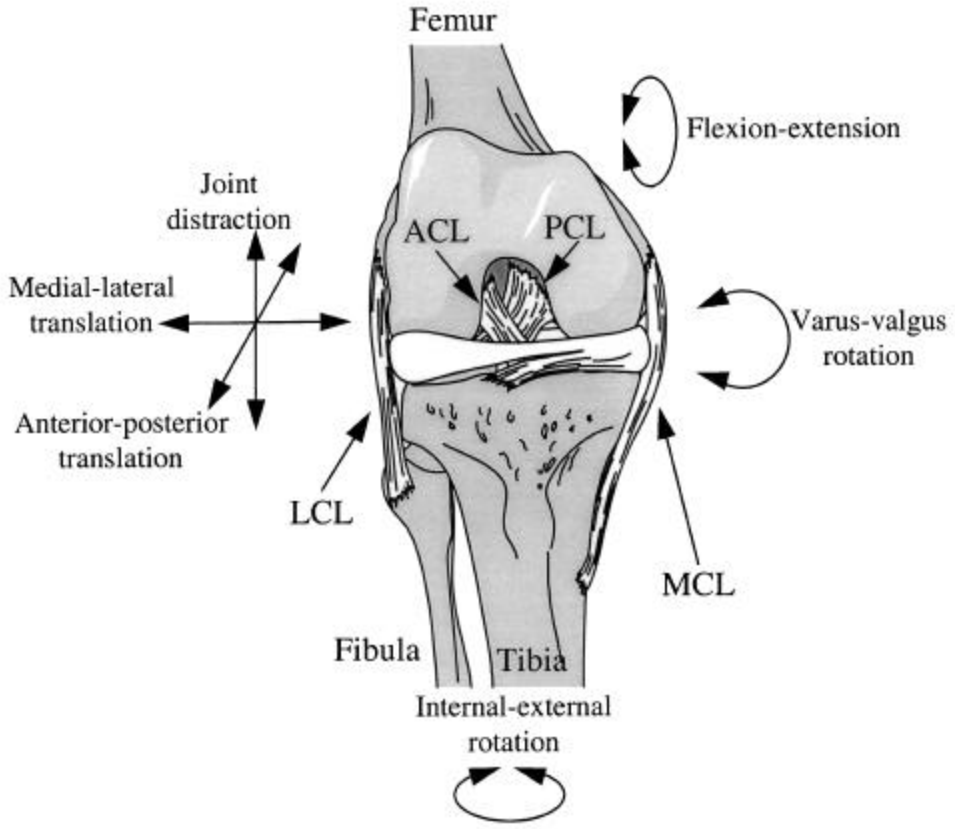

FIGURE5. Anterior view of the knee joint. The femur, tibia, and fibula are connected by the anterior cruciate ligament (ACL), posterior cruciate ligament (PCL), medial collateral ligament (MCL), and lateral collateral ligament (LCL). The clinical rotations and translations of Grood and Suntay are defined (Grood and Suntay, 1983).

restraint to varus rotations.[58,59] For most ligament cutting studies, the MCL has been divided into the superficial MCL and the deep MCL. The superficial MCL has been shown to be the primary structure resisting valgus rotations of the knee.[52,55,61,62] Both the superficial and deep MCL also act as primary restraints to internal tibial rotation[52,55,62,63] and secondary restraints to anterior tibial displacement.[52,56] The LCL provides a primary restraint to varus rotation[52,53,58,59,61] and external tibial rotation[52,58,59] and a secondary restraint to anterior and posterior tibial displacement.[52,53,58,59,61]

C. Material Testing of Ligaments

To properly discuss the material properties of ligaments, it is essential to consider aspects of the experimental testing protocols that have been used to measure these properties. In experimental studies of ligaments, it is important to distinguish between structural proper-

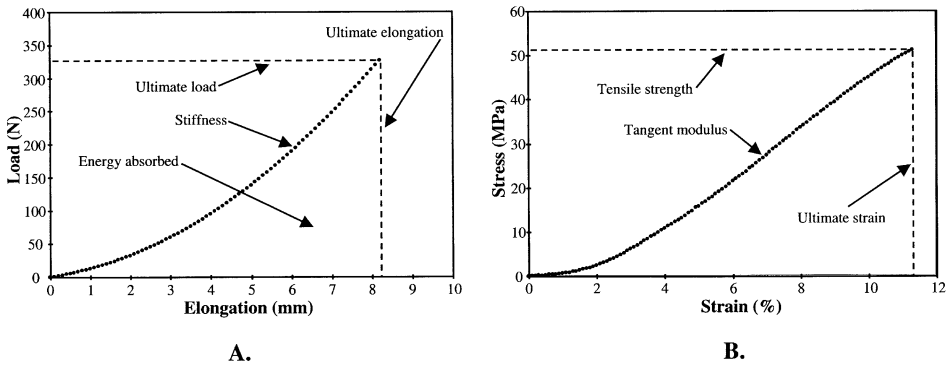

FIGURE6. Load-elongation and stress-strain curves for a bone-ligament-bone complex under uniaxial tension. (A) Structural properties represented in a load-elongation curve, (B) Material properties represented in a stress-strain curve.

ties and material properties. Structural properties are derived from tests of entire bone-ligament-bone structures, whereas material properties are derived from tests of isolated ligament tissue[64] or from a bone-ligament-bone complex.[42] Material properties must be determined from a test that provides a region in the center of the ligamentous tissue that is under a state of homogenous uniaxial strain. Structural properties are typically represented by a load-elongation curve (Figure 6a). From this curve, properties such as ultimate load, ultimate elongation, stiffness, and energy absorbed at failure can be determined. The ultimate load and elongation are determined at the point of failure of the bone-ligament-bone complex and the stiffness is the slope of the linear portion of the curve. The energy absorbed to failure is equal to the area under the load-elongation curve up to failure. Failure may occur in the ligament midsubstance or at the insertion sites. Structural properties depend on the material properties of the ligamentous tissue and also on the geometry of the bone-ligament-bone structure and the material properties of the insertion sites. Material properties of ligaments describe the material behavior irrespective of ligament geometry and do not include information about the strength of the insertion sites. The stress-strain relationship for ligament material can be determined by combining load-elongation data with the initial cross-sectional area of the ligament and strain measurements from the ligament substance. Material properties such as tensile strength, ultimate strain, and tangent modulus can be obtained from the stress-strain curve (Figure 6b). Stress is determined by dividing the applied load by the initial cross-sectional area of the tissue, whereas strain can be approximated by dividing the change in gage length by initial gage length. The tangent modulus is the slope of the linear portion of the stress-strain curve. However, if the test complex does not fail within the substance of the ligament, the tensile strength and ultimate strain of the material were not achieved and thus cannot be reported.

Testing considerations can drastically affect the material properties of ligaments. It is important to decide what information is desired and what test would be appropriate to yield that information. Depending on the specific goals, a variety of tests may be performed such as uniaxial tension,[64] strip biaxial tension,[65] and shear.[66,67] These test configurations can be used to perform testing at a fixed strain rate, to assess the effects of cyclic loading,[68] or to

AU: No callout for Figure 7 (should be somewhere between pp. 24–29)

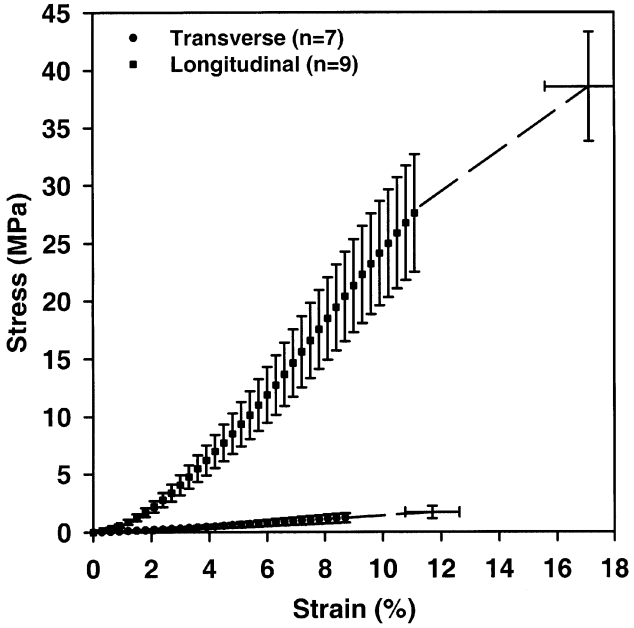

FIGURE7. Stress-strain curves for human MCL tested parallel and transverse to the collagen fiber direction. The final point in each curve was the average failure point for the specimens. The error bars indicate the standard error for the average ultimate strain and tensile stress. The tangent modulus of the longitudinal curve was over an order of magnitude greater than the tangent modulus of the transverse curve. (Reprinted with permission from Quapp and Weiss, 1998.)

investigate viscoelastic behavior under creep or stress relaxation conditions.[69,70] Uniaxial tensile tests are commonly used to characterize ligament behavior and are performed on specimens with high length-to-width ratios. These tests provide data on the one-dimensional, tensile behavior of ligaments. Strip biaxial tests are performed on samples with low length-to-width ratios to minimize the tissue's lateral stretch. This test can provide additional two-dimensional information on the material behavior. The strip biaxial test is similar to a (more general) biaxial test configuration, but the objective is to maintain the stretch ratio in the lateral direction at a value of 1.0. This will in general produce a "stiffer" stress-strain curve than a uniaxial configuration since the tissue is prevented from contracting in the lateral direction. Simple shear tests provide an additional means to learn about the multiaxial behavior of ligaments.[66] Depending on the orientation of the collagen fibers with respect to the shear deformation, the relative contributions of the fibers and the ground substance matrix to the material response may be determined. Unconfined or confined compression tests may be utilized to further characterize the behavior of ligaments.[29] Compressibility is an important quantity that dictates how a constitutive model may be formulated. Creep and stress relaxation tests are often used to gain insight into the viscoelastic properties of ligaments. Creep tests are performed by subjecting a tissue to a constant stress level and observing the change in strain. For stress relaxation testing, a constant strain is held and the reduction in stress over

time is measured. Cyclic tests may also be used to determine the viscoelastic behavior of ligaments. By noting the changes in peak stress (creep testing) or peak strain (stress relaxation) with each cycle, viscoelastic material coefficients may be estimated. Insights into the elastic and viscoelastic behavior of ligaments may also be yielded through experiments that quantify tissue permeability.[71] The role of fluid flow in the mechanics of ligaments may be assessed through such experiments.

Tensile testing of isolated ligamentous tissue introduces numerous experimental difficulties. Most of these difficulties are related to the poor interface between ligamentous soft tissue and the rigid clamps of a material testing machine. It is common for ligaments to slip from these clamps during testing or to fail at the stress concentration that is induced as soft tissue is compressed between the rigid clamps. Some investigators have used liquid nitrogen or dry ice to freeze the tissue grasped by the clamps.[72–75] This provides a local hardening of the tissue at the clamped area of the specimen, preventing slippage or failure. One must be careful to ensure that the temperature in the gage length is not changed appreciably to avoid alterations in material properties. Additionally, isolated ligaments often have poor aspect ratios and irregular geometries that induce nonuniformities in the stresses and strains during testing. To achieve uniform loading conditions, samples with appropriate length-to-width ratios are often cut from intact ligaments. Dog-bone shaped samples reduce cross-sectional area in the specimen midsubstance to ensure that failure will occur within the gage length and not at the clamped ends.[64,76] For tests of bone-ligament-bone complexes, special fixtures are often used to ensure a strong grip on the bones and to position the bones so that the tensile load is applied along the longitudinal axis of the ligament.[42]

The measurement techniques that are used during material testing of ligaments deserve special attention. The calculation of stress in ligaments under uniaxial tension requires accurate measurement of the tissue cross-sectional area and the applied load. The measurement of load is relatively straightforward and is usually accomplished using a load cell positioned in series with the clamping system. Measurement of cross-sectional area can be quite difficult since the ligament cross-section is rarely uniform and can vary considerably along the length of the ligament.[77] Calipers have been used extensively but require the assumption of a regular cross-sectional shape (rectangular,[64] circular, or ellipsoid[78]). Calipers may also introduce errors by deforming the tissue.[77] Despite the disadvantages, calipers are often used because of their ease of use and their sufficient level of accuracy for many applications. Area micrometers have also been used to measure cross-sectional area. These devices compress the specimen into a well-defined cross-sectional shape via a prescribed transverse pressure. This method underestimates the actual cross-sectional area due to tissue deformation as pressure is applied by the micrometer.[79] However, it does provide a repeatable measurement method. In recent years, noncontact methods such as laser micrometers have been developed for measuring the cross-sectional shape and area of ligaments.[77,80] The accuracy of these methods is not limited by measurement-induced deformations or assumptions about cross-sectional shape. Some disadvantages of these techniques are the longer time required to perform measurements and the inability to measure surface concavities for some techniques.

Numerous techniques have been used to measure strain in soft tissues such as ligaments. Historically, many investigators used the crosshead displacement of the material testing machine and specimen initial length to derive ligament strain. Large errors can be introduced due to slack in the system, specimen slippage in the clamps, clamp compliance,

or inhomogeneities in the ligament strain field. This has been shown to be an extremely inaccurate method for measuring local ligament surface strains, especially when bone-ligament-bone complexes are used for tensile testing.[81] Other investigators have attached pins to the ligament insertion sites and measured the distance between the pins using calipers at different joint orientations as an indicator of ligament length.[62,82] A similar technique has been used by Hollis et al.[83] to measure elongation in different bundles of the ACL. An instrumented spatial linkage (ISL) was used to digitize the coordinates of the ligament insertion sites in different joint positions. Both of these techniques assume a homogeneous strain field between the insertion sites, which is rarely attained. Roentgenographic techniques have also been used to measure the length of ligaments *in vivo*. The accuracy of this method also relies on homogeneous strain fields between the insertion sites. More recently, investigators have used liquid metal strain gages[85–89] or Hall effect strain transducers (HEST)[90–93] for localized measurement of ligament strain. These devices attach directly to the tissue substance and measure displacement between attachment points. This provides a one-dimensional measurement that also assumes homogeneous strain between attachment locations. Liquid metal strain gages and HESTs are considered to be more accurate than some of the earlier techniques of strain measurement, but they still have some associated problems. The devices require suturing or barbs for attachment to the ligament substance which may alter *in situ* strains. In spite of the small size of these devices, they are still large enough that they may impinge on surrounding tissues during joint motion, altering normal ligament deformation.

Noncontact, optical techniques have been used by many investigators for strain measurement in biological soft tissues. The video dimension analyzer (VDA) was originally described by Yin et al.[94] based on the earlier work of Gardner and Warner[95] and has been used in the biomechanics field for measurement of deformations in skin,[96] blood vessels,[97] and articular cartilage.[98] Woo et al.[42,99] pioneered the use of the VDA for the measurement of ligament strain. The VDA utilizes a video image of the test specimen to determine strain. Prior to testing, two or more reference lines are drawn on the ligament surface perpendicular to the loading axis. The reference lines define a gage length for strain measurement. The VDA system automatically tracks the distance between the reference lines during testing and converts this distance into a voltage. The voltage can be calibrated to represent percentage strain of the tissue. The VDA can be used to measure strain in real-time; however, a test is typically recorded on videotape for later analysis. A disadvantage of the VDA system is that it performs only a one-dimensional measurement across the video image. Even in simple uniaxial tests, the reference lines will often experience some shearing motion that cannot be quantified by the one-dimensional VDA measurement.

A similar video-based method has been used for measurement of ligament and other soft tissue strain.[100–103] This technique also utilizes a video recording of testing, but the images are analyzed with a motion analysis system or other custom software. With this method, small contrast markers are stained or glued on the ligament surface and then videotaped during mechanical testing. The video system is calibrated by filming an object of known dimensions. This allows the two-dimensional location of the markers to be tracked and the surface strain calculated between marker pairs. In addition to providing a two-dimensional measure of ligament strain, this method also has a greater potential for attaching multiple markers to a ligament's surface and quantifying strain inhomogeneities. The recent availability of systems that are not limited by the conventions of NTSC-based video has improved the utility of strain and motion measurement systems. These new systems

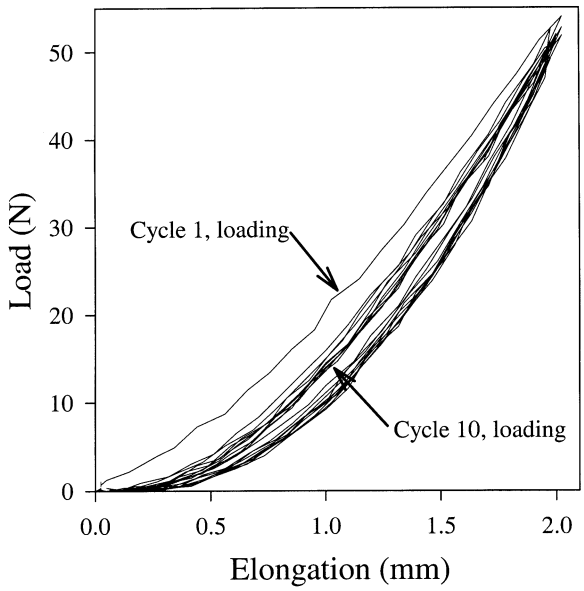

FIGURE8. Cyclic load-elongation behavior of human fascia lata tested along the collagen fiber direction. The hysteresis decreases with increasing cycle number, and the loading-unloading curves become repeatable. (Reproduced with permission from Weiss et al., 1996.)

typically provide accuracy and resolution that are 1 to 2 orders of magnitude better than video-based systems. Several systems perform the image processing necessary to track markers on the camera.

The use of video techniques with motion analysis software has been extended to three-dimensional strain measurements.[47,104–106] Most motion analysis systems utilize a Direct Linear Transformation (DLT) to obtain three-dimensional coordinate data from multiple two-dimensional views.[107] By digitizing a calibration object with known coordinates, the DLT method provides a direct linear relationship between the digitized points from multiple two-dimensional camera views and their three-dimensional space coordinates. Our laboratory[47,104] has measured the three-dimensional strain distribution across the surface of the human MCL by attaching multiple rows of markers to the ligament surface along the collagen fiber direction. Two video cameras were used to determine the three-dimensional coordinates of the markers and record their positions during varus-valgus cycling. This allowed calculation of strain in different regions of the MCL.

Video techniques provide numerous benefits over other strain measurement methods. Video methods are less invasive than other techniques and they can provide a three-dimensional strain measurement at multiple locations on a single ligament. An experimental study by To et al.[108] simultaneously measured the two-dimensional strains on opposite surfaces of ligaments during uniaxial tensile tests. The strain magnitudes were found to be nearly equal, which suggests that measured surface strains correspond well with the strain state located deeper within the ligament substance. Despite the benefits of video strain

measurement, these techniques have certain inherent limitations. For two-dimensional measurements, rigid body motions such as rotations will cause the markers to move out of the measurement plane and will introduce significant errors in the measured strains.[100,109] Further inaccuracies may be caused by radial distortion induced by the camera lens. Also, the effects of tissue stain and adhesive markers on the local material properties have not been assessed.[110] The alcohol content of Verhoff's stain may cause tissue dehydration, and adhesive markers may locally harden soft tissue. A final drawback of video systems is the long analysis time needed for calibration and digitization of the video images. Recent improvements in motion analysis systems minimize those problems.

Recent efforts have been made to measure ligament strain using photoelastic methods.[111–113] The entire surface of a ligament is coated with a thin layer of polyurethane possessing optically high fringe sensitivity. During deformation, fringe patterns are generated on the ligament surface when viewed with polarized light that may be recorded with a video system and analyzed to estimate local strain values. Advantages of this system include an improved potential for measuring strain inhomogeneities over an entire surface. Unfortunately, it may be extremely difficult to find a photoelastic coating material that binds sufficiently well to the ligament without altering the tissue properties. Also, despite of the relative differences in strain that are visible through fringe patterns, quantifying these with actual strain values can be challenging. In addition, it is not currently possible to quantify initial strain with this technique.

Forces in ligaments have been directly measured by attaching devices such as buckle transducers[114–118] or implantable force transducers[119,120] to ligament tissue and also by strain gage attachment to bone near ligament insertion sites.[121] These devices have yielded significant information about the forces in ligaments, but they all require the invasive attachment of mechanical devices. This may limit the accuracy by altering the normal ligament deformation. Markolf et al.[122] have developed a technique for mechanically isolating a bone plug containing a ligament's insertion site with a coring cutter. A load cell was used to hold the bone plug and directly measure the resultant ligament forces as the knee was loaded. This technique has been used to measure forces in the ACL and PCL of cadaveric human knees.[123,124] Fujie et al.[125] developed a new method to determine the magnitude and direction of ligament forces utilizing a six-degree-of-freedom force-moment sensing robot. The robot was used to simultaneously measure the six-degree-of-freedom motion and externally applied forces and moments during kinematic testing of joints. Individual ligaments were cut and the robot was utilized to recreate the kinematics measured prior to ligament transection. Utilizing the principle of superposition, the change in the measured forces and moments was used to indicate the magnitude and direction of force present in the individual ligaments.

Measurement of *in situ* stress and strain poses extreme experimental difficulties. Many investigators have been forced to measure changes in ligament stress and strain from unknown reference configuration because of the inability to determine a unique zero-stress reference length. Optical and video-based measurement techniques have been used to determine a reference state of zero stress and thus provide a measurement of *in situ* strain.[46,47] Markers were filmed with the joint in a neutral position and then the ligament was cut from its insertion sites allowing the ligament to assume its stress-free configuration. From the new coordinates of the markers, it was possible to determine *in situ* strain distribution. If the ligament material properties are also known, the *in situ* stress can be determined from the *in situ* strain. Howe et al.[126] utilized a HEST to determine the stress-

Table 1. *Material Properties of Human and Animal Ligaments and Tendons (Mean ± SEM)*

Specimen type	Tangent modulus (MPa)	Tensile strength (MPa)	Ultimate strain (%)
Human MCL[64]	332.2 ± 58.3	38.6 ± 4.8	17.1 ± 1.5
Rabbit MCL[139]	740 ± 90	77.7 ± 1.9	12.9 ± 1.2
Human PCL, anterolateral bundle[280,*]	248 ± 119	35.9 ± 15.2	18.0 ± 5.3
Rabbit ACL[142]	516 ± 64	62.3 ± 5.2	12.5 ± 1.5
Human ACL, LCL, PCL[141,*]	345.0 ± 22.4	36.4 ± 2.5	15.0 ± 0.8
Human patellar tendon[141,*]	643.1 ± 53.0	68.5 ± 6.0	13.5 ± 0.7
Goat patellar tendon[143,**]	1639.1 ± 435.9	126.8 ± 20.8	15.2 ± 3.9

Note: Tests were performed using noncontact strain measurement techniques that isolated the ligament/tendon substance except those marked by "*". The reference marked by "**" utilized an area micrometer technique that has been shown to underestimate cross-sectional area. Thus the values for tangent modulus and tensile strength from this study are likely to be overestimated.

free length of the anteromedial band (AMB) of the human ACL. The knee was subjected to anterior-posterior shear loads, and the applied load was plotted against the HEST displacement. The resultant curve demonstrated a lax region during the transition from posterior to anterior-directed tibial shear loading. There was an inflection point in the lax region that was found to correspond with the slack-taut transition for the AMB. The accuracy of the "inflection point" method for determining a zero strain reference for ligaments has been assessed using an arthroscopic force probe.[127] An advantage of the inflection point method is that destructive sectioning of the ligament is not required. However, this technique will not work for ligaments that cannot be completely unloaded *in vivo*.

To study the viscoelastic properties of ligaments, special test protocols must be utilized. The strain rate used for tensile test experiments has been shown to affect the measured ligament material properties. Although the stress-strain behavior of ligaments is relatively insensitive to strain rate over several decades of variation,[128] high rate loading will produce a stiffening response.[129,130] After repeated loading cycles, ligaments reach a "preconditioned" state and there is a minimal amount of hysteresis as loading and unloading cycles become nearly repeatable (Figure 8). Preconditioning soft tissue also minimizes the observed relaxation and creep and the peak stress during cyclic loading will no longer decrease with subsequent cycling. This provides a consistent starting point for subsequent material tests.

Changes in experimentally determined material properties can be introduced by the environment in which the testing is performed. It is extremely important for ligaments to remain hydrated for determination of accurate material properties. This can be achieved by testing in a saline bath, by keeping the ligament covered in saline soaked gauze, or with regular sprays of saline mist. A decrease in ligament hydration has been shown to cause a decrease in tissue stiffness and strength.[131] Increased hydration has also been shown to

cause a larger relaxation in stress relaxation tests.[132,133] Temperature also affects material properties, but not as strongly as hydration. Increases in temperature are accompanied by a decrease in tissue stiffness.[134] Many investigators perform ligament material testing in heated saline baths. This allows simultaneous control of both hydration and temperature.

The storage history of the test specimen may also affect ligament material properties. Several studies have compared the properties of fresh ligaments with those that have been frozen and stored.[135–137] There have been slightly conflicting results from these studies, but most have reported no significant changes in the structural or material properties of ligaments. Woo et al.[137] reported a significant decrease in the area of hysteresis during the first few loading cycles of previously frozen rabbit MCLs but did not observe any other changes in the structural or material properties.

The effects of skeletal maturity and aging on the properties of ligaments and their insertions have been extensively studied.[46,130,135,138,139] Woo et al.[130] showed that MCLs from immature rabbits almost always failed by avulsion from the periosteum at the tibial insertion site, whereas mature rabbit MCLs usually experienced midsubstance failures. This change in failure mode corresponded to an increase in ligament structural properties from puberty to adulthood. The effect was attributed to mineralization of the matrix surrounding collagen at the tibial insertion site. Histological evaluation showed that the extent of mineralization increased toward skeletal maturation, as defined by closure of the epiphyses. Changes in material properties have also been observed in specimens with aging and the onset of senescence.[135,139] Noyes and Grood[135] reported that the ACLs of younger donors possessed structural properties two to three times greater than specimens from younger donors. In addition, most of the young ligaments failed in the midsubstance, whereas the ligaments from older donors failed by bony avulsion. Woo et al.[139] reported only a slight decrease in rabbit MCL structural properties and no change in failure mode in comparisons between skeletally mature (1 to 3 year old) and senescent (four-year-old) animals. There was a difference in the rate of skeletal maturation between male and female animals as measured by the ultimate load of the femur-MCL-tibia complex (FMTC). The ultimate load of male FMTCs reached a plateau at 6 months of age, whereas the female FMTCs did not plateau until 12 months of age. The modes of failure correlated well with closure of the epiphyses in both sexes (i.e., tibial avulsion failure for the skeletally immature groups and midsubstance for the skeletally mature groups). Clearly the age and sex of specimens must be considered when assigning structural and/or material properties for a model of ligament mechanics, or when attempting to predict failure locations.

D. Material Properties of Ligaments

The previously described testing techniques have been used to characterize the material behavior of ligaments. The stress-strain curve resulting from a tensile test of isolated ligamentous tissue or a bone-ligament-bone complex reflects the material behavior of the constituent materials (Figure 6b). Tensile tests have nearly always been performed along the collagen fiber direction as this is the predominant loading axis *in vivo*. The stress-strain relationship of ligaments tested along the collagen fiber direction is nonlinear. With initial lengthening of ligament tissue, the curve is upwardly concave as the collagen crimp pattern is straightened.[140] This portion of the stress-strain curve is known as the "toe" region and is often described as having the shape of an exponential or polynomial relationship. The toe region typically extends to a strain of 2 to 3%, although there can be considerable inter-

Table 2. *Effects of strain rate on the material properties of rabbit MCL(Mean ± SEM)*

Strain rate (mm/s)	Tangent modulus (MPa)	Tensile strength (MPa)	Ultimate strain (%)
0.008	700 ± 70	75.2 ± 2.4	9.5 ± 0.5
0.1	840 ± 150	81.4 ± 7.4	10.0 ± 0.5
1.0	800 ± 60	85.7 ± 7.7	11.0 ± 0.5
10.0	910 ± 50	87.2 ± 6.0	11.5 ± 1.0
113.0	760 ± 160	106.7 ± 6.8	13.0 ± 1.0

Note: Data indicate that large variations in strain rate have relatively small effects on ligament material properties. From Woo et al.[130]

specimen variability. At the end of the toe region, there is a gradual transition into the linear region of the stress-strain curve as the collagen is straightened. This portion of the curve is dominated by the material behavior of the straightened collagen. The uniaxial stress-strain curve remains essentially linear until failure.[13,30] The peak stress value is the tensile strength and the corresponding strain is the ultimate strain. Continued straining beyond this point results in catastrophic failure of collagen fibers.

Although much of the published research on ligament mechanics only includes structural properties, the material properties of many different human and animal ligaments have been determined (Table 1). The tangent modulus for ligamentous tissue ranges from 250 to over 1600 MPa, whereas the tensile strength ranges between 35 and 125 MPa. Ultimate strain has been reported to be between 12 and 18%. Some of the variation in material properties of Table 1 can be attributed to differences in experimental methods. Butler et al.[141] used clamp-to-clamp measurements to determine ligament strains whereas Quapp et al.,[64] Woo et al.,[139,142] and Gibbons et al.[143] used noncontact video methods. There were also differences in strain rate, specimen age, specimen type, and other testing conditions between the studies. In spite of the large differences in testing procedures, specimen type, and species, the experimentally measured material properties reported in Table 1 are remarkably similar. This can be attributed to the collagen reinforced structure of ligaments that remains quite similar between different ligaments and even between different species.

The ultimate strain for human and animal knee ligaments is between 12% and 18% (Table 1) and even under physiological conditions, strain levels as high as 5 to 8% are normal. Traditional linear elasticity theory assumes that the magnitude of both strains and rotations are "small". Because rotations are not present in a uniaxial tensile test and infinitesimal uniaxial strain can be readily converted (i.e., to Green-Lagrange strain for this simple deformation), it is permissible to use infinitesimal strain to represent the results of a tensile test. One should always keep in mind the numerical difference between the magnitude of the infinitesimal strain and Green-Lagrange strain.[144] For a uniaxial tensile test of a specimen experiencing a stretch λ, the infinitesimal strain is calculated as

$$\varepsilon_{11} = \lambda - 1 \tag{17}$$

The Green-Lagrange strain is calculated as

$$E_{11} = \frac{1}{2}(\lambda^2 - 1) \tag{18}$$

As an example, the infinitesimal strain underestimates the Green-Lagrange strain by more than 1% strain (7% error) for a 15% uniaxial extension. Although this approach can be used to describe uniaxial tensile data, it cannot be used to formulate two- or three-dimensional constitutive models for ligaments and tendons because of the presence of large rotations under *in vivo* deformation. As shown in Equation 5, the large strains and rotations experienced by ligaments *in vivo* require the use of finite deformation theory. A similar argument can be made regarding the stress.[144] Normally, "engineering stress", σ, is reported for uniaxial tensile tests of ligaments and tendons. This is calculated using the initial cross-sectional area A_0:

$$\sigma = \frac{F}{A_0} \tag{19}$$

For a uniaxial tensile test, the Cauchy stress $\boldsymbol{T}$ (typically used in the equations of motion) is defined as

$$T = \frac{F}{A} \tag{20}$$

where A represents the current cross-sectional area. Direct measurement of the current cross-sectional area complicates the tensile test experiment considerably. Constitutive assumptions such as incompressiblity can eliminate the need to measure A. For a detailed discussion of the differences between the stress and strain measures, the reader is referred to Fung,[128] section 7.10.

Ligaments are highly anisotropic because of their fibrous structure. Collagen provides the primary resistance to tensile loading but offers negligible resistance to compression. Ligaments also offer little resistance to bending, as illustrated by the fact that they will fold under their own weight when held vertically from the bottom. Quapp and Weiss[64] performed tensile tests on samples from human MCLs harvested both parallel and transverse to the collagen fiber direction. These data showed that the tensile strength, ultimate strain, and tangent modulus were significantly higher for tests oriented along the collagen direction. In addition, the toe region was absent from the stress-strain curves of transverse specimens (Figure 7). Chuong et al.[76] studied the anisotropy of the canine diaphragmatic central tendon. Tensile tests were performed on samples oriented parallel and transverse to the predominant fiber direction. The results showed significantly higher tangent modulus and tensile strength for the samples oriented parallel to the fiber direction. The ultimate strains were not significantly different between the two groups.

Ligaments have time- and history-dependent viscoelastic properties that arise from the interaction of water with the ground substance matrix and the inherent viscoelasticity of the solid phase. There have been numerous experimental investigations of the viscoelastic nature of ligaments.[70,130,132,145–149] The loading and unloading curves of ligaments under tension do not follow the same path. A hysteresis loop is typically observed during tensile testing due to internal energy losses (Figure 8). Creep, an increase in deformation over time under a constant load, and stress relaxation, a reduction in stress over time under a constant deformation can both be observed in ligaments.[70] The effects of conditions such as temperature[146] and hydration level[132] on the iscoelastic behavior of ligaments has also been investigated. The variation of ligament stress-strain behavior with strain rate is another indicator of the viscoelastic nature of the tissue. Woo et al.[130] compared the material properties of rabbit MCLs tested at five different strain rates (Table 2). Although some strain rate dependency can be seen, results showed thatchanges in strain rate of over four orders of magnitude had relatively small effects on ligament material properties. Tensile strength and ultimate strain increased slightly with increasing strain rate, whereas tangent modulus remained essentially unchanged.

Although often assumed to be incompressible due to their high water content, experimental evidence suggests ligaments undergo some volume change during deformations.[28,29] This volume change may occur due to fluid exudation[26] or as a result of inherent compressibility of the solid phase. Because of the limited availability of experimental data describing interstitial fluid flow in ligaments and tendons, FE models have been used to gain a better understanding of the flow behavior.[150,151] Chen et al.[151] created a microstructural model to study interstitial flow parallel and transverse to the collagen fibril direction based on previously measured values for fibril diameter and water content. Results indicated that ligaments are likely much more permeable to flow in the longitudinal direction than in the transverse direction. Experimental data suggests that permeability transverse to the collagen fiber direction in ligaments is approximately an order of magnitude less than the permeability of cartilage.[71]

Material inhomogeneities are present within individual ligaments. Butler et al.[152] compared the material properties between different bundles of the human ACL. The anteromedial bundle and anterolateral bundles were found to have significantly higher modulus, ultimate stress, and strain energy density than the posterior bundle. The ultimate strain was not significantly different between the three bundles. Differences in the biochemical composition of ligaments has been studied in an effort to explain the observed material property inhomogeneities.[153,154] Frank et al.[153] studied the normal rabbit MCL and found different levels of water content, glycosaminoglycan content and collagen concentration along the length of the ligament. Mommersteeg et al.[154] showed that collagen density is nonuniformly distributed throughout human knee ligaments. The variations in collagen density measured by Mommersteeg et al.[154] appeared to correspond with variations in modulus found throughout the ACL and PCL in separate studies by Butler et al.[152,155] Material inhomogeneities are believed to be especially common near the insertion sites,[153] although this has not been well quantified experimentally due to the difficulties in performing mechanical measurements in such a small region of tissue. This is an area where further research is greatly needed.

IV. MATERIAL MODELS for LIGAMENTS

Numerous material models have been developed to represent biological soft tissues such as ligaments. These models have helped to further the understanding of the contribution of different tissue components to the material behavior of the overall tissue for both the normal tissues and for tissues affected by injury, healing, immobilization, exercise, and other conditions that alter the homeostatic state of the tissue. Material models may also be used to predict responses from independent experimental tests. In addition, material models provide a framework for representing the properties of tissue in a FE or analytical context. The construction of accurate constitutive models is difficult because ligaments are nonlinear, anisotropic, inhomogeneous, viscoelastic, and undergo large deformations. In this section, an overview of the development of ligament material models is presented. Models for other biological soft tissues such as tendon, skin, and heart muscle are also briefly reviewed. Although these tissues differ in structure and function from ligaments, their overall mechanical behavior is governed by the mechanical behavior of collagen. The discussed models are divided into elastic and viscoelastic groups. Recent efforts in the development of poroelastic and homogenization models are also reviewed.

A. Microstructural Versus Phenomenological Models

Ligament material models can be categorized roughly as either microstructural or phenomenological depending on their basis of formulation. Microstructural models are based on explicit representation of the different components of the tissue microstructure. The responses of the individual constituents of a tissue are combined to determine an overall description of its material behavior. These models are useful in explaining the relationship between tissue microstructure and mechanical properties. The continuum response of many microstructural models is based on an assumed structural configuration of mechanical response of the collagen fibrils. Phenomenological models describe the material behavior but do not necessarily have an explicit relationship to the components or structure of the tissue. The material coefficients obtained from phenomenological models generally do not have a direct physical interpretation.

B. Elastic Models

As described earlier, the material behavior of ligaments is relatively insensitive to strain rate over several decades of variation. In addition, these tissues reach a “preconditioned” state after repeated loadings and there is a minimal amount of hysteresis. This has prompted many investigators to neglect the time- and rate-dependent components of tissue behavior and concentrate on modeling the nonlinear elastic response. Most models have been one-dimensional or have assumed that the three-dimensional behavior is isotropic.

There are two general approaches that have been used in forming microstructural models of ligaments. Both of these have described the uniaxial response of ligaments by explaining the toe region based on collagen structure. One general approach used numerous elastic elements that were sequentially recruited causing nonlinear, elastic behavior.

The second approach has been to describe toe region behavior by directly modeling collagen fiber geometry.

A simplified explanation for the upwardly concave stress-strain behavior of ligaments was proposed by Viidik[156] and subsequently presented in more detail by Frisen et al.[157] The elastic response of ligaments was represented by numerous individual linearly elastic components, each of which represented a collagen fibril of different initial length in its unloaded and crimped form. As the ligament was loaded, additional fibrils were recruited yielding the nonlinear behavior characteristic of the toe region. At higher loads, all the fibrils were loaded and the ligament stress-strain curve became linear. This approach provides a compact description of the uniaxial response of ligaments.

Other proposed microstructural models have utilized an approach similar to that of Viidik[156] and Frisen et al.[157] Kastelic et al.[158] developed a structural representation for tendons referred to as the sequential straightening and loading model. It was assumed that crimped fibrils had negligible resistance to extension and that tensile resistance arose only from the elasticity of previously straightened fibrils. Crimp angles varied among morphologically based values throughout the width of the tendon, which caused a gradual recruitment of fibrils. This was in contrast to previous structural models in which crimp configuration was constant throughout the tissue.[18,19,159] Decraemer et al.[160] proposed a similar model consisting of a large number of purely elastic fibers embedded in a gelatin-like liquid. Identical values for the modulus and cross-sectional area of each fiber were assumed. The fibers were of different lengths with a normal distribution spread about an assumed mean. Belkoff and Haut[161] formulated a structural model for skin undergoing uniaxial tension based on earlier models[159,160,162] that was later adapted to model human patellar tendon.[163] The model assumed that the collagen fibrils had a normally distributed slack length that caused a gradual disappearance of the crimp pattern as the individual fibers became straight and began to carry a load. Kwan and Woo[164] created a structural model featuring a bilinear stress-strain curve for each fibril with different slopes for the toe and linear regions. Constitutive equations for individual fibers were superposed to form an equation for the entire ligament. This is similar to the approach that was earlier used by Soong and Hung[165] and Lanir.[20,159] Liao and Belkoff[166] recently extended earlier models of sequential recruitment[159,160,162] to include failure. Once recruited, individual fibers behaved linear elastically until exceeding a limit strain at which point brittle failure occurred.

The uniaxial behavior of ligaments has also been described by directly modeling collagen fibril geometry. Diamant et al.[19] proposed a microstructural model for ligaments and tendons that represented the collagen crimp structure with straight elastic segments joined by rigid hinges. A similar structural model was developed for human patellar tendons by Stouffer et al.[167] The collagen crimp pattern was represented by a kinematic chain composed of short elements connected by pins and torsion springs. A light microscope system was used to measure crimp pattern at different positions and under different loads to quantify model parameters. Individual link parameters were defined as functions of position to account for variations in crimp pattern. Comninou and Yannas[18] utilized a sinusoidal waveform to model the collagen crimp structure. Constitutive equations for uniaxial extension were formulated for a single fiber as well as for a bundle of fibers embedded in a matrix. A constant crimp configuration was assumed that restricted this model to small strains. Lanir[20,159] also proposed a structural model for biological soft tissues that directly modeled the collagen fibrils. The model assumed that the collagen fibril crimp was induced and sustained by elastic fibers attached to each collagen fiber at numerous points along its length.

Initial stretching was resisted primarily by the elastic fibers and with increasing stretch, the stiffer collagen fibrils began to straighten and carry more of the load.

All of the one-dimensional models have been successful at describing the uniaxial behavior of biological soft tissues. However, because they are limited to one dimension there are no independent tests that can be performed to test their predictive value. These models are not able to describe or predict the three-dimensional, anisotropic behavior of ligaments, the contribution of the ground substance matrix to ligament material behavior, and shear or transverse loading.

Three-dimensional continuum models have also been developed to represent the material behavior of ligaments. Advantages over the one-dimensional approach include the ability to predict two- and three-dimensional material behavior. Beskos and Jenkins[168] proposed a continuum model that represented tendon as a fiber-reinforced composite. Inextensible fibers were arranged in a helical pattern and were embedded in an incompressible, hollow right circular cylinder. Fung[169] proposed a phenomenological model using an exponential stress-strain relationship based on uniaxial experimental results from rabbit mesentery. This formulation included the nonlinearity and finite deformation associated with uniaxial tensile tests. This work was later extended by Hildebrandt et al.[170] to two- and three-dimensional isotropic forms.

Ault and Hoffmann[171,172] developed a three-dimensional constitutive law for soft connective tissues that used a previously developed linearly elastic composite materials approach.[173,174] The collagen fibrils and ground substance matrix were modeled over a representative material volume. The cylindrical fibril was assumed to be surrounded by a concentric cylinder of matrix material. Although the fibril and the matrix were both assumed to be isotropic and linearly elastic solids, the fiber-reinforced geometry of the representative volume induced transversely isotropic symmetry. Large regions of soft tissue were represented by aggregations of the single fiber subunits using methods described by Whitney and McCullough.[175] A distribution function was used to describe fiber orientation. By applying boundary conditions of uniform strain and uniform stress to the aggregate model, it was possible to predict upper and lower bounds, respectively, for tissue stiffness. Changes in fibril orientation with deformation were not considered. Model predictions were compared with experimental data from rat tail tendon and cat knee joint capsule.

Lanir[162] used a strain energy approach to form a continuum model for fibrous connective tissue. The energy of deformation was assumed to arise from the tensile stretch in the collagen fibers, with the only contribution from the matrix being a simple hydrostatic pressure. The model described an incompressible composite of undulating collagen fibers embedded in a fluid matrix. The model assumed that the collagen fibers buckle under a compressive load and the unfolding of the fibers during deformation squeezed the matrix, resulting in an internal hydrostatic pressure. The stress due to deformation was described by:

$$\boldsymbol{T} = \lambda W_{\lambda} \boldsymbol{a} \otimes \boldsymbol{a} + p\mathbf{1} \tag{21}$$

where λ is the collagen fiber stretch, W_{λ} is the strain energy contribution from the collagen fibers, $\boldsymbol{a}$ is a unit vector describing the local fiber direction, and p is the hydrostatic pressure arising from the matrix. For a uniaxial tensile test along the fiber direction, the model reduces to one dimension with the entire stress carried by the collagen fibers and $p = 0$.

Hurschler et al.[176] recently proposed a three-dimensional model for tendon and ligament that included both microstructural and tissue level aspects in its formulation. Similar to the approach used by Lanir,[162] it was assumed that the fibrils contributed to strain energy only when in tension and the only contribution of the matrix was a hydrostatic pressure. A probability distribution function was used to describe the initial orientation of the collagen fibers in the tissue. Fiber deformation was assumed to be incompressible and axisymmetric. Individual fibrils were assumed to deform in a linear manner. Stretch-based failure criteria were established at both the fiber and fibril level to model damage and failure. A simplified version of the model was used to describe uniaxial tensile data. The model required a large number of material parameters. Many of these parameters were difficult or impossible to determine experimentally.

Three-dimensional isotropic models are capable of describing uniaxial data, but the use of isotropic symmetry for fiber-reinforced structures such as ligaments may introduce large inaccuracies in computational models. A better description of material behavior may be achieved by recognizing the anisotropy of ligaments arising from their collagen-reinforced structure. Our laboratory developed a structurally motivated continuum model to represent ligaments and tendons as incompressible, transversely isotropic, hyperelastic materials.[65,177] The formulation used a strain energy approach that allowed for a relatively straightforward finite element implementation of the model. The model formulation also allowed for easy determination of coefficients from material testing. The model assumed that transversely isotropic symmetry occurs in ligaments as a result of a single family of collagen fibers. A unit vector field $\boldsymbol{a}^0$ in the undeformed configuration was used to describe the local fiber direction and the strain energy was required to depend on this vector. By standard arguments,[178] the strain energy was an isotropic function of $\boldsymbol{C}$ and $\boldsymbol{a}^0$. When the material undergoes deformation, $\boldsymbol{a}^0(\boldsymbol{X})$ will deform with the body. After deformation, the fiber direction may be described by a unit vector field $\boldsymbol{a}(\boldsymbol{x}(\boldsymbol{X}))$. In general the fibers will also undergo length change. The fiber stretch, λ, is then

$$\lambda \boldsymbol{a} = \boldsymbol{F} \cdot \boldsymbol{a}^0 \tag{22}$$

where $\boldsymbol{F}$ is the deformation gradient tensor. A material with the above symmetry is *transversely isotropic*.

The elastic response of the tissue was assumed to arise from the resistance of the collagen fiber family, the ground substance matrix, and their interaction. Further, it was assumed that the ground substance matrix was isotropic. Finally, the composite structure was assumed incompressible because of the large amount of trapped water in the tissue. With these assumptions, the strain energy was written as:

$$W = F_1(I_1, I_2) + F_2(\lambda + F_3(I_1, I_2, \lambda) \tag{23}$$

The function F_1 represented the material response of the isotropic ground substance matrix, F_2 represented the contribution from the collagen fiber family, and F_3 was the contribution from interactions between the fibers and matrix, such as a shear coupling. I_1 and

I_2 were the standard invariants of the right Cauchy-Green deformation tensor and are the complete set of invariants associated with incompressible isotropic material behavior:

$$I_1 = \text{tr } \boldsymbol{C}\ I_2 = \frac{1}{2}\left[(\text{tr } \boldsymbol{C})^2 - \text{tr } \boldsymbol{C}^2\right] \tag{24}$$

The dependence on λ arose directly from the reinforcing fiber family.

The second Piola-Kirchoff (P-K) stress for an incompressible material with strain energy given by Equation 23 is

$$\boldsymbol{S}^e = 2\frac{\partial W}{\partial \boldsymbol{C}} = 2\{(W_1 + I_1 W_2)\mathbf{1} - W_2 \boldsymbol{C}\} + \frac{1}{\lambda} W_\lambda \boldsymbol{a}^0 \otimes \boldsymbol{a}^0 + p\,\boldsymbol{C}^{-1} \tag{25}$$

For Equation 23, the following identifications can be made in Equation 25:

$$W_1 = \frac{\partial F_1}{\partial I_1} + \frac{\partial F_3}{\partial I_1} \qquad W_2 = \frac{\partial F_1}{\partial I_2} + \frac{\partial F_3}{\partial I_2} \qquad W_\lambda = \frac{\partial F_2}{\partial \lambda} + \frac{\partial F_3}{\partial \lambda} \tag{26}$$

Equation 23 is similar to many constitutive equations that have been successfully used in the past to describe biological soft tissues such as cardiac muscle.[179–182]

An experimental study was performed to evaluate the ability of a simplified form of Equation 23 to describe and predict the material behavior of human fascia lata.[65] The simplification was used to demonstrate the characteristics of the strain energy function without including the interaction term F_3, for which experimental data were not readily obtainable. A simple form that describes an isotropic material was used for the matrix:

$$F_1 = \frac{C_1}{2}(I_1 - 3) + \frac{C_2}{2}(I_2 - 3) \tag{27}$$

This represented the Mooney-Rivlin model.[183] Several observations about the mechanical behavior of collagen fibers were incorporated into the form for F_2. First, collagen does not support a significant compressive load, and structures that are composed of mostly collagen will tend to buckle under small compressive forces. Second, the tensile stress-stretch relation for ligaments and tendons can be well approximated by an exponential in the toe region and subsequently by a line. These observations led to the following choice for the strain energy derivatives of the collagen fibers:

$$\begin{aligned} W_\lambda &= 0 && \lambda \le 1 \\ W_\lambda &= C_3(\exp(C_4(\lambda - 1)) - 1) && 1 < \lambda < \lambda^* \\ W_\lambda &= C_5\lambda + C_6 && \lambda \ge \lambda^* \end{aligned} \tag{28}$$

Here, λ^* was the stretch at which the collagen fibers were straightened, C_3 scaled the exponential stresses, C_4 was the rate of collagen fiber uncrimping, and C_5 was the modulus of the straightened collagen. The y-intercept of the linear region, C_6, was determined from the condition that the stress was C^0 continuous at λ^*:

$$C_6 = C_3(\exp\,(C_4(\lambda^* - 1)) - 1) - C_5\lambda^* \tag{29}$$

Our laboratory has performed experimental work to evaluate the descriptive[64,65] and predictive[65] capabilities of this transversely isotropic hyperelastic material model. In one study,[65] human fascia lata was subjected to uniaxial tensile tests both parallel and transverse to the collagen fiber direction. This allowed determination of material parameters and evaluation of the model's ability to describe three-dimensional behavior. The model was then used to predict the results of an experimental strip biaxial test. In a separate study,[64] the model was successfully used to describe uniaxial tensile data from human MCLs tested both parallel and transverse to the collagen fiber direction (Figure 9).

C. Viscoelastic Models

Although ligaments are relatively insensitive to strain rate,[128] tissue viscoelasticity does play a significant role in the response of joints to high-rate loading or impact scenarios.[129] Viscoelastic effects are also important when considering cyclic loading,[68] creep, or stress relaxation.[69,70] Tissue pathologies can cause alterations in viscoelastic behavior. The time- and history-dependent behavior of ligaments has been the topic of study in many experimental studies of ligaments, and viscoelasticity has been incorporated into several constitutive models for ligaments. Once again, these models may be divided into microstructural and phenomenological categories.

Microstructural viscoelastic models have been formulated with a similar basis as some of the previously discussed microstructural elastic models. Viidik[156] and Frisen et al.[157] proposed microstructural models for parallel fibered viscoelastic tissues consisting of spring and dashpot combinations. These general discrete element models of viscoelastic behavior were also modified to include the nonlinearity of the elastic response.[156,157] Lanir[184] extended his structural elastic model by assuming that the individual fibers were linearly viscoelastic. This model was further extended to incorporate three-dimensional viscoelasticity theory.[162] Viscoelasticity was similarly added to the structural model of Decraemer et al.[185] by assuming internal friction between fibers and between fibers and the surrounding matrix. The damping was introduced by assigning linear viscoelastic properties to the fibers with a relaxation function.

Phenomenological viscoelastic models have also been used to model ligaments. Barbenel et al.[186] generalized spring and dashpot models by incorporating a logarithmic relaxation spectrum. Sanjeevi et al.[187,188] described the viscoelastic behavior of biological soft tissues with an equation similar to that of a Voigt-type spring and dashpot model. Dehoff[89] and Bingham and Dehoff[90] modified a continuum-based constitutive equation that had been used to characterize the nonlinear viscoelasticity of polymers to describe the behavior of soft biological tissues. Ligaments were modeled as an isotropic, viscoelastic material with fading memory.

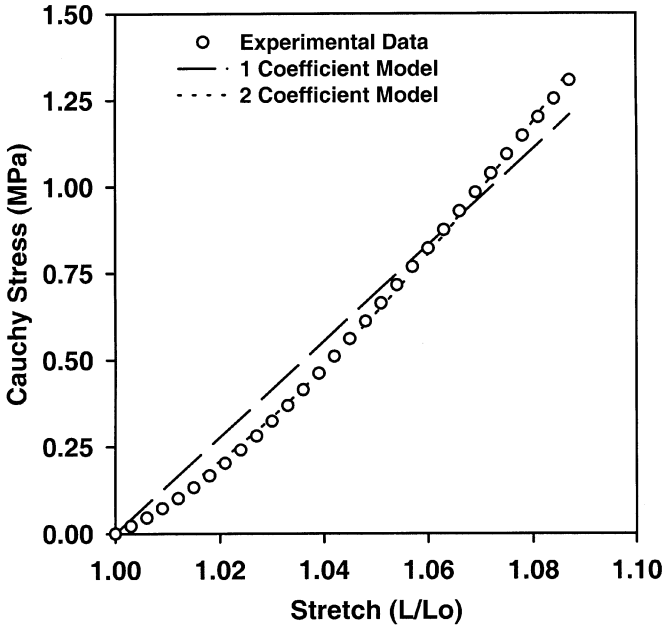

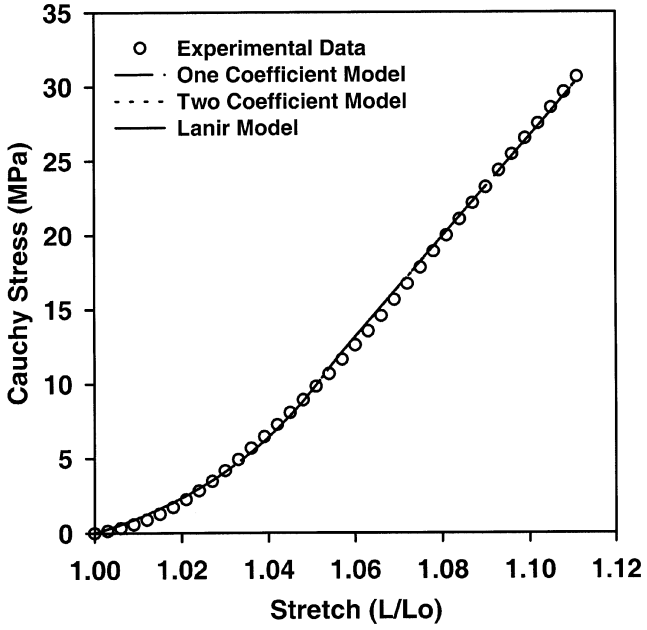

FIGURE9. (A) Cauchy stress-stretch curves for the specimens transverse to and (B) along the collagen fiber direction, and the material model curve fits. The Two-Coefficient model provided a better description of the transverse data, while all three models provided a good description of the longitudinal data. In B, the lines representing the model fits are coincident. (Reproduced with permission from Quapp and Weiss, 1998.)

As with elastic models, one-dimensional viscoelastic representations for ligaments can describe one-dimensional behavior, but are incapable of describing and predicting complex three-dimensional behavior. Continuum viscoelasticity theory can be applied to circumvent this shortcoming of one-dimensional approaches. In addition, continuum hyperelastic models can be readily extended to continuum viscoelasticity.

1. General Viscoelasticity Theory

The most general viscoelastic behavior can be described by the definition of a *simple material*:

$$\boldsymbol{S}(t) = \boldsymbol{S}_e(\boldsymbol{C}(t) + \boldsymbol{Z}_{s=0}^{\infty}\{\boldsymbol{G}(t-s);\ \boldsymbol{C}(t)\}) \tag{30}$$

where $\boldsymbol{S}(t)$ is the time-dependent second P-K stress, $\boldsymbol{S}_e(\boldsymbol{C}(t))$ is the equilibrium stress representing the long-time elastic material behavior, $\boldsymbol{C}(t)$ is the right deformation tensor, and $\boldsymbol{Z}$ is a functional representing the history of $\boldsymbol{G}(t-s) = \boldsymbol{C}(t-s) - \boldsymbol{C}(t)$. This general constitutive law requires the history of the right deformation tensor $\boldsymbol{C}(t)$ at all past times to calculate the second P-K stress $\boldsymbol{S}(t)$.

Equation 30 specifies that the current stress state depends on the entire history of deformations. A common simplification of this theory is the *Principle of Fading Memory*. This states that deformations that occurred in the distant past have less of an effect on the present stress than those that have occurred more recently.[191] The principle of fading memory may be introduced by defining an *influence function* or *obliviator* which characterizes the rate at which the memory fades.[192] A common form of the principle of fading memory utilizes an integral relationship between stress and strain in a first order theory:

$$\boldsymbol{S}(t) = \boldsymbol{S}_e(\boldsymbol{C}(t)) + \int_0^{\infty} \Upsilon(\boldsymbol{G}(t-s), s;\ \boldsymbol{C}(t))\, ds \tag{31}$$

where Υ is a general tensor-valued function with the variables $\boldsymbol{G}(t-s)$ and s and the parameter $\boldsymbol{C}$. Truesdell and Noll[192] have referred to materials with an integral relationship between the stress and strain as *materials of the integral type*.

Coleman and Noll[191] formulated a nonlinear theory known as finite linear viscoelasticity. This theory restricts the deformation to be slowly changing in the recent past. With this approach, the current stress can be determined by linearly integrating the deformation history with reference to the current configuration. In contrast to the infinitesimal theory, the integrating functions in the constitutive integrals are nonlinear functions of the current deformation state. Equation 31 reduces to finite linear viscoelasticity when a linear function is used for Υ.

If only a very short part of the history of $\boldsymbol{C}$ has an influence on the stress, the deformation tensor $\boldsymbol{C}(t-s)$ can be approximated by its Taylor expansion as s approaches zero. Truesdell and Noll[192] referred to materials in which the stress depends on only a finite

number of these time derivatives as *materials of the differential type*. It has often been assumed that the viscous stress $\boldsymbol{S}_v$ depended only on the strain and on the strain rate that reduced the description to first order. The general equation for a first-order viscoelastic material of the differential type is:

$$\boldsymbol{S}(t) = \boldsymbol{S}_e(\boldsymbol{C}(t)) + \boldsymbol{S}_v(\dot{\boldsymbol{C}}(t);\ \boldsymbol{C}(t)) \tag{32}$$

3. Applications of Viscoelasticity Theory to Ligaments and Tendons

Pioletti[4,147,193] recently developed a three-dimensional, viscoelastic model for ligament and tendon behavior that included nonlinear elastic behavior, short-term memory effects, and long-term memory effects. The short-term memory effects described the behavior for which stress depended on strain rate (material of the differential type) and the long-term memory effects described stress relaxation on a longer time scale (material of the integral type). The model was limited by considering specimens to be isotropic, homogeneous, and incompressible.

A general relationship for the description of soft tissue viscoelasticity was obtained by combining Equation 31 and Equation 32:

$$\boldsymbol{S}(t) = \boldsymbol{S}_e(\boldsymbol{C}(t)) + \boldsymbol{S}_v(\dot{\boldsymbol{C}}(t);\ \boldsymbol{C}(t)) + \int_0^{\infty} \sum (\boldsymbol{G}(t-s),\ s;\ \boldsymbol{C}(t))\,ds \tag{33}$$

where the three terms of Equation 33 represent the elastic, short-term memory, and long-term memory response of the material, respectively. The assumptions of isotropic, homogeneous, incompressible material behavior allows Equation 33 to be expressed as:

$$\boldsymbol{S}(t) = \left[-p\boldsymbol{C}^{-1} + \left(\frac{\partial W_e}{\partial I_1} + I_1\frac{\partial W_e}{\partial I_2}\right)\boldsymbol{I} - \frac{\partial W_e}{\partial I_2}\boldsymbol{C}\right] + \frac{\partial W_v}{\partial \dot{\boldsymbol{C}}}$$

$$+ \int_{\delta}^{\infty} \sum (\boldsymbol{G}(t-s),\ s;\ \boldsymbol{C}(t))\,ds \tag{34}$$

where W_e is the previously defined strain energy function for a hyperelastic material and W_v is a similarly defined *dissipative potential* for short-term memory effects from which the viscous stress is derived. This description decoupled the different mechanical behaviors, which was useful for determination of material coefficients.

Johnson et al.[194,195] proposed a viscoelastic model called the single integral finite strain (SIFS) model. This model describes a material of the integral type with fading mem-

ory. A single integral was used to relate stress and strain for an isotropic, incompressible material. Different constitutive equations were used to describe the mechanical behavior of ligaments at different elongations using the concept of constitutive branching.[196] A one-dimensional form of this model was applied to uniaxial tensile testing data from ligaments and tendons. The nonlinear viscoelastic response utilized by SIFS theory was first proposed by Pipkin and Rogers.[197] The Cauchy stress $\boldsymbol{T}$ was defined to be of the form

$$\boldsymbol{T}(t) = -p\boldsymbol{I} + \boldsymbol{F}(t)\left\{\boldsymbol{R}(\boldsymbol{C}(t), 0) + \int_0^t \frac{\partial}{\partial(t-s)}(\boldsymbol{R}[\boldsymbol{C}(s), t-s])ds\right\}\boldsymbol{F}^T(t) \quad (35)$$

where p was the indeterminate part of the stress arising due to the incompressibility constraint, $\boldsymbol{I}$ was the identity tensor, $\boldsymbol{F}$ was the deformation gradient tensor, $\boldsymbol{C}$ was the right Cauchy-Green stretch tensor, and $\boldsymbol{R}$ was a strain-dependent tensorial relaxation function. The term $\boldsymbol{R}[\boldsymbol{C}(t), 0]$ in Equation 35 represented an instantaneous deformation occurring at $t = 0$. The strain-dependent tensorial relaxation function was defined to be

$$\boldsymbol{R} = \phi_0\boldsymbol{I} + \phi_1\boldsymbol{C} + \phi_2\boldsymbol{C}^2 \quad (36)$$

where ϕ_0, ϕ_1, and ϕ_2 are scalar functions of t and the principle invariants of $\boldsymbol{C}$. Linearization of Equation 35 leads to isotropic linear viscoelasticity. If the equations are not linearized, quasi-linear viscoelasticity (QLV)[128,169,198] may be obtained with proper selection of ϕ_0, ϕ_1, and ϕ_2. QLV theory is described below.

By substituting a scalar relaxation function, $G(t-s)$ for the tensorial relaxation function $\boldsymbol{R}$, Equation 35 was rewritten as

$$\begin{aligned}\boldsymbol{T}(t) &= -p\boldsymbol{I} + C_0\{[1+\mu I(t)]\boldsymbol{B}(t) - \mu\boldsymbol{B}^2(t)\} \\ &- C_0(1-\gamma)\int_0^t \dot{G}(t-s)\{[1+\mu I(s)]\boldsymbol{B}(t) - \mu\boldsymbol{F}(t)\boldsymbol{C}(s)\boldsymbol{F}^T(t)\}ds \quad (37)\end{aligned}$$

where C_0 was the initial modulus, C_∞ was the long-time modulus, $\gamma = C_\infty/C_0$, μ was the shear modulus, $\boldsymbol{B}$ was the left Cauchy-Green strain tensor, and $I(s) = \text{tr}\,\boldsymbol{C}(s)$. The term $\dot{G}(t-s)$ ensured recent strain states had a greater importance than older strain states.

Experimental data from uniaxial tests of human patellar tendons and canine MCLs were used to validate a one-dimensional form of SIFS theory. Material coefficients were extracted from stress relaxation and stress-strain data. The model was then used to predict material behavior for stress relaxation and cyclic loading. Predicted model behavior corresponded well with experimental data.Fung[128,169,198] introduced a viscoelasticity theory that has become the most widely used theory in soft tissue biomechanics. This theory is

referred to as QLV. The basis of this theory is that (1) the stress at a given time can be described by a convolution integral representation, separating the elastic response and the relaxation function; and (2) the relaxation function has a specific continuous spectrum.

The formulation of QLV theory is similar to finite linear viscoelasticity. It is assumed that the stress relaxation function can be expressed as a convolution of a relaxation function with an elastic response:

$$\boldsymbol{S}(t) = \boldsymbol{G}(t) * \boldsymbol{S}^{e}(\boldsymbol{E}) \tag{38}$$

where $\boldsymbol{S}^{e}(\boldsymbol{E})$ is the elastic response and $\boldsymbol{G}(t)$ is the reduced relaxation function. In general, $\boldsymbol{G}(t)$ is a fourth-order tensor providing direction-dependent relaxation phenomena.

Using the superposition principle and representing the strain history as a series of infinitesimal step strains, the overall stress relaxation function can be expressed as the sum of all individual relaxations. For a general strain history, the stress at time t, $\boldsymbol{S}(t)$, is given by the strain history and the convolution integral over time of $\boldsymbol{G}(t)$:

$$\boldsymbol{S}(t) = \int_{-\infty}^{t} \boldsymbol{G}(t-\tau) : \frac{\partial \boldsymbol{S}^{e}(\boldsymbol{E})}{\partial \boldsymbol{E}} : \frac{\partial \boldsymbol{E}}{\partial \tau} d\tau \tag{39}$$

For biological soft tissues, Fung proposed a continuous relaxation representation for $\boldsymbol{G}(t)$. It was assumed that the relaxation function was the same in all directions which reduced $\boldsymbol{G}(t)$ to a scalar, $G(t)$:

$$G(t) = \frac{\{1 + c[E_1(t/\tau_2) - E_2(t/\tau_1)]\}}{1 + c\ln(\tau_2/\tau_1)} \tag{40}$$

where $E_1(t)$ was the exponential integral function,

$$E_1(t) = \int_{z}^{\infty} \frac{e^{-t}}{t} t \tag{41}$$

This relaxation function provides a smooth, linear decrease from short to long relaxation times (Figure 10). The stiffness (real part of complex modulus) increases with increasing frequency, whereas the damping (imaginary part) is relatively constant over a wide range of frequencies.[199] This yields a hysteresis loop that is relatively insensitive to strain rate over several decades of change, a feature often observed for soft tissues. The three viscoelastic material coefficients, τ_1, τ_2, and c, can be determined from the analysis of a stress

relaxation experiment. τ_1 and τ_2 represent time constants that bind the lower and upper limits of the constant damping range of the relaxation function and c is a dimensionless constant that scales the degree to which viscous effects are present. Although the QLV approach was independently formulated by Fung and colleagues, the specific continuous relaxation spectrum has a history of use in other fields as well. Neubert[200] provides an overview of the relaxation spectrum. Complete details and history of the QLV theory can be found in Fung,[128] section 7.6.

QLV has been successfully used by many investigators to model the time- and history-dependent behavior of biological soft tissues. Haut and Little[201] applied QLV to describe relaxation tests of collagen fiber bundles extracted from the tails of rats. The model was then used to predict the results of constant strain rate tests, hysteresis loops, and sinusoidal tests. Woo et al.[148] performed an experimental investigation of the viscoelastic properties of the canine MCL. It was shown that QLV theory could describe the observed time- and history-dependent behavior.

The widespread use of QLV theory has motivated investigators to develop optimal methods for estimating QLV parameters.[202–205] Dortmans et al.[202] studied the discrepancies that occur in parameter estimation due to the inability to produce a true step change in strain experimentally. A similarly motivated study was performed by Nigul and Nigul.[203] Myers et al.[204] proposed a method for reducing parameter estimation errors induced by finite rate relaxation testing. Sauren and Rousseau[205] performed a sensitivity analysis to examine the effects of the parameters τ_1, τ_2, and c on QLV behavior. It was shown that c has the strongest influence on the degree to which viscous effects are present. The time constants τ_1 and τ_2 were shown to govern the "fast" and "slow" viscous phenomena, respectively.

One of the advantages of QLV theory is that it decouples the elastic contribution to the stress from the time- and rate-dependent contributions. This makes it relatively easy to use any hyperelastic model for the elastic contribution since the viscoelastic portion will remain unaffected. However, the FE implementation of QLV and other viscoelasticity the-

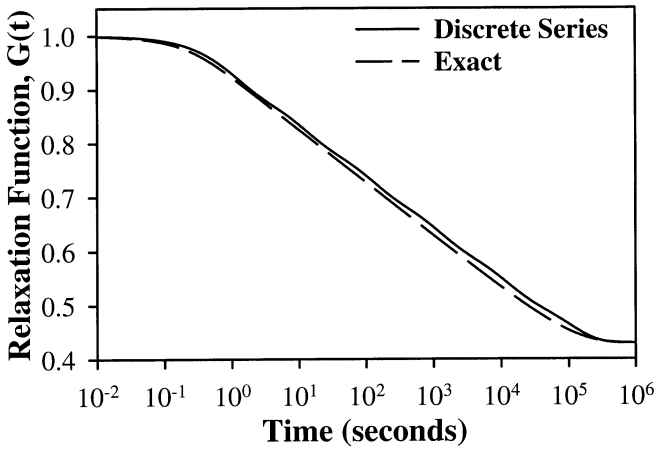

FIGURE10. Relaxation functions $G(t)$ given by the quasi-linear viscoelastic function and the discrete spectrum approximation.}

ories is made difficult by the large amounts of computer storage that are required. To compute stresses at each time-step, it is necessary to store a second-order tensor at each integration point, for each element, at each previous time-step. This is due to the continuous relaxation spectrum that is used in the convolution representation for the QLV theory. For even the smallest problems, these storage requirements are prohibitive.

Puso and Weiss[3] developed a FE implementation of QLV using a discrete spectrum approximation. This approach was used to reduce the large amounts of storage required for a continuous relaxation function. This implementation utilized an exponential series approximation to Equation 40. A log plot of Equation 40 shows a linear transition region between short and long times (Figure 10). A series of exponentials with equal spectral strengths and relaxation times spread one decade apart provides such qualitative behavior.[199] Based on this observation, the following approximation to Equation 40 was made:

$$G(t) = G_e + \frac{G_0 - G_e}{N_d + 1} \sum_{I=0}^{N_d} \exp(t/10^{(I+I_0)}) \tag{42}$$

where G_e is the equilibrium modulus, G_0 is the initial modulus, N_d is the span of the transition region in decades, and 10^{I_0} is the lowest discernible relaxation time. The span of the transition region is chosen so that it includes the nonlinear curve sections on each end of the central linear region, as shown in Figure 10. This ensures that the transition regions will be represented accurately in the discrete spectrum approximation. All required coefficients G_e, G_0, N_d and I_0 can be determined graphically from a log plot of $G(t)$, as in Figure 10.

Recent work by Thornton et al.[206] shows that QLV and linear viscoelastic models are not successful at predicting ligament creep behavior based on relaxation experiments or predicting relaxation behavior based on creep experiments. This suggests that these viscoelastic phenomena occur by fundamentally different mechanisms and raises concern over the general applicability of QLV theory for modeling the time-dependent behavior of ligaments. Lakes and Vanderby[207] have attempted to address this limitation of QLV theory by interrelating creep and relaxation in a single-integral nonlinear superposition model.

D. Poroelastic Models

Poroelastic models provide a quantitative description of the relative contributions of the solid and fluid phases in soft tissue to the material behavior of the composite structure. Poroelastic material models were originally developed to describe soil mechanics[208,209] and have been utilized in the biomechanics field for the description of cartilage[210] and interveterbral disks.[211] Material models of this type have been implemented into commercial FE codes.[212,213] Although experimental investigations have indicated that the material behavior of ligaments and tendons is a function of tissue hydration,[131,132] few models have incorporated fluid effects into their formulation. Knowledge of the fluid flow in ligaments

and tendons may also help to elucidate the possibility that fluid transport contributes to the nutrition of the tissue,[214] as is known to be the case in articular cartilage.[215]

Atkinson et al.[216] created a microstructurally based FE model of a collagen fascicle that included fluid effects. The model consisted of a fibrous outer ring with helically oriented fibrils surrounding an internal region consisting of a water-based matrix. Although permeability is known to be a nonlinear function of deformation for other soft tissues,[217] it was assumed to be constant in this representation. A nonlinear poroelastic representation was used for the central core of each fascicle that is similar to the biphasic model often used to model articular cartilage.[217,218] This material stiffens under compression, which was controlled through the definition of the shear modulus:

$$G = \left[\frac{3(1-2\nu)(1+e_0)}{2(1+\nu)\kappa}\right](p+P_t)\exp(\varepsilon_{vol}^{el}) \tag{43}$$

where G is the shear modulus, e_0 is the initial void ratio (volume fraction of fluid/volume fraction of solid), p is the internal pressure, P_t is the elastic ultimate strength, $\varepsilon_{vol}^{el} = \ln(J^{el})$ is the elastic portion of volume change, ν is Poisson's ratio, and κ is the log bulk modulus. Fluid flow in the model was assumed to obey Darcy's law,

$$v = -k\frac{dp}{dr} \tag{44}$$

where v is the fluid velocity, k is the permeability, and p is the pressure. The fibrous outer ring was represented by an orthotropic poroelastic material. The tensile modulus along the fibril direction was assumed to be 600 MPa and the transverse fibril modulus was assumed to be 60 MPa. The outer ring was also capable of holding water and similar permeabilities and void ratios were used as for the inner core.

Stress relaxation tests, cyclic extension, and uniaxial tensile tests were simulated with the model. Parametric studies were conducted examining the effects of variations in moduli, permeability, and void ratio in both the outer ring and inner core. The model was able to predict general phenomenological behavior observed experimentally by other investigators. It was shown that the relaxation response and internal pressures were highly sensitive to changes in permeability and water content.

Although this model was able to predict many behaviors that have been observed experimentally, there are still many issues that have limited the usefulness of this approach. The most fundamental problem is that many of the material parameters such as tissue permeability are not widely available. Although these quantities may be difficult to quantify experimentally, they are essential for construction of accurate models and can in fact be determined through well-planned experiments.[71] Atkinson et al.[216] have used assumed values for the material properties and varied them in parameterized studies. This allowed an assessment of model sensitivity to these parameters, but the accuracy of the model is unknown.

E. Homogenization Models

Homogenization modeling techniques offer advantages over traditional continuum level or microstructural approaches for the analysis of composite materials such as biological tissue. Homogenization theory was developed specifically for the analysis of microstructured materials[219,220] and it has been extensively used in the study of composites.[221,222] Using homogenization theory, it is possible to perform microstructural and continuum analyses independently and then combine the results to predict stress and strain fields on microstructural levels throughout a large region of material. Continuum analyses use apparent mechanical properties to determine a stress-strain distribution. This method is relatively inexpensive computationally, which allows the analysis of large-scale systems but it is not possible to predict the stress-strain inhomogeneities occurring within the microstructure of a composite material. Microstructural methods assume a specific representative geometry, which is analyzed to predict apparent moduli and stress distributions within the material microstructure. Unfortunately, the computational expense of microstructural analyses prohibits their use for large-scale systems. The knowledge of the microstructural mechanical environment of biological tissues that can be gained through homogenization modeling can provide insight into the role of individual tissue constituents and their interaction. The microstructural tissue stress and strain levels are believed to play significant roles in mediating tissue homeostasis.[223]

Linear forms of homogenization theory have been used to represent the mechanics of hard tissue. Hollister et al.[224,225] used homogenization theory for the study of trabecular bone mechanics. The formulation assumed linear elastic deformations within the trabecular tissue. The total tissue strain was separated into an apparent strain plus a fluctuating component:[221]

$$\{\varepsilon_{tissue}\} = \{\varepsilon_{app}\} + \{\varepsilon^*\} \tag{45}$$

where $\{\varepsilon_{tissue}\}$ was the total tissue strain, $\{\varepsilon_{app}\}$ was the apparent strain which varied only on a macroscopic level, and $\{\varepsilon^*\}$ was a fluctuating component that varied on both the macroscopic and microscopic levels. In addition, the microstructure was assumed to be locally periodic,[220] which assured that $\{\varepsilon^*\}$ was periodic on the microstructural scale. The resulting variational form of the microstructural equilibrium equation was:

$$\int_{V_{cell}} \{\varepsilon(v)\}^T[\boldsymbol{C}]\{\mathbf{e}^*\}dV_{cell} = -\int_{V_{cell}} \{\varepsilon(v)\}^T[\boldsymbol{C}]\{\mathbf{e}_{app}\}dV_{cell} \tag{46}$$

where $\{\varepsilon(v)\}$ was the virtual strain vector, $[\boldsymbol{C}]$ was the tissue stiffness matrix, and V_{cell} was the volume of the microstructural model. Validation of homogenization theory for modeling trabecular bone mechanics has been assessed both analytically and experimentally.[224,225]

The analysis of ligaments with homogenization theory requires a formulation capable of describing finite deformations. Livesay et al.[226,227] extended homogenization theory to encompass large deformations. New relations were developed between the microstructural

and continuum levels, allowing the total deformation gradient to be expressed as a multiplicative combination of the deformation gradients at the microstructural and continuum levels:

$$\boldsymbol{F}_{total} = \boldsymbol{F}_{cont} * \boldsymbol{F}_{micro} \tag{47}$$

Here, $\boldsymbol{F}_{cont}$ describes the continuum level deformation gradient and $\boldsymbol{F}_{micro}$ describes the microstructural level deformation gradient. The extension of homogenization theory to include finite deformations should allow it to be applied to biological soft tissues such as ligaments and tendons.

V. APPLICATIONS in JOINT MODELING

Computational models of diarthroidal joints have the potential to provide a powerful tool for the study of ligament function, prosthesis design, and the effects of ligament reconstruction. Models offer the potential to predict quantities that are difficult or impossible to measure experimentally. The construction of accurate and useful models requires integration of the mechanics concepts, experimental results, and material models described previously. A general approach that has been commonly used in forming joint models has been to predict quasi-static equilibrium positions for given external loads and kinematic constraints.

Similar to the pattern observed in experimental work, the human knee joint has been the most commonly modeled joint. There have been great advancements in the complexity and utility of models since the early work of Strasser[228] that represented the knee as a four-bar linkage. In this section, we will present an overview of joint models that have incorporated ligament mechanics into their formulations. Models will be divided into groups that use one-dimensional, two-dimensional, or three-dimensional representations for the ligaments. Model characteristics will be critically reviewed with emphasis given to the ligament formulation.

A. One-Dimensional Representation of Ligaments

Nearly all mathematical models of joints have used a one-dimensional representation of the ligaments. This simplification has been used because the primary function of ligaments is to resist tensile forces. The one-dimensional discrete element representation of ligaments has usually been simple linear or nonlinear springs. Discrete elements allow the entire representation of ligaments to be reduced to a load-elongation relationship. This greatly reduces model complexity while still enabling investigators to predict quantities such as joint kinematics. However, this simplification does not allow prediction of ligamentous stresses and load cannot be transferred between soft tissue and bone at points other than the discrete element insertion sites.

Strasser[228] proposed a model for the human knee more than 80 years ago by observing that the cruciate ligaments in combination with the tibia and femur formed a mechanism that could be approximated by a four-bar linkage. This approach has been utilized more recently as well.[229,230] In this two-dimensional model, the point where the cruciate links cross each other defines the instant center of rotation between the femur and tibia. This

model has also been used to describe the shape of the femoral and tibial condyles and the migration of the tibio-femoral contact point with knee flexion. Although the four-bar approach has been useful for describing simplified knee kinematics, the assumption of rigid cruciate ligaments is inadequate for representing the complex interactions between the cruciates and the tibia and femur.

Joint models can be broadly categorized as using either analytical or FE solution methods. Quasi-static analytical models generate a system of equations by balancing forces or minimizing total system energy from which equilibrium joint positions may be predicted. The FE method utilizes similar overall methods, but the discretization of geometry into a FE mesh allows complex systems to be more easily studied. A large number of both analytical and FE models of joints featuring a discrete element representation of ligaments have been published in recent decades. Rather than providing an exhaustive description of each of these models, a summary of general modeling approaches and characteristics will be provided in the following paragraphs.

A discrete element representation of ligaments requires investigators to specify a force-elongation relationship for each element. Linear[231,232] and quadratic[233–241] force-elongation functions have often been used to describe ligaments in joint models. A common approach has been to specify a reference length below which the element force was equal to zero. At low strains, a nonlinear (quadratic) function was used to describe toe-region behavior and at higher strains a linear function was used.[239] In models that have utilized linear springs to represent the ligaments, nonlinear joint stiffness has been observed as a result of changes in ligament orientation.[231]

Ligaments have been represented by individual discrete elements or in some cases they have been represented by two or more elements representing different fiber bundles.[239–241] It is thought that multiple line elements will be more capable of representing the inhomogeneities that exist in ligaments. Mommersteeg et al.[240] studied the effects of using different numbers of line elements to represent the ligaments of the human knee. It was shown that models utilizing three or less line elements per ligament were very sensitive to geometrical parameters, whereas models with seven or more line elements were mathematically redundant. The ideal compromise will always be specific to the model and loading conditions.

The *in situ* strain observed in ligaments has been included in some discrete element joint models. Unfortunately, there are little data available quantifying *in situ* strain levels so many investigators have either neglected *in situ* strain or assumed a uniform initial strain for all ligaments. Discrete element models of ligaments are also limited in that they are unable to represent the strain inhomogeneities that occur across individual ligaments *in situ*.[46] Blankevoort et al.[239,240] have developed a method for applying a nonuniform initial strain to each ligament element in their three-dimensional knee model. An optimization technique was used to alter the initial strain of each ligament until the model reproduced kinematics that had been previously measured experimentally. Although this technique allows a model to be formulated that describes joint kinematics, the reference strains that it predicts are often physiologically unrealistic. In one study,[239] initial ligament strains ranged between –25% for the anterior bundle of the LCL to 10% for the posterior bundle of the ACL. Also, this approach for the determination of *in situ* strain does not guarantee a unique solution.

Ligaments *in vivo* often wrap around each other (ACL-PCL) or around bones (MCL-tibia). This causes soft tissue load to be transferred at locations other than the insertion

sites and alters the direction of load transfer at the insertion sites. Most one-dimensional representations of ligaments have only allowed forces that act in a straight line between insertion sites.[239] However, significant exceptions have been described in the literature.[242–245] Hefzy and Grood[242] extended their previously published analytical knee model[246] to include geometric nonlinearities such as ligament wrapping. Blankevoort and Huiskes[243] incorporated the model proposed by Hefzy and Grood[242] that allowed their line elements to follow the curved edge of a contacting bone (Figure 11). Frictionless contact between the ligament and the bone was assumed. This algorithm was used to model the contact that occurs between the MCL and the tibia. When compared to a model without bony interactions, it was shown that the bony edge redirected the ligament force to more effectively counterbalance valgus moments on the tibia.

Discrete element joint models have also been expanded to include articular contact. Contact allows loads to be transferred directly between two bones, rather than just through

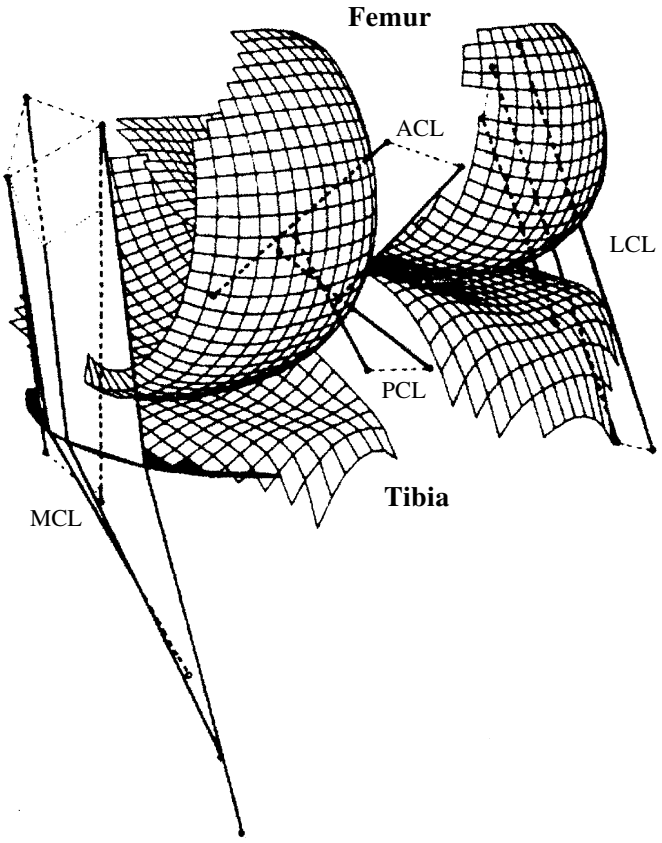

FIGURE11. FE model of the human knee joint featuring a discrete element representation of the ligaments. An algorithm has been used that allows for wrapping of the MCL around the medial edge of the tibia. (Adapted from Blankevoort and Huiskes, 1991.)

connecting ligaments. It also permits joint contact area and stress to be predicted. The three-dimensional quasi-static knee model developed by Wismans et al.[233] was one of the first to include contact in its formulation. Rigid contact was required to occur between the femur and tibia at a single point on each condyle throughout all joint motions. Varus-valgus motions could not be studied with this implementation of joint contact. Recent work has made use of deformable contact to achieve predictions of joint contact area and stress.[231,238,239] Andriacchi et al.[231] included deformable contact between the rigid femur and tibia in their three-dimensional knee model by introducing hydrostatic elements representing the contact surface. Essinger et al.[238] implemented deformable contact by describing elastic compression springs at discrete points on the joint surface. Blankevoort et al.[239] compared rigid and deformable contact in a three-dimensional FE knee model. For the deformable case, a thin layer of isotropic linear elastic material was attached to the rigid bone surface representing a cartilage layer. For both the rigid and deformable cases, frictionless contact was assumed. It was shown that the rigid contact model was much more sensitive to changes in surface geometry. The detailed FE knee model of Li et al.[241] included a deformable representation for both the cartilage and the menisci. Cartilage was modeled as a linearly elastic solid with material properties based on previously published experimental values. The menisci were represented by a number of discrete spring elements with stiffness determined through an optimization procedure.

Discrete element joint models have been developed to simulate the response of joints to dynamically applied loads.[236,237,247–250] The inertial effects of bones were included in these joint models; however, soft and hard tissue viscoelasticity was neglected in all cases as the ligaments were represented by simple elastic springs and the bones were modeled as rigid bodies. The approach used by Moeinzadeh and Engin et al.[247–249] in the development of a two-dimensional, sagittal plane knee joint model is representative of the other modeling efforts in this group. Nonlinear elastic spring ligaments were used to connect the rigid bones. The model was used to predict ligament and joint contact forces with the application of dynamic loads to the tibia.

Sensitivity analyses have been performed to assess the dependence of discrete element models on different parameters. Wismans et al.[233] studied the effects of changing ligament stiffness, initial strain, insertion site locations, and ligament sectioning on the anterior-posterior laxity of the knee. Changes in initial ligament strain had larger effects than the insertion site locations or ligament stiffness. Ligament cutting simulations showed the cruciate ligaments to have the greatest influence on anterior-posterior laxity. A sensitivity analysis performed by Beynnon et al.[235] on a two-dimensional knee model showed a greater sensitivity to insertion site location and articular surface geometry than ligament stiffness and initial strain.

In addition to the simulation of normal joint kinematics, models have also been utilized to study joint pathologies and to examine the effects of various surgical procedures.[232–234,238,244,241] Wismans et al.[233] and Crowninshield et al.[234] simulated the effects of ligament sectioning by removing discrete elements from their knee models. Gibson et al.[232] used the model of Andriacchi et al.[231] to simulate the surgical effects of using Müller's anterolateral femorotibial ligament (ALFTL) graft[251] as an ACL substitute or as an adjunct to an ACL reconstruction for an ACL-deficient knee. Additional spring elements were added to represent the surgically constructed ALFTL graft. Essinger et al.[238] and Garg and Walker[244] developed models to simulate the effects of total knee replacement.

One-dimensional ligaments have been represented in models of other joints as well. Gilbertson et al.[252] recently published a review of FE models of the spine. Many of these models have featured a detailed three-dimensional representation of the vertebral bodies and discs, including anisotropy[253,254] and fluid effects[211,255] for the annular fibers and nucleus. Ligaments have been modeled only as discrete spring elements.[256–258]

B. Two-Dimensional Representation of Ligaments

Models featuring two-dimensional representations of ligaments are able to predict quantities such as soft tissue stress, which is not possible with a one-dimensional representation. Two-dimensional representations offer many of the advantages of three-dimensional representations, yet they are computationally more simple. A two-dimensional, plane stress FE model of the rabbit MCL in the midcoronal plane was developed by Matyas et al.[43] using experimentally determined geometry. Linearly elastic, isotropic, homogeneous material properties were used for the MCL. The MCL was rigidly attached to the femur and tibia at the insertion sites and frictionless contact was enforced between the MCL and bones at contact areas other than the insertion sites. The tibia was displaced to induce a 2% tensile strain. The model predicted that the highest levels of tensile stress occurred in the tissue midsubstance, whereas high levels of hydrostatic compressive stress were found near the insertion sites. The areas of high compressive stress correlated with regions of rounded, fibrocartilagenous cells rather than the elongated cells of ligament midsubstance. This model featured geometry and boundary conditions that were developed earlier by Simbeya et al.[259-261] The model of Simbeya[261] introduced anisotropy by modeling the two-dimensional ligament as a composite of tension only cable elements embedded within isotropic quadrilateral elements. The model was also used to simulate tensile tests of the rabbit femur-MCL-tibia complex. Significant compressive and shear stresses were predicted in the ligament near the femoral and tibial insertions, respectively. Giori et al.[44] created a two-dimensional FE model to study the stresses that developed as tendons wrapped around bones. This model also predicted hydrostatic compressive stresses near the bony contact areas that corresponded with areas of fibrocartilagenous tissue.

The preceding group of models featuring a two-dimensional representation of ligaments illustrates some of the insufficiencies of discrete element models. Although discrete elements are only able to support tensile loads, each of the two-dimensional models predicted that regions of tissue were also subjected to compressive and shear loading. The ability to correlate microstructural differences in tissue type with differences in the mechanical environment has many implications in terms of the ability to understand healthy and pathological soft tissues.

C. Three-Dimensional Representation of Ligaments

To accurately model ligament stresses and interactions with surrounding soft tissues and bone, it is necessary to use a three-dimensional continuum representation for their structure. Although one-dimensional representations can be used to predict ligament forces, they are unable to predict stress distributions throughout the ligament. One-dimensional representations may be used to predict joint kinematics, but load transfer via contact

with other soft or hard tissue structures will not be represented correctly. In addition, joint models featuring one-dimensional ligaments do not provide unique solutions for ligament load-sharing. Any number of one-dimensional elements, with different insertion site locations on the bones, can produce a model with similar joint stiffness characteristics. Two-dimensional representations of ligaments are also insufficient for describing and predicting the complex three-dimensional behavior of ligaments. Despite the inaccuracies induced by simplifying ligaments to one and two dimensions, few investigators have utilized three-dimensional representations for ligaments when modeling joint kinematics due to the difficulties associated with their formulation and additional complexity in representing the constitutive behavior of ligaments. The few efforts at representing ligaments in three dimensions that have been reported in the literature have ranged from three-dimensional groupings of discrete elements to continuum models featuring either isotropic or transversely isotropic representations for ligament. Each approach will be discussed in the following section.

1. Discrete Element Network

Martelli et al.[262] created detailed models of the ACL consisting of a large network of viscoelastic discrete elements. Ten "fibers" were used to describe the curved surface geometry between the femoral and tibial insertions of the ACL. Twenty equidistant "knots" were defined on each fiber and each knot was connected to the adjacent knots on the same fiber through a linear spring in series with a linear dashpot and also through an angular damper. Knots on adjacent fibers were connected by linear dashpots. The model was used to predict fiber strain during passive flexion of the knee. Although this three-dimensional network of discrete elements may offer some advantages over simpler one-dimensional representations in the ability to predict regional variations in tissue strain, the utility of this model is somewhat limited. The particular number and configuration of discrete elements is not based on any actual tissue characteristics. For example, the model would presumably behave much differently if the discrete elements were arranged in parallel rather than in series. Also, the stiffness and viscosity values for the individual discrete elements were unknown, forcing the use of somewhat arbitrary values. A final important limitation of this model is that once again tissue stresses cannot be predicted, indicating that a continuum representation may be more appropriate.

2. Isotropic Material Symmetry

Pioletti et al.[4,263] developed a three-dimensional FE model of the human ACL. Curves describing the external geometry of the insertion sites were determined experimentally. The actual geometry of the ligament substance was not measured. Rather, a solid was created that joined the two curves describing the measured geometry of the insertion sites. The bony insertions into the femur and tibia were both represented by rectangular blocks containing distinct zones for the cortical and cancellous bones. An isotropic, elastic material model was used to represent the ACL. The cortical and cancellous bone were both modeled as isotropic, linear elastic materials. *In situ* stress was included in the model by applying a 100-Newton force along the ligament axis at full extension. Three-dimensional

kinematics were determined in a separate experimental study performed by Heegaard[264] wherein knees were subjected to flexion between 0 and 150 degrees. A tibial drawer test was simulated by passively flexing the knee model to 20 degrees and then applying 4 mm of anterior tibial displacement.

The model predicted inhomogeneous stress fields in the ACL during flexion and anterior drawer tests. Model results predicted that with increasing knee flexion, increases in Von Mises stress and hydrostatic stress could be found near the anterior femoral insertion of the ligament. Stresses around the tibial insertion were found to be only slightly increased with increasing flexion angle. Internal rotation was also shown to cause an increase in ligament stress relative to knees with no internal rotation. The tibial drawer tests predicted a large increase in ligament stresses at all flexion angles. The general trends observed in these results agreed with numerous previously published experimental studies.[122,265–268]

Although this model was able to predict experimentally observed trends, there were several limitations to its accuracy. The ligament was represented by an isotropic material model that can introduce large errors in fiber-reinforced structures such as ligaments. The material properties were assumed to be homogeneous throughout the ligament, which neglects the inhomogeneities that have been reported experimentally. In addition, the geometry of the ligament was simplified. Rather than following the curved fibers of the ACL *in vivo*, the unknown ligament geometry was "extruded" in a straight line between the two known insertion sites. It was also assumed that the ACL consisted of a single bundle although it has been shown that the ACL consists of two main bundles, the AMB and the posteriorlateral bundle (PLB). This assumption may have neglected important interactions between the AMB and PLB. Interactions between the ACL and PCL were also neglected due to the lack of a PCL in the model.

3. Transversely Isotropic Material Symmetry

Wilson et al.[269,270] developed a three-dimensional FE model of the rabbit femur-MCL-tibia complex. Geometry was generated by sectioning the harvested knee of a skeletally mature female rabbit. The ligament was modeled using isotropic poroelastic elements. Anisotropy was introduced by the addition of discrete nonlinear spring elements to represent collagen fibers. This provides a relatively simple means of extending continuum models to anisotropy; however, the fiber-matrix coupling only allows load transfer to occur at discrete nodal points.[271] The bones were modeled as linearly elastic materials. Local spring stiffnesses were adjusted until the model could reproduce the force-displacement behavior of MCL tensile tests. Areas of compressive stress were predicted in the MCL near the femoral insertion and just proximal to the tibial insertion as the MCL wraps around the tibia. Model validation was achieved by making local comparisons of predicted MCL strains with those measured experimentally. In general, the correspondence between measured and predicted MCL strains was good, with the poorest correspondence found near the femoral insertion.

A three-dimensional FE model of the human ACL has been published recently by Hirokawa and Tsuruno.[272] The ACL was represented by a hyperelastic material model that featured an isotropic ground substance matrix (Mooney-Rivlin model) reinforced by nonlinear fibers.[164] This constitutive model is similar to the model earlier developed by Weiss et al.[65,177] ACL geometry and kinematics were determined from a previous experimental

study.[273] The model was loaded by prescribing displacements of the insertion sites to simulate passive flexion and anterior tibial displacement. Results indicated there was an inhomogeneous distribution of stress in the ACL and that this distribution changed with flexion angle. Application of an anterior tibial displacement caused stresses in the ACL to increase. There were numerous characteristics that have limited the utility of this model. Nearly all of the material parameters were unknown by the authors so they have estimated values based on previous theoretical and experimental papers. The initial stress distribution in the ligament was also unknown and was generated by moving the ACL insertion sites from a nonphysiological position into their position at full extension. This generated an arbitrary initial stress state upon which all following measurements were based.

Our laboratory has developed three-dimensional FE models of the human MCL.[3,47,274] These models have utilized the transversely isotropic, hyperelastic constitutive model of Weiss et al.[65,177] for representing the MCL and have been used to predict the stress-strain distribution in the human MCL as a function of flexion angle and valgus rotation.[47,274] A subject-specific modeling approach was used to create the FE model based on inputs determined from experimental testing. The overlying muscle and periarticular soft tissue, including the patella and patellar tendon, was dissected from a fresh frozen cadaveric knee. CT scans were taken at 1.0-mm intervals with the knee at zero degrees flexion. Prior to kinematic testing, an ISL was mounted to the femur and tibia for measuring the six-degree-of-freedom motion of the knee. To measure strain in the MCL, 15 black markers were applied to the MCL using cyanoacrylate. Specially designed fixtures were used to apply 10 cycles of ±5 degrees of varus-valgus rotation at fixed flexion angles (0, 45, and 90 degrees). Tibial axial rotation, medial-lateral translation, and joint distraction were unconstrained while anterior-posterior tibial displacement was constrained. The stretch ratio along the collagen fibers on the MCL surface was determined using a three-dimensional video motion analysis system. After completion of the kinematic testing, the knee was positioned at full extension and the MCL was sectioned from its attachments. Three-dimensional video analysis was used to measure the stress-free position of the markers from which the *in situ* strain could be determined. This information was used to apply an initial stretch to the MCL in the computational model.[275] Custom punches were used to cut tensile test specimens parallel and transverse to the collagen fiber direction of the MCL.[64] Data from tensile tests of these specimens were collected using a 25-lb. load cell and two-dimensional video strain measurement. The stress-strain relationship was then determined for both the longitudinal and transverse samples. The experimental data were fit to our transversely isotropic constitutive model.[177]

Surfaces of the femur and tibia were extracted from the CT data using the marching cubes[276] and decimation[277] algorithms. The cross-sectional contours of the superficial MCL were manually digitized from each CT slice. These contours were then laced together with triangles to form a polygonal surface. The polygon surfaces of the femur, MCL, and tibia were imported into a commercial FE preprocessing program where block-structured, hexahedral FE meshes were constructed for each of the three structures (Fig. 12).

The nonlinear, implicit FE code NIKE3D was used for all analyses. The MCL was modeled using the previously described transversely isotropic, hyperelastic constitutive model.[177] The bones were represented as rigid, and their six-degree-of-freedom motion was completely prescribed using the experimentally measured kinematic data from the last valgus loading cycle. Contact between the MCL and tibia and the MCL and femur was enforced using the penalty method. The experimentally measured initial stretch was applied to the MCL with the bones held fixed. The joint motion measured by the ISL during experiments

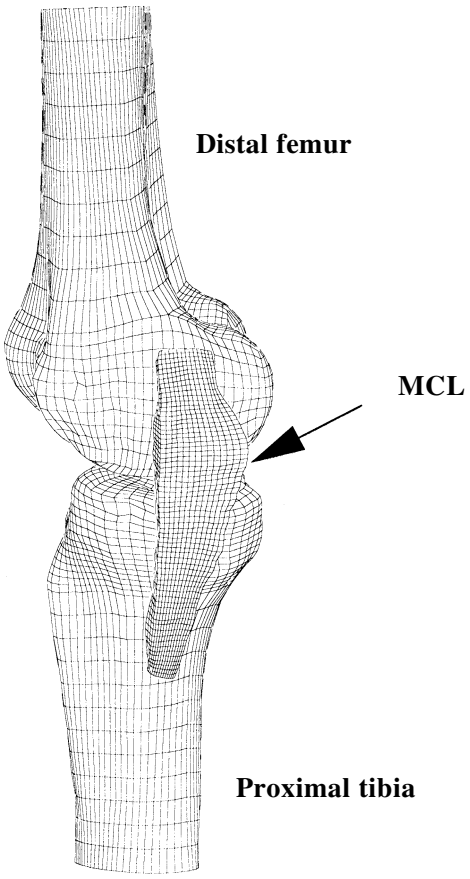

FIGURE12. FE mesh of the femur-MCL-tibia complex. The bones were represented as rigid and the MCL was modeled as a transversely isotropic, hyperelastic material. Experimentally measured kinematics were used to drive the model.

was then applied to the tibia with the femur held fixed. NIKE3D was allowed to iterate to convergence at all steps using a quasi-Newton (BFGS) solution method.

The ability of a three-dimensional FE model to predict inhomogeneous stress-and-strain distributions throughout an entire ligament is demonstrated by this model. The predicted MCL stress-and-strain distribution may be used to indicate joint configurations and loading conditions where the ligament is vulnerable to injury. The model results showed that at zero degrees flexion the *in situ* stress and strain were highest in the posterior fibers of the MCL (Fig. 13). With increasing flexion angles, the load in the posterior fibers decreased, whereas the load in the anterior fibers increased. The application of 5 degrees of valgus rotation increased the ligament stresses at all flexion angles (Fig. 14). An experimental study by Hull et al.[278] reported similar strain values for the anterior fibers. The experimentally measured MCL strains with five degrees of applied valgus rotation were used to validate the model

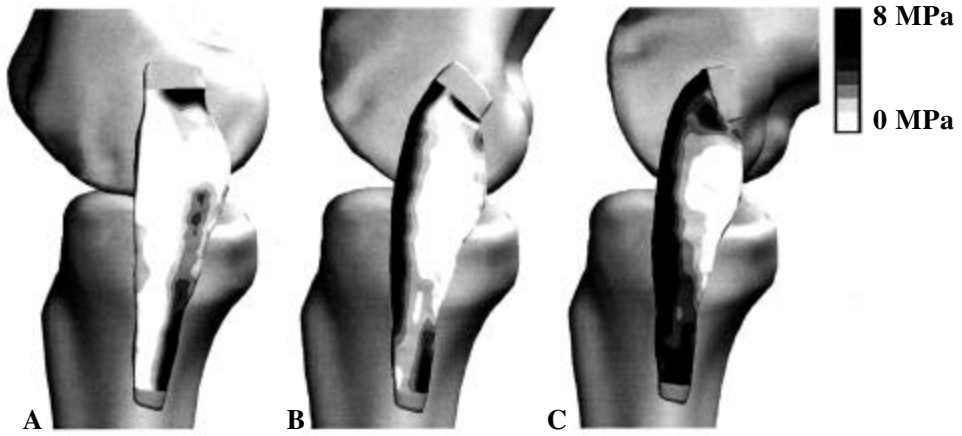

FIGURE13. Predicted Von Mises stress in the human MCL as a function of passive knee flexion. (A) zero degrees; (B) 45 degrees; (C) 90 degrees.

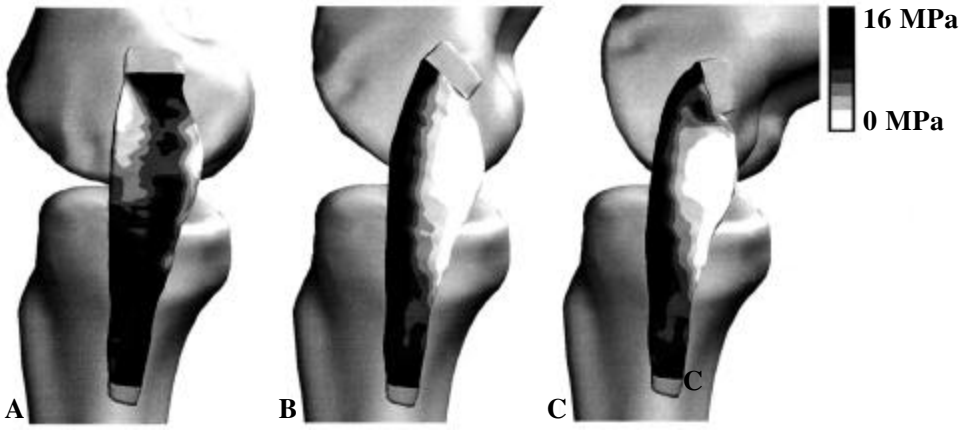

FIGURE14. Predicted Von Mises stress in the human MCL as a function of passive knee flexion and 5 degrees applied valgus rotation. (A) zero degrees; (B) 45 degrees; (C) 90 degrees.

results (Fig. 15). In general, a good correspondence was found between the experimental and computational results. The correspondence was best in the ligament midsubstance and worsened toward the ligament insertions to bone. These results highlight the need for improvement in the algorithms used for attaching ligaments to bones in computational joint models. A gradual change in material properties at insertion sites to more closely simulate *in vivo* behavior would likely improve future models. Other improvements in modeling accuracy could be achieved by including inhomogeneities in MCL material properties that occur

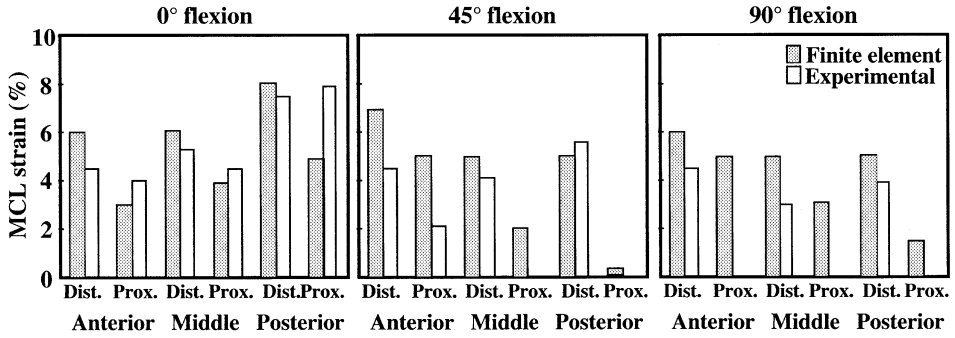

FIGURE15. Comparison of experimental and FE MCL strains with 5 degrees of applied valgus rotation. Ligament buckling prevented experimental measurements in the proximal region at 45 and 90 degrees.

throughout the ligament midsubstance. Additional limitations of this model include the assumption that the superficial MCL does not significantly interact with the medial meniscus or the deep fibers of the MCL and that a viscoelastic representation for the MCL is not necessary for the low rate loading that was simulated.

Similar methods have been used recently to generate a FE model of the human forearm featuring the radius, ulna, and a three-dimensional representation of the interosseous ligament (IOL).[279] This was a subject-specific model with geometry, kinematics, and initial IOL strain based on experimental inputs. IOL insertion site kinematics were prescribed for the FE model based on experimentally measured values during forearm compression with the arm in pronation, supination, and neutral rotation. The IOL strains predicted by the FE model were nonuniform across the surface of the IOL and were highest in neutral rotation and lowest in pronation. The magnitude and relative distribution of IOL strains followed the general trends that were observed experimentally.

VI. CONCLUSIONS

Ligamentous injuries are common and often lead to significant joint degeneration and loss of function. Experimental studies of ligaments have yielded insight into their function and mechanisms of injury; however, many aspects of their behavior are still unknown. Computational models of ligaments offer the potential to provide information regarding ligament mechanics that would be difficult or impossible to measure experimentally. The complex material properties of ligaments make the accurate modeling of their material behavior a challenge.

In this articles, we have provided a critical review of the constitutive models that have been developed to represent ligaments and tendons. These models have developed from rather simplistic descriptors of one-dimensional behavior to models capable of describing and predicting three-dimensional anisotropic behavior. The simplifying assumptions of each modeling approach have been discussed as well as their relative strengths and weak-

nesses. The application of these constitutive relationships in the context of joint modeling has also been reviewed.

The ultimate goal of these modeling efforts is to improve the clinical diagnosis and treatment of ligamentous injuries. The models may also identify means by which to prevent injuries, such as through the use of protective equipment in the case of sports-related injuries. Despite the significant advances in recent years in both the complexity and accuracy of computational models of ligaments, current models are still incapable of completely describing and predicting ligamentous behavior. Improvement in future models will be achieved through research in a number of different areas. Experimental methods need to be improved to allow inhomogeneities in material properties and *in situ* strain to be more accurately quantified. This need is especially urgent for accurate modeling of the insertion sites. More data are also needed to quantify the multiaxial material properties of ligaments. Better material models will allow ligament elastic and viscoelastic behavior to be more accurately represented. These models need to be capable of representing healing and diseased ligaments as well as healthy tissue. Improvements in computational algorithms and computer hardware also will allow large-scale problems to be analyzed more quickly. With advances in these fundamental areas, accurate subject-specific models for entire joints will eventually be feasible.

ACKNOWLEDGMENTS

Financial support from Whitaker Foundation Biomedical Research and Transition Grants, and NIH Grant #AR47369 is gratefully acknowledged.

REFERENCES

1. Spencer AJM. Continuum Mechanics. New York: Longman; 1980.
2. Simo JC, Taylor RL, Pister KS. Variational and projection methods for the volume constraint in finite deformation elastoplasticity. Comp Meth Appl Mech Eng 1985;51:177–208.
3. Puso MA, Weiss JA. Finite element implementation of anisotropic quasilinear viscoelasticity. ASME J Biomech Eng 1998;120(1):62–70.
4. Pioletti DP. Viscoelastic properties of soft tissues: application to knee ligaments and tendons. Ph.D. Dissertation, Department of Physics, Ecole Polytechnique Federale de Lausanne; 1997.
5. Simon BR. Multiphasic poroelastic finite element models for soft tissue structures. Appl Mech Rev 1992;45:191–218.
6. Kwan MK, Lai WM, Mow VC. A finite deformation theory for cartilage and other soft hydrated connective tissues–i. equilibrium results. J Biomechanics 1990;23(2):145–155.
7. Govindjee S, Simo JC. Mullins' effect and the strain amplitude dependence of the storage modulus. Int J Solids Struct. 1992;29:1737–51
8. Zienkiewicz OC, Taylor RL. The Finite Element Method, Volume 1: Basic Formulation and Linear Problems. London: McGraw-Hill; 1989.
9. Bathe K-J. Finite Element Procedures. New Jersey: Prentice-Hall; 1996.
10. Bertsekas DP. Constrained Optimization and Lagrange Multiplier Methods. New York: Academic Press; 1982.
11. Fortin M, Glowlnski R. Augmented Lagrangian Methods: Applications to the Numerical Solution of Boundary-Value Problems. Amsterdam: Elsevier Science Publishers; 1983.

12. Daniel DM, Akeson WH, O'Connor JJ. Knee Ligaments: Structure, Function, Injury and Repair. New York: Raven Press; 1990.
13. Woo SL-Y, Buckwalter JA. Injury and Repair of the Musculoskeletal Soft Tissues. American Academy of Orthopaedic Surgeons. Illinois: Park Ridge; 1988.
14. Amiel D, Frank C, Harwood F, Fronek J, Akeson W. Tendons and ligaments: a morphological and biochemical comparison. J Orthop Res 1984;1(3):257–265.
15. Nimni ME. Collagen: structure, function, and metabolism in normal and fibrotic tissues. Semin Arthritis Rheum 1983;13(1):1–86.
16. Viidik A. Structure and function of normal and healing tendons and ligaments. In Biomechanics of Diarthrodial Joints. New York: Springer-Verlag; 1990:3–38.
17. Kastelic J, Palley I, and Baer E. The multicomposite ultrastructure of tendon. Conn Tiss Res 1978;6:11–23.
18. Comninou M, Yannas IV. Dependence of stress-strain nonlinearity of connective tissues on the geometry of collagen fibers. J Biomechanics 1976;9:427–433.
19. Diamant J, Keller A, Baer E, Litt M, Arridge RGC. Collagen; ultrastructure and its relation to mechanical properties as a function of ageing. Proc R Soc Lond 1972;180(B):293–315.
20. Lanir Y. Structure-function relations in mammalian tendon: The effect of geometrical nonuniformity. Journal of Bioeng 1978;2:119–128.
21. Dale WC, Baer E. Fibre-buckling in composite systems: A model for the ultra-structure of uncalcified collagen tissue. J Mater Sci 1974;9:369–382.
22. Tanzer ML. Cross-linking of collagen. Science 1973;180:357–370.
23. Bailey AJ, Robins SP, Balian G. Biological significance of the intermolecular crosslinks of collagen. Nature 1974;251(5471):105–109.
24. Neuberger A, Slack HGB. Metabolism of collagen from liver, bone, skin, and tendon in normal rat. Biochem J 1953;53:47–52.
25. Ogston AG. The biological functions of the glycosaminoglycans. In: Balasz EA, editor, Chemistry and Molecular Biology of the Intercellular Matrix, volume 3. London: Academic Press; 1970.
26. Hannafin JA and Arnoczky SP. Effect of cyclic and static tensile loading on water content and solute diffusion in canine flexor tendons: An *in vitro* study. J Orthop Res 1994;12:350–356.
27. Hvidberg E. Investigations into the effect of mechanical pressure on the water content of isolated skin. Acta Pharmac (Kobenhavn) 1960;16:245–259.
28. Thieike RJ, Vanderby R, Grood ES. Volumetric changes in ligaments under tension. Proc ASME Bioeng Conf 1995;29:197–198.
29. Weiss J, Lai A, Loui S, and Nisbet J. Behavior of human medial collateral ligament in unconfined compression. Trans 46th Meeting Orthop Res Soc 2000;25:781.
30. Woo SL-Y, An K-N, Arnoczky SP, Wayne JS, Fithian DC, Myers BS. Anatomy, biology, and biomechanics of tendon, ligament and meniscus. In: Simon SR, editor. Orthopaedic Basic Science. American Academy of Orthopaedic Surgeons; 1994:47–74.
31. Rosenbloom J. Elastin: Biosynthesis, structure, degradation, and role in disease processes. Conn Tiss Res 1982;10:73–91.
32. Minns RJ, Soden PD, Jackson DS. The role of the fibrous components and ground substance in the mechanical properties of biological tissues: A preliminary investigation. J Biomechanics 1973;6:153–165.
33. Kirby MC, Sikoryn TA, Hukins DW, Aspden RM. Structure and mechanical properties of the longitudinal ligaments and ligamentum flavum of the spine. J Biomed Eng 1989;11(3): 192–196.
34. Cooper RR, Misol S. Tendon and ligament insertion. A light and electron microscopic study. J Bone Joint Surg 1970;52A:1–20.
35. Benjamin M, Evans EJ, Copp L. The histology of tendon attachments to bone in man. J Anat 1986;149:89–100.

36. Noyes FR, Torvik PJ, Hyde WB, LeLucas MS. Biomechanics of ligament failure II. An analysis of immobilization, exercise and reconditioning effects in primates. J Bone Joint Surg 1974;56A:1406–18.
37. Tipton CM, Matthes RD, Martin RR. Influence of age and sex on the strength of bone-ligament junctions in knee joints of rats. J Bone Joint Surg 1978;60A:230–234.
38. Vailas AC, Tipton CM, Matthew RD, Gant M. Physical activity and its influence on the repair process of medial collateral ligaments. Connect Tiss Res 1981;9:25–31.
39. Woo SL-Y, Gomez MA, Sites TJ, Newton PO, Orlando CA, Akeson WH. The biomechanical and morphological changes in the medial collateral ligament of the rabbit after immobilization and remobilizatlon. J Bone Joint Surg 1987;69A:1200–11.
40. Weiss JA, Woo SL-Y, Ohiand KJ, Horibe S, Newton PO. Evaluation of a new injury model to study medial collateral ligament healing: Primary repair versus non-operative treatment. J Orthop Res 1991;9:516–528.
41. Noyes FR, Bulter DL, Grood ES, Zernicke RF, Hefzy MS. Biomechanical analysis of human ligament grafts used in knee-ligament repairs and reconstructions. J Bone Joint Surg 1984; 66A:344–352.
42. Woo SL-Y, Gomez MA, Seguchi Y, Endo CM, Akeson WH. Measurement of mechanical properties of ligament substance from a bone-ligament-bone preparation. J Orthop Res 1983; 1:22–29.
43. Matyas JR, Anton MG, Shrive NG, Frank CB. Stress governs tissue phenotype at the femoral insertion of the rabbit MCL. J Biomechanics 1995;28(2):147–157.
44. Giori NJ, Beaupre GS, Carter DR. Cellular shape and pressure may mediate mechanical control of tissue composition in tendons. J Orthop Res 1993;11(4):581–591.
45. Weiss JA, Schauer DA, Gardiner JC. Modeling contact in biological joints using penalty and augmented Lagrangian methods. Proc ASME Winter Annual Meeting 1996;BED-33: 347–348.
46. Woo SL-Y, Weiss JA, Gomez MA, and Hawkins DA. Measurement of changes in ligament tension with knee motion and skeletal maturation. ASME J Biomech Eng 1990;112(1):46–51.
47. Gardiner JC and Weiss JA. Effects of flexion angle and valgus rotation on stresses in the human medial collateral ligament. Proc ASME Bioeng Conf 1997;BED-35:27–28.
48. Woo SL-Y, Orlando CA, Frank CB, Gomez MA, Akeson WH. Tensile properties of medial collateral ligament as a function of age. J Orthop Res 1986;4:133–141.
49. Grood ES, Suntay WJ. A joint coordinate system for the clinical description of three-dimensional motions: Application to the knee. ASME J Biomech Eng 1983;105:136–144.
50. Blankevoort L, Huiskes R, de Lange A. Recruitment of knee joint ligaments. ASME J Biomech Eng 1991;113(1):94–103.
51. Fukubayashi T, Torzilli PA, Sherman MF, Warren RF. An *in vitro* biomechanical evaluation of anterior-posterior motion of the knee. J Bone Joint Surg 1982;64A:258–264.
52. Markolf KL, Mensch JS, Amstutz HC. Stiffness and laxity of the knee—the contributions of the supporting structures. A quantitative *in vitro* study. J Bone Joint Surg 1976;58A:583–594.
53. Piziali RL, Seering WP, Nagel DA, Schurman DJ. The function of the primary ligaments of the knee in anterior-posterior and medial-lateral motions. J Biomechanics 1980;13:777–784.
54. Markolf KL, Bargar WL, Shoemaker SC, Amstutz HC. The role of joint load in knee stability. J Bone Joint Surg 1981;63A:570–585.
55. Seering WP, Piziali RL, Nagel DA, Schurman DJ. The function of the primary ligaments of the knee in varus-valgus and axial rotation. J Biomechanics 1980;13:785–794.
56. Shoemaker SC, Markolf KL. Effects of joint load on the stiffness and laxity of ligament-deficient knees. An *in vitro* study of the anterior cruciate and medial collateral ligaments. J Bone Joint Surg 1985;67A:136–146.
57. Butler DL, Noyes FR, Grood ES. Ligamentous restraints to anterior-posterior drawer in the human knee. J Bone Joint Surg 1980;62A:259–270.

58. Gollehon DL, Torzilli PA, Warren RF. The role of the posterolateral and cruciate ligaments in the stability of the human knee. J Bone Joint Surg 1987;69A:234–242.
59. Grood ES, Stowers SF, and Noyes FR. Limits of motion in the human knee. Effect of sectioning the posterior cruciate ligament and posterolateral structures. J Bone Joint Surg 1988;70A: 88–97.
60. Kennedy JC, Grainger RW. The posterior cruciate ligament. J Trauma 1967;7:367–377.
61. Grood ES, Noyes FR, Butler DL, Suntay WJ. Ligamentous and capsular restraints preventing straight medial and lateral laxity in intact human cadaver knees. J Bone Joint Surg 1981;63A: 1257–69.
62. Warren LF, Marshall JL, Girgis F. The prime static stabilizer of the medial side of the knee. J Bone Joint Surg 1974;56-A:665–674.
63. Shoemaker SC, Markolf KL. The role of the meniscus in the anterior-posterior stability of the loaded anterior cruciate-deficient knee. J Bone Joint Surg 1986;68A:71–79.
64. Quapp KM, Weiss JA. Material characterization of human medial collateral ligament. ASME J Biomech Eng 1998;120:757–763.
65. Weiss JA. A constitutive model and finite element representation for transversely isotropic soft tissues. Ph.D. Dissertation, Department of Bioengineering, University of Utah; 1994.
66. Gardiner JC, Weiss JA. Simple shear testing of parallel-fibered planar soft tissues. ASME J Biomech Eng 2001 April.
67. Gardiner JC, Cordaro N, Weiss JA. Elastic and viscoelastic shear properties of the medial collateral ligament. Trans 46th Meeting Orthop Res Soc 2000;25:63.
68. Yahia LH, Drouin G. Study of the hysteresis phenomenon in canine anterior cruciate ligaments. J Biomedical Eng 1990;12:57–62.
69. Hughes DW, Kirby MC, Sikoryn TA, Apsden RM, Cox AJ. Comparison of structure, mechanical properties, and functions of lumbar spinal ligaments. Spine 1990;15(8):787–795.
70. Kwan MK, Lin TH, Woo SL-Y. On the viscoelastic properties of the anteromedial bundle of the anterior cruciate ligament. J Biomechanics 1993;26(4–5):447–452.
71. Weiss J, Maakestad B, Nisbet J. The permeability of human medial collateral ligament. Trans 46th Meeting Orthop Res Soc 2000;25:783.
72. Riemersa DJ, Schamhardt HC. The cryo-jaw, a clamp designed for *in vitro* rheology studies of horse digital flexor tendon. J Biomechanics 1982;15(8):619–620.
73. Powell ES, Trail IA, Noble J. Non-suture repair of tendons. J Biomed Eng 1989;11(3): 215–218.
74. Liggins AB, Shemerluk R, Hardie R, Finlay JB. Technique for the application of physiological loading to soft tissue *in vitro*. J Biomed Eng 1992;14(5):440–441.
75. Sharkey NA, Smith TS, Lundmark DC. Freeze clamping musculo-tendinous junctions for *in vitro* simulation of joint mechanics. J Biomechanics 1995;28(5):631–635.
76. Chuong CJ, Sacks MS, Johnson RL, Reynolds R. On the anisotropy of the canine diaphragmatic central tendon. J Biomechanics 1991;24:563–576.
77. Lee TQ, Woo SL-Y. A new method for determining cross-sectional shape and area of soft tissues. ASME J Biomech Eng 1988;110:110–114.
78. Haut RC, Little RW. Rheological properties of canine anterior cruciate ligaments. J Biomechanics 1969;2:289–298.
79. Allard P, Thirty PS, A Bourgault, and G Drouin. Pressure dependence of the area micrometer method in evaluation of cruciate ligament cross-section. J Orthop Res 1979;1:265–267.
80. Iaconis F, Steindler R, Marinozzi G. Measurements of cross-sectional area of collagen structures (knee ligaments) by means of an optical method. J Biomechanics 1987;20(10):1003–10.
81. Butler DL, Grood ES, Noyes FR, Zernicke RF, Brackett K. Effects of structure and strain measurement technique on the material properties of young human tendons and fascia. J Biomechanics 1984;17(8):579–596.
82. Wang CJ, Walker PS, Wolf B. The effects of flexion and rotation on the length patterns of the ligaments of the knee. J Biomechanics 1973;6:587–596.

83. Hollis JM, Takai S, Adams DJ, Horibe S, Woo SL-Y. The effects of knee motion and external loading on the length of the anterior cruciate ligament (ACL): A kinematic study. ASME J Biomech Eng 1991;113(2):208–214.
84. van Dijk R, Huiskes R, Selvik G. Roentgenstereophotogrammetric methods for the evaluation of the three dimensional kinematic behavior and cruciate ligament length patterns of the human knee joint. J Biomechanics 1979;12:727–731.
85. Edwards RG, Lafferty JF, Lange KO. Ligament strain in the human knee joint. J Basic Eng 1970;92:131–136.
86. Bach JM, Hull ML, Patterson HA. Direct measurement of strain in the posterolateral bundle of the anterior cruciate ligament. J Biomechanics 1997;30(3):281–283.
87. Kear M, Smith RN. A method for recording tendon strain in sheep during locomotion. Acta Orthop Scand 1975;46:896–905.
88. Kennedy JC, Hawkins RJ, Willis RB. Strain gauge analysis of knee ligaments. Clin Orthop 1977;129:225–229.
89. Monahan JJ, Grigg P, Pappas AM, Leclair WJ, Marks T, Fowler DP, Sullivan TJ. *In vivo* strain patterns in the four major canine knee ligaments. J Orthop Res 1984;2:408–418.
90. Arms SW, Boyle J, Johnson RJ, Pope MH. Strain measurement in the medial collateral ligament of the human knee: An autopsy study. J Biomechanics 1983;16:491–496.
91. Beynnon B, Howe JG, Pope MH, Johnson RJ, Fleming BC. The measurement of anterior cruciate ligament strain *in vivo*. Int Orthop 1992;16(1):1–12.
92. Fleming BC, Beynnon BD, Nichols CE, Johnson RJ, Pope MH. An *in vivo* comparison of anterior tibial translation and strain in the anteromedial band of the anterior cruciate ligament. J Biomechanics 1993;26(1):51–58.
93. Renstrom P, Arms SW, Stanwyck TS, Johnson RJ, Pope MH. Strain within the anterior cruciate ligament during hamstring and quadriceps activity. Amer J Sports Med 1986;14(1):83–87.
94. Yin FC, Tompkins WR, Peterson KL, Intaglietta M. A video-dimension analyzer. IEEE Tans Biomed Engng 1972;19:376–381.
95. Gardner RM, Warner HR. Dynamic aortic diameter measurements *in vivo.* Computers in Biomedical Research 1967;1:50–64.
96. Lanir Y, Fung YC. Two-dimensional mechanical properties of rabbit skin. I. Experimental system. J Biomechanics 1974;7(1):29–34.
97. Fronek K, Schmid-Schoenbein G, Fung YC. A noncontact method for three-dimensional analysis of vascular elasticity *in vivo* and *in vitro*. J Appl Physiol 1976;40(4):634–637.
98. Woo SL-Y, Akeson WH, and Jemmott GF. Measurements of nonhomogeneous, directional mechanical properties of articular cartilage in tension. J Biomechanics 1976;9:785–791.
99. Woo SL-Y. Mechanical properties of tendons and ligaments I. Quasi-static and nonlinear viscoelastic properties. Biorheology 1982;19:385–396.
100. Derwin KA, Soslowsky LJ, Green WD, Elder SH. A new optical system for the determination of deformations and strains: calibration characteristics and experimental results. J Biomechamcs 1994;27(10):1277–85.
101. Neumann L, Ekstrom LA, Keller TS, Perry L, Hansson TH. Aging, vertebral density, and disc degeneration alter the tensile stress-strain characteristics of the human anterior longitudinal ligament. J Orthop Res 1994;12(1):103–112.
102. Weiss JA, France EP, Bagley AM, Blomstrom G. Measurement of 2-D strains in ligaments under uniaxial tension. Trans 38th Meeting Orthop Res Soc 1992;17(2):662.
103. Smutz WP, Drexler M, Berglund LJ, Growney E, An KN. Accuracy of a video strain measurement system. J Biomechanics 1996;29(6):813–817.
104. Gardiner JC, Weiss JA. Strain in the human medial collateral ligament during valgus loading. Trans 46th Meeting Orthop Res Soc 2000;25:774.
105. Runco TJ. A study of the nonuniform *in situ* strains on the surface of the anterior cruciate ligament. M.S. Dissertation, Department of Mechanical Engineering, University of Pittsburgh; 1996.

106. Runco TJ, Sakane M, Woo SL-Y. Non-contact evaluation of *in-situ* surface strain distribution of the anterior cruciate ligament. Proc ASME Winter Annual Meeting 1996;BED-33: 173–174.
107. Shapiro R. Direct linear transformation method for three-dimensional cinematography. Research Quarterly 1978;49:197–205.
108. To SY, Kwan MK, Woo SL-Y. Simultaneous measurements of strains on two surfaces of tendons and ligaments. J Biomechanics 1988;21(6):511–514.
109. Lam TC, Frank CB, Shrive NG. Calibration characteristics of a video dimension analyzer system. J Biomechanics 1992;25(10):1227–31.
110. Shrive NG. Soft tissue strain measurement. In: Orr JF, Shelton JC, editors, Optical Measurement Methods in Biomechanics. London: Chapman and Hall; 1997:154–172.
111. Hirokawa S, Yamamota K, Kawada T. A photoelastic study of ligament strain. IEEE Trans Rehabil Eng 1998;6(3):300–308.
112. Yamamoto K, Hirokawa S, Kawada T. Strain distribution in the ligament using photoelasticity. A direct application to the human AGL. Med Eng Phys 1998;20:161–168.
113. Kawada T, Abe T, Yamamoto K, Hirokawa S, Soejima T, Tanaka N, Inoue A. Analysis of strain distribution in the medial collateral ligament using a photoelastic coating method. Med Eng Phys 1999;21:279–291.
114. Ahmed AM, Hyder A, Burke DL, Chan KH. *In vitro* ligament tension pattern in the flexed knee in passive loading. J Orthop Res 1987;5(2):217–230.
115. Barry D, Ahmed AM. Design and performance of a modified buckle transducer for the measurement of ligament tension. ASME J Biomech Eng 1986;108:149–152.
116. Komi P. Relevance of *in vivo* force measurements to human biomechanics. J Biomechanics 1990;23:23–34.
117. Lew WD, Lewis JL. The effect of knee-prosthesis geometry on cruciate ligament mechanics during flexion. J Bone Joint Surg 1982;64:734–739.
118. Lewis JL, Lew WD, Schmidt J. A note on the application and evaluation of the buckle transducer for knee ligament force measurement. ASME J Biomech Eng 1982;104:125–128.
119. Glos DL, Butler DL, Grood ES, Levy MS. *In vitro* evaluation of an implantable force transducer (IFT) in a patellar tendon model. ASME J Biomech Eng 1993;115:335–343.
120. Holden JP, Grood ES, Korvick DL, Cummings JF, Butler DL, Bylski-Austrow DI. *In vivo* forces in the anterior cruciate ligament: Direct measurements during walking and trotting in a quadruped. J Biomechanics 1994;27(5):517–526.
121. France EP, Daniels AU, Goble EM, Dunn HK. Simultaneous quantitation of knee ligament forces. J Biomechanics 1983;16(8):553–564.
122. Markolf KL, Gorek JF, Kabo JM, Shapiro MS. Direct measurement of resultant forces in the anterior cruciate ligament. An *in vitro* study performed with a new experimental technique. J Bone Joint Surg 1990;72A(4):557–567.
123. Markolf KL, Burchfield DM, Shapiro MS, Cha CW, Finerman GA, Slauterbeck JL. Biomechanical consequences of replacement of the anterior cruciate ligament with a patellar ligament allograft. Part II: Forces in the graft compared with forces in the intact ligament. J Bone Joint Surg 1996;78A(11):1728–34.
124. Markolf KL, Slauterbeck JL, Armstrong KL, Shapiro GA, Finerman MS. A biomechanical study of replacement of the posterior cruciate ligament with a graft. Part II: Forces in the graft compared with forces in the intact ligament. J Bone Joint Surg 1997;79A(3):381–386.
125. Fujie H, Mabuchi K, Woo SL-Y, Livesay GA, Arai S, Tsukamoto Y. The use of robotics technology to study human joint kinematics: a new methodology. ASME J Biomech Eng 1993; 115:211–217.
126. Howe JG, Wertheimer C, Johnson RJ, Nichols CE, Pope MH, Beynnon B. Arthroscopic strain gauge measurement of the normal anterior cruciate ligament. Arthroscopy 1990;6:198–204.

127. Fleming BC, Beynnon BD, Tohyama H, Johnson RJ, Nichols CE, Renstrom P, Pope MH. Determination of a zero strain reference for the anteromedial band of the anterior cruciate ligament. J Orthop Res 1994;12:789–795.
128. Fung YC. Biomechanics: Mechanical Properties of Living Tissues, 2nd Edition. New York: Springer-Verlag; 1993.
129. Danto MI, Woo SL-Y. The mechanical properties of skeletally mature rabbit anterior cruciate ligament and patellar tendon over a range of strain rates. J Orthop Res 1993;11(1):58–67.
130. Woo SL-Y, Peterson RH, Ohiand KJ, Sites TJ, Danto MI. The effects of strain rate on the properties of the medial collateral ligament in skeletally immature and mature rabbits: A biomechanical and histological study. J Orthop Res 1990;8:712–721
131. Haut RC, Powlison AC. The effects of test environment and cyclic stretching on the failure properties of human patellar tendons. J Orthop Res 1990;8(4):532–540
132. Chimich D, Shrive N, Frank C, Marchuk L, and Bray R. Water content alters viscoelastic behavior of the normal adolescent rabbit medial collateral ligament. J Biomechanics, 1992;25: 831–837
133. Haut TL, Haut RC. The state of tissue hydration determines the strain-rate-sensitive stiffness of human patellar tendon. J Biomechanics 1997;30(1):79–81.
134. Woo SL-Y, Lee TQ, Gomez MA, Sato S, Field FP. Temperature dependent behavior of the canine medial collateral ligament. ASME J Biomech Eng 1987;109:68–71.
135. Noyes FR, Grood ES. The strength of the anterior cruciate ligament in humans and rhesus monkeys: Age-related and species-related changes. J Bone Joint Surg 1976;58A:1074–82.
136. Viidik A, Sanquist L, Magi M. Influence of postmortem storage on tensile strength characteristics and histology of rabbit ligaments. Acta Orthop Scand 1965;79:1–38.
137. Woo SL-Y, Orlando CA, Camp JT, Akeson WH. Effects of postmortem storage by freezing on ligament tensile behavior. J Biomechanics 1986;19:399–404.
138. Haut RC. Age-dependent influence of strain rate on the tensile failure of rat-tail tendon. ASME J Biomech Eng 1983;105:296–299.
139. Woo SL-Y, Ohiand KJ, Weiss JA. Aging and sex-related changes in the biomechanical properties of the rabbit medial collateral ligament. Mechanisms of Ageing and Development 1990; 56:129–142.
140. Viidik A and Ekholm R. Light and electron microscopic studies of collagen fibers under strain. Z Anat Entwickl Gesch 1968;127:154–164.
141. Butler DL, Kay MD, and Stouffer DC. Comparison of material properties in fascicle-bone units from human patellar tendon and knee ligaments. J Biomechanics 1986;19:425–432.
142. Woo SL-Y, Newton PO, Mackenna DA, and Lyon RM. A comparative evaluation of the mechanical properties of the rabbit medial collateral and anterior cruciate ligaments. J Biomechamcs 1986;25(4):377–386.
143. Gibbons MJ, Butler DL, Grood ES, Bylski-Austrow DI, Levy MS, Noyes FR. Effects of γ-irradiation on the initial mechanical and material properties of goat bone-patellar tendon-bone allografts. J Orthop Res 1991;9:209–218.
144. Kohles SS, Thielke RJ, Vanderby R. Finite elasticity formulations for evaluation of ligamentous tissue. Biomed Mater Eng 1997;7(6):387–390.
145. Cohen RE, Hooley CJ, McCrum NG. Viscoelastic creep in collagenous tissue. J Biomechanics 1976;9:175–184.
146. Lam TC, Thomas CG, Shrive NG, Frank CB, Sabiston CP. The effects of temperature on the viscoelastic properties of the rabbit medial collateral ligament. ASME J Biomech Eng 1990; 112(2):147–152.
147. Pioletti DP, Rakotomanana L, Gillieron C, Leyvraz PF, Benvenuti JF. Nonlinear viscoelasticity of the ACL: Experiments and theory. In: Middleton J, Jones ML, Pande GN, editors. Computer Methods in Biomechanics and Biomedical Engineering. Gordon and Breach; 1996: 271–280.

148. Woo SL-Y, Gomez MA, Akeson WH. The time and history-dependent viscoelastic properties of the canine medial collateral ligament. ASME J Biomech Eng 1981;103:293–298.
149. Yahia LH, Audet J, Drouin G. Rheological properties of the human lumbar spine ligaments. J Biomedical Eng 1991;13(5):399–406.
150. Butler DL, Kohles SS, Thieike RJ, Chen C, Vanderby R. Interstitial fluid flow in tendons and ligaments: a porous medium finite element solution. Med Biol Eng Comput 1997;35(6): 742–746.
151. Chen CT, Malkus DS, Vanderby R. A fiber matrix model for interstitial fluid flow and permeability in ligaments and tendons. Biorheology 1998;35(2):103–118.
152. Butler DL, Guan Y, Kay MD, Cummings JF, Feder SM, Levy MS. Location-dependent variations in the material properties of the anterior cruciate ligament. J Biomechamcs 1992;25(5): 511–518.
153. Frank C, McDonald D, Lieber R, Sabiston P. Biochemical heterogeneity within the maturing rabbit medial collateral ligament. Clin Orthop 1988;236:279–285.
154. Mommersteeg TJ, Blankevoort L, Kooloos JG, Hendriks JC, Kauer JM, Huiskes R. Nonuniform distribution of collagen density in human knee ligaments. J Orthop Res 1994;12: 238–245.
155. Butler DL, Sheh MY, Stouffer DC, Samaranayake VA, Levy MS. Surface strain variation in human patellar tendon and knee cruciate ligaments. ASME J Biomech Eng 1990;112:38–45.
156. Viidik A. A rheological model for uncalcified parallel-fibred collagenous tissue. J Biomechanics 1968;1:3–11.
157. Frisen M, Magi M, Sonnerup L, Viidik A. Rheological analysis of soft collagenous tissue. Part I: Theoretical considerations. J Biomechanics 1969;2:13–20.
158. Kastelic J, Palley I, Baer E. A structural mechanical model for tendon crimping. J Biomechanics 1980;13:887–893.
159. Lanir Y. A structural theory for the homogeneous biaxial stress-strain relationships in flat collagenous tissues. J Biomechanics 1979;12:423–436.
160. Decraemer WF, Maes MA, Vanhuyse VJ. An elastic stress-strain relation for soft biological tissues based on a structural model. J Biomechanics 1980;13:463–468.
161. Belkoff SM, Haut RC. A structural model used to evaluate the changing microstructure of maturing rat skin. J Biomechanics 1991;24:711–720.
162. Lanir Y. Constitutive equations for fibrous connective tissues. J Biomechanics 1983;16(1): 1–12.
163. Belkoff SM, Haut RC. Microstructurally based model analysis of γ-irradiated tendon allografts. J Orthop Res 1992;10:461–464.
164. Kwan MK, Woo SL-Y. A structural model to describe the nonlinear stress-strain behavior for parallel-fibered collagenous tissues. ASME J Biomech Eng 1989;111:361–363.
165. Soong YT, and Huang WN. A stochastic model for biological tissue elasticity in simple elongation. J Biomechanics 1973;6:451–458.
166. Liao H, Belkoff SM. A failure model for ligaments. J Biomechanics 1999;32(2):183–188.
167. Stouffer DC, Butler DL, Hosny D. The relationship between crimp pattern and mechanical response of human patellar tendon-bone units. ASME J Biomech Eng 1985;107:158–165.
168. Beskos DE, Jenkins JT. A mechanical model for mammalian tendon. J Appl Math 1975;42: 755–758.
169. Fung YC. Elasticity of soft tissues in simple elongation. Am J Physiol 1967;213:1532–44.
170. Hildebrandt J, Fukaya H, Martin CJ. Simple uniaxial and uniform biaxial deformation of nearly isotropic incompressible tissues. Biophysical J 1969;9:781–791.
171. Ault HK, Hoffman AH. A composite micromechanical model for connective tissues: Part I—Theory. ASME J Biomech Eng 1992;114(1):137–141.
172. Ault HK, Hoffman AH. A composite micromechanical model for connective tissues: Part II—Application to rat tail tendon and joint capsule. ASME J Biomech Eng 1992;114(1):142–146.

173. Hashin Z, Rosen BW. The elastic moduli of fiber-reinforced materials. ASME J Appl Mech 1964;31:223–232.
174. Hill R. Theory of mechanical properties of fibre-strengthened materials: I. Elastic behavior. J Mech Phys Solids 1964;12:199–212.
175. Whitney JM, McCullough. Composites Design Guide, Vol. 2, Analytical Design Methods. University of Delaware; 1980.
176. Hurschler C, Loit-Ramage B, Vanderby R. A structurally based stress-stretch relationship for tendon and ligament. ASME J Biomech Eng 1997;119:392–399.
177. Weiss JA, Maker BN, Govindjee S. Finite element implementation of incompressible, transversely isotropic hyperelasticity. Comp Meth Appl Mech Eng 1996;135:107–128.
178. Marsden JE, Hughes TJR. The Mathematical Foundations of Elascitity. New York: Dover Publications, Inc.; 1993.
179. Choung CJ, Fung YC. Residual stress in arteries. In Frontiers in Biomechanics. New York: Springer-Verlag; 1986:117–179.
180. Horowitz A, Sheinman I, Lanir Y. Nonlinear incompressible finite element for simulating loading of cardiac tissue—Part II: Three dimensional formulation for thick ventricular wall segments. ASME J Biomech Eng 1988;110:62–68.
181. Humphrey JD, Strumph RK, Yin FCP. Determination of a constitutive relation for passive myocardium. I. A new functional form. ASME J Biomech Eng 1990;112:333–339.
182. Humphrey JD, Yin FCP. On constitutive relations and finite deformations of passive cardiac tissue: I. A pseudostrain-energy approach. ASME J Biomech Eng 1987;109:298–304.
183. Mooney M. A theory of large elastic deformation. J Appl Phys 1940;11:582–592.
184. Lanir Y. A microstructure model for the rheology of mammalian tendon. ASME J Biomech Eng 1980;102:332–339.
185. Decraemer WF, Maes MA, Vanhuyse VJ, Vanpeperstraete P. A nonlinear viscoelastic constitutive equation for soft biological tissues based upon a structural model. J Biomechanics 1980; 13:559–564.
186. Barbenel JC, Evans JH, Finlay JB. Stress-strain-time relations for soft connective tissues. In: Kenedi, editor. Perspectives in Biomedical Engineering. New York: McMillan; 1973: 165–172.
187. Sanjeevi R. A viscoelastic model for the mechanical properties of biological materials. J Biomechanics 1982;15(2):107–109.
188. Sanjeevi R, Somanathan N, Ramaswamy D. A viscoelastic model for collagen fibers. J Biomechanics 1982;15(3):181–183.
189. Dehoff PH. On the nonlinear viscoelastic behavior of soft biological tissues. J Biomechanics 1978;11:35–40.
190. Bingham DN, Dehoff PH. A constitutive equation for the canine anterior cruciate ligament. ASME J Biomech Eng 1979;101:15–22.
191. Coleman BD, Noll W. Foundations of linear viscoelasticity. Rev Modern Physics 1961;3(2): 239–249.
192. Truesdell C, Noll W. The Non-linear Field Theories of Mechanics. New York: Springer-Verlag; 1992.
193. Pioletti DP, Rakotomanana LR, Benvenuti JF, Leyvraz PF. Viscoelastic constitutive law in large deformations: applications to human knee ligaments and tendons. J Biomechanics 1998; 31:753–757.
194. Johnson GA, Rajagopal KR, Woo SL-Y. A single integral finite strain (SIFS) model of ligaments and tendons. ASME Adv Bioeng 1992;22:245–248.
195. Johnson GA, Livesay GA, Woo SL-Y, Rajagopal KR. A single integral finite strain viscoelastic model of ligaments and tendons. ASME J Biomech Eng 1996;118(2):221–226.
196. Rajagopal KR, Wineman AS. A constitutive equation for nonlinear solids which undergo deformation induced microstructural changes. Intl J Plasticity 1992;8:385–395.

197. Pipkin AC, Rogers TG. A non-linear integral representation for viscoelastic behavior. J Mech Phys Solids 1968;16:59–74.
198. YC Fung. Biomechanics: its scope, history, and some problems of continuum mechanics in physiology. Appl Mech Rev 1968;21:1–20.
199. Tschoegl NW. The Phenomenological Theory of Linear Viscoelastic Behavior. New York: Springer-Verlag; 1989.
200. Neubert HKP. A simple model representing internal damping in solid materials. Aeronautical Quarterly 1963;14:187–210.
201. Haut RC, Little RW. A constitutive equation for collagen fibers. J Biomechanics 1972;5: 421–430.
202. Dortmans LJ, Sauren AA, Rousseau EP. Parameter estimation using the quasi-linear viscoelastic model proposed by Fung. ASME J Biomech Eng 1984;106:198–203.
203. Nigul I, Nigul U. On algorithms of evaluation of Fung's relaxation function parameters. J Biomechanics 1987;20(4):343–352.
204. Myers BS, McElhaney JH, Doherty BJ. The viscoelastic responses of the human cervical spine in torsion: Experimental limitations of the quasi-linear theory, and a method for reducing these effects. J Biomechanics 1991;24(9):811–817.
205. Sauren AA, Rousseau EP. A concise sensitivity analysis of the quasi-linear model proposed by Fung. ASME J Biomech Eng 1983;105:92–95.
206. Thornton GM, Oliynyk A, Frank CB, Shrive NG. Ligament creep cannot be predicted from stress relaxation at low stresses: A biomechanical study of the rabbit medial collateral ligament. J Orthop Res 1997;15:652–656.
207. Lakes RS, Vanderby R. Interrelation of creep and relaxation: a modeling approach for ligament. ASME J Biomech Eng 1999;121(6):612–615.
208. Terzaghi K. Theoretical Soil Mechanics. New York: John Wiley and Sons; 1943.
209. Truesdell C, Toupin R. The classical field theories. In Handbuck der Physik. Berlin: Springer-Verlag; 1960:226–793.
210. Mow VC, Kuei SC, Lai WM, Armstrong CG. Biphasic creep and stress relaxation of articular cartilage: Theory and experiments. ASME J Biomech Eng 1980;102:73–84.
211. Simon BR, Wu JS, Carlton MW, Evans JH, Kazarian LE. Structural models for human spinal motion segments based on a poroelastic view of the intervertebral disk. ASME J Biomech Eng 1985;107(4):327–335.
212. Prendergast PJ, van Driel WD, Kuiper J-H. A comparison of finite element codes for the solution of biphasic poroelastic problems. Proc Inst Mech Eng [H] 1996;210:131–136.
213. Wu JZ, Herzog W, Epstein M. Evaluation of the finite element software ABAQUS for biomechanical modelling of biphasic tissues. J Biomechanics 1998;31:165–169.
214. Manske PR, Lesker PA. Flexor tendon nutrition. Hand Clinics 1985;1(1):13–24.
215. O'Hara BP, Urban JP, Maroudas A. Influence of cyclic loading on the nutrition of articular cartilage. Ann Rheum Dis 1990;49(7):536–539.
216. Atkinson TS, Haut RC, Altiero NJ. A poroelastic model that predicts some phenomological responses of ligaments and tendons. ASME J Biomech Eng 1997;119:400–405.
217. Mow VC, Holmes MH, Lai WM. Fluid transport and mechanical properties of articular cartilage: A review. J Biomechanics 1984;17(5):377–394.
218. Suh JK, Spilker RL. Indentation analysis of biphasic articular cartilage: Nonlinear phenomena under finite deformation. ASME J Biomech Eng 1994;1166:1–9.
219. Bensoussan A, Lions JL, Papanicolaou G. Asymptotic Analysis for Periodic Structures. Amsterdam: North-Holland; 1978.
220. Sanchez-Palencia E. Non-Homogeneous Media and Vibration Theory. Berlin: Springer; 1980.
221. Suquet PM. Elements of homogenization theory for inelastic solid mechanics. In: Sanchez-Palencia E, Zaoui A, editors. Homogenization Techniques for Composite Media. Berlin: Springer; 1985.

222. Guedes JM. Nonlinear computational models for composite materials using homogenization. Ph.D. Dissertation, University of Michigan; 1990.
223. Brand RA. What do tissues and cells know of mechanics? Ann Med 1997;29(4):267–269.
224. Hollister SJ, Fyhrie DP, Jepsen KJ, Goldstein SA. Application of homogenization theory to the study of trabecular bone mechanics. J Biomechanics 1991;24(9):825–839.
225. Hollister SJ, Brennan JM, Kikuchi N. A homogenization sampling procedure for calculating trabecular bone effective stiffness and tissue level stress. J Biomechanics 1994;27(4): 433–444.
226. Livesay GA, Suh J-K, Woo SL-Y. Extensions to homogenization theory for soft tissues undergoing finite elastic deformation. Proc BMES Fall Meeting; 1997.
227. Livesay GA, Suh J-K, Woo SL-Y. Extensions of homogenization theory for the analysis of ligaments under finite elastic deformation. Proc 3rd World Congress Biomech, page 125a; 1998.
228. Strasser H. Lehrbuch der muskel und gelenkmechanik, volume 3, Berlin: Springer; 1917.
229. Bradley J, FitzPatrick D, Daniel D, Shercliff T, O'Connor J. Orientation of the cruciate ligament in the sagittal plane, a method of predicting its length-change with flexion. J Bone Joint Surg 1988;70B(1):94–99.
230. Charlebois SJ, DiAngelo DJ. Development of a linkage model to study the role of the cruciate and collateral ligaments of the knee. 21st Meeting Amer Soc Biomech; 1997.
231. Andriacchi TP, Mikosz RP, Hampton SJ, Galante JO. Model studies of the stiffness characteristics of the human knee joint. J Biomechanics 1983;16:23–29.
232. Gibson M, Mikosz R, Reider B, Andriacchi T. Analysis of the Muller anterolateral femorotibial ligament reconstruction using a computerized knee model. Amer J Sports Med 1986;14: 371–375.
233. Wismans J, Veldpaus F, Janssen J, Huson A, Struben P. A three-dimensional mathematical model of the knee-joint. J Biomechanics 1980;13:677–685.
234. Crowninshield R, Pope MH, Johnson RJ. An analytical model of the knee. J Biomechamcs 1976;9:397–405.
235. Beynnon B, Yu J, Huston D, Fleming B, Johnson R, Haugh L, Pope MH. A sagittal plane model of the knee and cruciate ligaments with application of a sensitivity analysis. ASME J Biomech Eng 1996;118:227–238.
236. Wongchaisuwat C, Hemami H, Buchner HJ. Control of sliding and rolling at natural joints. ASME J Biomech Eng 1984;106:368–375.
237. Abdel-Rahman E, Hefzy MS. A two-dimensional dynamic anatomical model of the human knee joint. ASME J Biomech Eng 1993;115(4A):357–365.
238. Essinger JR, Leyvraz PF, Heegaard JH, Robertson DD. A mathematical model for the evaluation of the behavior during flexion of condylar-type knee prostheses. J Biomechamcs 1989; 22(11–12):1229–41.
239. Blankevoort L, Kuiper JH, Huiskes R, Grootenboer HJ. Articular contact in a three-dimensional model of the knee. J Biomechamcs 1991;24(11):1019–31.
240. Mommersteeg TJ, Blankevoort L, Huiskes R, Kooloos JG, Kauer JM. Characterization of the mechanical behavior of human knee ligaments: A numerical-experimental approach. J Biomechanics 1996;29(2):151–160.
241. Li G, Kanamori A, Woo SL. A validated three-dimensional computational model of a human knee joint. ASME J Biomech Eng 1999;121(6):657–662.
242. Hefzy MS, Grood ES. An analytical technique for modelling knee joint stiffness—Part II: Ligamentous geometric nonlinearities. ASME J Biomech Eng 1983;105(2):145–153.
243. Blankevoort L, Huiskes R. Ligament-bone interaction in a three-dimensional model of the knee. ASME J Biomech Eng 1991;113(3):263–269.
244. Garg A, Walker PS. Prediction of total knee motion using a three-dimensional computer-graphics model. J Biomechanics 1990;23(1):45–58.
245. van Eijden TMGJ, Kouwenhoven E, Verburg J, Weijs WA. A mathematical model of the patello-femoral joint. J Biomechanics 1986;19:219–229.

246. Grood ES, Hefzy MS. An analytical technique for modeling knee joint stiffness—Part I: Ligamentous forces. ASME J Biomech Eng 1982;104(4):330–337.
247. Moeinzadeh MH, Engin AE, Akkas N. Two-dimensional dynamic modelling of human knee joint. J Biomechanics 1983;16(4):253–264.
248. Moeinzadeh MH, Engin AE. Response of a two-dimensional dynamic model of the human knee to the externally applied forces and moments. J Biomed Eng 1983;5(4):281–291.
249. Engin AE, Moeinzadeh MH. Dynamic modeling of human articulating joints. Mathematical Modeling 1983;4:117–141.
250. Abdel-Rahman EM, Hefzy MS. Three-dimensional dynamic behavior of the human knee joint under impact loading. Med Eng Phys 1998;20(4):276–290.
251. Muller W. The Knee: Form, Function, and Ligament Reconstruction. New York: Springer-Verlag; 1983.
252. Gilbertson LG, Goel VK, Kong WZ. Finite element methods in spine biomechanics research. Crit Rev Biomed Eng 1995;23(5–6):411–473.
253. Shirazi-Adl A, Shrivastava SC, Ahmed AM. Stress analysis of the lumbar disc-body unit in compression. A three-dimensional nonlinear finite element study. Spine 1984;9(2):120–134.
254. Lavaste F, Skalli W, Robin S, Roy-Camille R, Mazel C. Three-dimensional geometrical and mechanical modeling of the lumbar spine. J Biomechanics 1992;25:1153–64.
255. Laible JP, Pflaster DS, Krag MH, Simon BR, Haugh LD. A poroelastic-swelling finite element model with application to the intervertebral disc. Spine 1993;18(5):659–670.
256. Shirazi-Adl A, Ahmed AM, Shrivastava SC. A finite element study of a lumbar motion segment subjected to pure sagittal plane moments. J Biomechanics 1986;19(4):331–350.
257. Goel VK, Kim YE, Lim TH, Weinstein JN. An analytical investigation of the mechanics of spinal instrumentation. Spine 1988;13(9):1003–11.
258. Goel VK, Yamanishi TM, Chang H. Development of a computer model to predict strains in the individual fibers of a ligament across the ligamentous occipito-atlanto-axial (c0-cl-c2) complex. Annals Biomed Eng 1992;20(6):667–686.
259. Simbeya KW. Ligament structure and function: a nonlinear finite element approach. Ph.D. Dissertation, University of Calgary; 1993.
260. Simbeya KW, Shrive NG, Frank CB, Matyas JR. A micromechanical finite element model of the rabbit medial collateral ligament. In: Middleton J, Pande G, Williams K, editors. Recent Advances in Computer Methods in Biomechanics and Biomedical Engineering. Books and Journals, Ltd.; 1992:240–249.
261. Simbeya KW, Shrive NG, Frank CB. Assessment with the FEM of the sensitivity of experimental results to experimental procedures in testing the rabbit medial collateral ligament. In: Middleton J, Jones ML, Pande GN, editors, Computer Methods in Biomechanics and Biomedical Engineering. Gordon and Breach; 1996:261–270.
262. Martelli S, Joukhadar A, Zaffagnini S, Marcacci M, Lavallee S, Champleboux G. Fiber-based anterior cruciate ligament model for biomechanical simulations. J Orthop Res 1998;16: 379–385.
263. Pioletti DP, Rakotomanana L, Benvenuti JF, Leyvraz PF. Finite element model of the human anterior cruciate ligament. Comp Meth in Biomech and Biomedical Eng; 1997.
264. Heegaard JH. Large slip contact in biomechanics: Kinematics and stress analysis of the patello-femoral joint. Ph.D. Dissertation, Ecole Polytechnique Federale de Lausanne; 1993.
265. Livesay GA, Fujie H, Kashiwaguchi S, Morrow DA, Fu FH, Woo SL-Y. Determination of the *in situ* forces and force distribution within the human anterior cruciate ligament. Annals Biomed Eng 1995;23(4):467–474.
266. Ahmed AM, Burke DL, Duncan NA, Chan KH. Ligament tension pattern in the flexed knee in combined passive anterior translation and axial rotation. J Orthop Res 1992;10(6):854–867.
267. Takai S, Adams DJ, Livesay GA, Woo SL-Y. Determination of the *in situ* loads on the human anterior cruciate ligament. J Orthop Res 1993;11:686–695.

268. Berns GS, Hull ML, Patterson HA. Strain in the anteromedial bundle of the anterior cruciate ligament under combination loading. J Orthop Res 1992;10(2):167–176.
269. Wilson AN, Shrive NG, Frank CB. Verification of a three-dimensional ligament model. In: Middleton J, Jones ML, Pande GN, editors. Computer Methods in Biomechanics and Biomedical Engineering, Gordon and Breach 1996;281–294.
270. Wilson AN, Shrive NG, and Frank CB. Three dimensional model of the rabbit medial collateral ligament using the finite element method. Proc Eng Systems Design Analysis Conf 1994; 17–26.
271. Gardiner JC, Weiss JA. Representation of anisotropy in constitutive models of biological soft tissues. Proc ASME Winter Annual Meeting 1998;BED-35:263–264.
272. Hirokawa S, Tsuruno R. Three-dimensional deformation and stress distribution in an analytical/computational model of the anterior cruciate ligament. J Biomechanics 2000;33:1069–77.
273. Hirokawa S, Solomonow M, Lu Y, Lou ZP, DAmbrosia R. Anterior-posterior and rotational displacement of the tibia elicited by quadriceps contraction. Amer J Sports Med 1992;20: 299–306.
274. Gardiner JC, Weiss JA. Experimental testing and computational modeling to determine the stress-strain distribution in the human medial collateral ligament. Trans 44th Annual ORS Meeting 1998;23:1027.
275. Weiss JA, Maker BN, Schauer DA. Treatment of initial stress in hyperelastic finite element models of soft tissues. Proc ASME Summer Bioengineering Conference 1995:105–106.
276. Lorensen WE, Cline HE. Marching cubes: A high resolution 3D surface construction algorithm. Computer Graphics (Proc SIGGRAPH) 1987;4:163–169.
277. Schroeder WJ, Zarge J, Lorensen WE. Decimation of triangle meshes. Computer Graphics (Proc SIGGRAPH) 1992;25.
278. Hull ML, Berns GS, Varma H, Patterson HA. Strain in the medial collateral ligament of the human knee under single and combined loads. J Biomechanics 1996;29(2):199–206.
279. Pfaeffle J, Weiss J, Gardiner J, Fischer K, Manson T, Tomaino M, Herndon J, Woo SL-Y. The stress and strain distribution in the interosseous ligament of the human forearm varies with forearm rotation. Trans 46th Meeting Orthop Res Soc 2000;25:140.
280. Race A, Amis AA. The mechanical properties of the two bundles of the human posterior cruciate ligament. J Biomech 1994;27(1):13–24.